FOULING CHARACTERISTICS OF CERAMIC MICROFILTRATION AND ULTRAFILTRATION MEMBRANES DURING SURFACE WATER TREATMENT

A Dissertation
Presented to
The Academic Faculty

by

Seungjin Lee

In Partial Fulfillment
of the Requirements for the Degree
Doctor of Philosophy in Environmental Engineering

Georgia Institute of Technology

August, 2013

FOULING CHARACTERISTICS OF CERAMIC MICROFILTRATION AND ULTRAFILTRATION MEMBRANES DURING SURFACE WATER TREATMENT

Approved by:

Dr. Jaehong Kim, Advisor
School of Civil and Environmental Engineering
Georgia Institute of Technology

Dr. Seung Soon Jang
School of Materials Science and Engineering
Georgia Institute of Technology

Dr. Ching-hua Huang
School of Civil and Environmental Engineering
Georgia Institute of Technology

Dr. Kerry Howe
Department of Civil Engineering
University of New Mexico

Dr. Yongsheng Chen
School of Civil and Environmental Engineering
Georgia Institute of Technology

Date Approved: June 21, 2013

To my parents, wife and children

ACKNOWLEDGEMENTS

Without the continuous support, advice and encouragement of my advisor, Dr. Jaehong Kim, my journey throughout graduate school would have been fruitless and sapless. He has been a man of exemplary character in every aspect of life. I cannot thank him enough for countless things, especially for being my big brother.

I wish to thank the committee members, Dr. Ching-Hua Huang, Dr. Yongsheng Chen, Dr. Seung Soon Jang, and Dr. Kerry Howe, for their time and guidance. Their precious comments and discussions with them were of great help to shape my research. Special thanks to Dr. Huang for her support during my former graduate study and having been my reference for the Environmental Protection Division, GA.

I owe a debt of thanks to Dr. Guangxuan Zhu for smoothening every single occasion when I was in need. Also lots of thanks to Ms. Jenny Eason, the late Mr. Earl Babbitt and Mr. Robert Simon for their consistent support. I am grateful to former and current research group members for helping me in the lab and office. They have endured my conundrums and cohabited with a midas. Thanks also to Mehmet Dilaver, Pyungkyu Park, and Min Cho who did not discontinue their support even from far away. I would like to extend my thanks to the Water Research Foundation and Dr. James Amburgey and Mr. Amir Alansari at the University of North Carolina at Charlotte, for the support.

Lastly, I am simply humble and speechless before my parents. They have walked with me throughout this journey for forty-one years. My wife, Inhee, and lovely children, Eunjae, Eunkhang, and Eunsaang, have been the reasons for my research and life.

TABLE OF CONTENTS

LIST OF TABLES

LIST OF FIGURES

LIST OF SYMBOLS

α	pore blockage parameter [m^2/kg]
A	membrane surface area [m^2]
C_b	bulk concentration of the feed solution [kg/m^3]
Δp	applied transmembrane pressure [Pa]
F	interaction force between a CML particle and membrane surface [N]
f'	fractional amount of foulant contributing to cake growth
H	Hamaker constant [J]
J	flux [m/s]
J_0	pure water flux of clean membrane [m/s]
J_{w0}	pure water flux of clean membrane [m/s]
k	fouling coefficient [variable unit depending on n]
k_1	a lumped parameter, $\alpha \Delta p C_b/\mu R_m$ [s^{-1}]
k_2	a lumped parameter, $2 f' R' \Delta p C_b/\mu(R_m+R_{p0})$ [s^{-1}]
k_{RC}	a proportionality coefficient between R_c and V/A [m^{-2}]
μ	viscosity [Pa·s]
n	filtration constant
p	pressure [Pa]
Q	volumetric filtrate flow rate through the membrane [m^3/s]
Q_0	initial value of Q
R'	specific cake layer resistance [m/kg]

R	radius of the CML particle (in Chapter 3) [m]
R	resistance [m^{-1}]
R_c	cake resistance [m^{-1}]
R_c	chemically reversible resistance (in Chapter 4) [m^{-1}]
R_{cp}	resistance due to concentration polarization [m^{-1}]
R_{cr}	chemically reversible resistance [m^{-1}]
R_{if}	chemically irreversible resistance [m^{-1}]
R_i	chemically irreversible resistance [m^{-1}]
R_m	intrinsic membrane resistance [m^{-1}]
R_p	physically removable fouling [m^{-1}]
R_{p0}	initial resistance of the deposit [m^{-1}]
R_{pr}	cake and pore deposit resistance removable by backwash [m^{-1}]
R_t	total resistance [m^{-1}]
R^2	coefficient of determination
t	filtration time [s]
V	cumulative permeate volume [m^3]
V_s	cumulative permeate volume per unit membrane surface area [m]
W	interaction energy per unit area between a particle and surface [J/m^2]
Z	total deflection or the sum of the cantilever deflection and the piezo position [m]

LIST OF ABBREVIATIONS

AFM	atomic force microscopy
alum	aluminum sulfate
BW	backwashing
CLSM	confocal laser scanning microscopy
CM	ceramic membrane
CML	carboxylate modified latex
DBP	disinfection by-product
DOC	dissolved organic carbon
DOM	dissolved organic matter
EIP	isoelectric point
GL	lake water from Georgia
GR	river water from Georgia
LMH	a unit of flux, liter per square meter per hour [$l/m^2/h$]
MGD	megagallon per day
MWCO	molecular weight cut-off
NL	lake water from North Carolina
NOM	natural organic matter
NR	river water from North Carolina
NTU	Nephelometric turbidity unit
PACl	polyaluminum chloride

PC	polycarbonate
PEG	polyethylene glycol
PES	polyether sulfone
PS	polysulfone
PVDF	polyvinylidene fluoride
QD	quantum dot
RC	regenerated cellulose
SEM	scanning electron microscopy
SRHA	Suwannee river humic acid
SSR	the smallest sum of squared residuals
SUVA	specific ultraviolet absorbance, UV_{254} (m^{-1}) divided by DOC (mg/l) [l/mg/m]
TEM	transmission electron microscopy
TOC	total organic carbon
UMFI	unified membrane fouling index
UV	ultraviolet
UV_{254}	ultraviolet absorbance at 254 nm

SUMMARY

Many advantages of ceramic membranes over conventional polymeric membranes have drawn attention, and ceramic membranes become a cost-competitive alternative to polymeric membranes. Coagulation-ceramic membrane processes can be robust options for surface water treatment through the utilization of the intrinsic mechanical durability and chemical resistivity of ceramic membranes and the optimization of coagulation pretreatment. Virtually no information on the performance and fouling mechanisms of ceramic membrane processes, however, is available to the industry, and questions related to the effective implementation of ceramic membranes for U.S. drinking water production remain unanswered. As in polymeric membrane processes, membrane fouling by natural organic matter (NOM) is an inevitable phenomenon and one of the greatest hurdles in ceramic membrane processes. Therefore, it is necessary to understand the fouling behavior of ceramic membrane processes, and the performance and optimization of coagulation-ceramic membrane processes need to be evaluated for drinking water production.

The objective of this study is to comparatively examine the similarities and dissimilarities between ceramic and polymeric membrane fouling to provide the water treatment industry with practical guidelines for the design and optimization of ceramic membrane processes. First, this study presents the fouling characteristics of ceramic microfiltration investigated using model feed solutions of polyethylene glycol or NOM as well as a synthetic river water. The fouling behavior was further analyzed, for the first time, using the combined pore blockage-cake filtration model, constant pressure filtration

laws, resistance-in-series model, and the unified membrane fouling index model. Second, the effects of solution chemistry parameters including ionic strength, divalent ion concentration and pH on the fouling behavior were examined for ceramic ultrafiltration of NOM. Experimental evaluations were expanded to visualization of fouling using quantum dots, batch adsorption tests, contact angle measurements, and foulant-membrane surface adhesion force measurements. Third, the effects of coagulation on the performance of coagulation-ceramic membrane filtration system were systematically investigated for selected U.S. surface waters. The performance of the hybrid system was evaluated in terms of pressure in a constant flow rate mode or flux in a constant pressure mode and the removal efficiency of NOM. Throughout the study, systematic comparison of the fouling characteristics between ceramic and polymeric membranes is provided via parallel experimental evaluation and analyses using polymeric membranes.

The fouling models agreed well with the ceramic membrane filtration results, and the ceramic membrane fouling was characterized by the shorter initial pore blocking mechanism and the earlier transition to the cake filtration mechanism than that of polymeric membranes. The results collectively suggest that less fouling tendency and better cleaning efficiency were characteristic of ceramic membranes, and physically removable resistances were dominant. On average, physically removable resistance for ceramic microfiltration was 72.5 % while it was 51.5 and 40.5 % for PVDF and polycarbonate membranes, respectively. The trends observed with the effects of solution chemistry on ceramic membrane fouling were similar to those on the polymeric counterparts while the extent varied depending on water quality parameters. The fouling of ceramic membranes with ZrO_2 surface was influence by pH more than polymeric

counterpart due to the charge inversion around pH 6.5. When pH changed from 4 to 6, 8 and 10, normalized flux for the ceramic membranes increased by 17, 13, and 4 %, respectively, while there was an increase of 6, 8 and 5 % for the polyethersulfone membranes with an isoelectric point around 3. The effect of calcium ions was significantly less with ceramic membranes where the normalized flux was reduced by 43 % and for polymeric membranes by 90 % at 5 mM. On the other hand, there was little difference in the effect of ionic strength between ceramic and polymeric membranes. The coagulation-ceramic microfiltration system performed better than the polymeric counterpart in terms of relative pressure and normalized flux in constant flow rate and pressure modes, respectively. The optimal coagulation condition may not be identical for ceramic and polymeric membranes. The operating pressure during the ceramic membrane filtration of a river water was reduced by 28.8 and 17.3 % with ferric chloride and aluminum sulfate, respectively, and it was 43.7 and 42.3 % with polymeric membranes. Less severe fouling and higher cleaning efficiency in the hybrid system was consistent with the findings obtained using simple model compounds. The final pressure at the end of the first cycle was 2.8 and 5.6 times the initial pressure with ceramic and polymeric membranes, respectively. The removal efficiency of NOM was comparable between the ceramic and polymeric membrane systems, and the SUVA values of source surface waters correlated well with the NOM rejection.

This study presents one of the first successful applications of filtration and fouling models to ceramic membrane systems and side-by-side evaluation of similarities and dissimilarities in the effects of membrane materials and solution chemistry. As the first work comparing the coagulation-membrane filtration systems between ceramic and

polymeric membranes under the same conditions, this study includes the performance of the coagulation-ceramic membrane system during the treatment of U.S. surface waters. The results of this study provide critical information to guide the industry practitioners, consultants, and regulatory agents considering early adoption of this new technology as well as fundamental knowledge upon which further in-depth studies can be built.

CHAPTER 1

INTRODUCTION

1.1 Motivation

Many advantages of ceramic membranes over conventional polymeric membranes have drawn attention and ceramic membranes becomes a cost-competitive alternative to polymeric membranes (Pendergast and Hoek, 2011). Virtually no information on the performance and fouling mechanisms of ceramic membrane processes, however, is available to the industry and the questions related to the effective implementation of ceramic membranes for U.S. drinking water production remains unanswered.

Membrane fouling by natural organic matter (NOM) is an inevitable phenomenon and one of the greatest hurdles in membrane processes to treat surface water for potable water production (Shao et al., 2011; Taniguchi et al., 2003). Fouling and/or biofilm formation are responsible for the poor production efficiency in polymeric membrane processes, and the suitability, performance and optimization of ceramic membrane processes need to be elucidated to meet the implementation of ceramic membrane processes for quality water production (Ciston et al., 2008). Previous studies have provided valuable insights on the factors that affect membrane fouling including membrane types (Gray et al., 2007), properties of membrane materials (Combe et al., 1999), process configuration (Tarabara et al., 2002), operating conditions (Meyn and Leiknes, 2010), water quality parameters(Howe and Clark, 2002), and cleaning strategies (Lee et al., 2001; Lim and Bai, 2003), but polymeric membranes have been almost

exclusively dealt with while alternative membrane materials have been receiving increasing interest only in recent years.

First of all, it is necessary to investigate the fouling characteristics of ceramic membranes, which can be realized by applying fouling/filtration models including the combined pore blockage-cake filtration model (Ho and Zydney, 2000), constant pressure filtration laws (Hermia, 1982; Huang et al., 2008), resistance-in-series model, and the unified membrane fouling index (UMFI) model (Huang et al., 2008). The results would suggest any similarity and differences between ceramic and polymeric membranes in terms of fouling mechanisms and their transitions. The identification of the dominant contributing resistances and relative contribution of the resistances would influence the cleaning strategy for different membrane materials.

Secondly, fundamental questions about the origin of the fouling characteristics of different membrane materials need to be answered, which can successfully describe the fouling characteristics of ceramic and polymeric membranes (de Lara and Benavente, 2009). Therefore, it is crucial to understand the effects of solution chemistry including ionic strength, divalent ion concentration and pH (Gray et al., 2008; Jones and O'Melia, 2000), the intrinsic membrane properties such surface charge (Benavente et al., 1993; Bowen and Mukhtar, 1993) and hydrophobicity/hydrophilicity (Yuan and Zydney, 2000; Zhang et al., 2009), and the interactions between solutes-membrane surface on the fouling behavior (Yuan and Zydney, 2000). Not only the flux and resistances analyses, but also the visualization of fouling and the measurements of the interaction forces between foulants and membranes would be of great significance, especially in a comparative context between different membrane materials.

Finally, the evaluation of the pretreatment conditions and fouling behavior of ceramic membrane process is prerequisite for the implementation of ceramic membrane processes for surface water treatment for drinking water production (Howe et al., 2006; Huang et al., 2009). Various pretreatment options, i.e., adsorption by powdered activated carbon (Huang et al., 2009), irradiation of ozone or ultraviolet, or coagulation, have been adopted to improve the efficiency membrane processes and the compatibility of feed water with membranes (Huang et al., 2009). Among those, coagulation is known to be one of the most effective pretreatments for the removal of natural organic matters (NOMs) in surface waters. Since little is known about a novel hybrid ceramic membrane processes while previous studies on the characteristics optimization of coagulation mainly dealt with polymeric membranes, the optimization of coagulation for the hybrid system will allow the application of ceramic membrane processes with confidence.

The knowledge about the effects of intrinsic physical properties of membranes such as pore size, molecular weight cut-off (MWCO) (Howe and Clark, 2002), roughness (Evans et al., 2008) and thickness of active and support layers will provide the water treatment industry and the manufacturers with practical guidelines for the selection of membranes with optimal performance.

1.2 Background

Membrane fouling can be analyzed by the filtration models developed for different modes of operations and driving forces, i.e., pressure or constant flow rate modes, cross-flow and dead-end modes (Arnot et al., 2000; Bowen et al., 1995; Hermia,

1982; Taniguchi et al., 2003). Since the fouling process is a combination of multiple mechanisms, not only a single dominant or apparent fouling mechanism but also the combined behavior needs to be analyzed. This study presents one of the first in-depth studies of fouling mechanisms of ceramic membranes. Dead-end, constant-pressure filtration experiments were performed with ceramic microfiltration membranes using polyethylene glycol (PEG) and Suwannee River Humic Acid (SRHA) solutions and a synthetic river water. PEG was chosen as a model organic matter since it has been widely used as a standard macromolecule in previous comparable studies examining polymeric membrane fouling (Ganguly and Bhattacharya, 1994; Ghose et al., 2000; Vincent-Vela et al., 2009). Flux data from ceramic membrane filtration were applied for the first time to a constant pressure filtration model taking into account the transition of fouling mechanisms from pore blocking to cake filtration, originally applied to polymeric membranes treating proteins (Ho and Zydney, 2000), and applied to identify the transitions of fouling mechanisms of NOM solutions (Taniguchi et al., 2003). The conventional cake filtration model and the recently developed unified membrane fouling index (UMFI) were used for comparison. The evaluation of mechanism(s) was further augmented by a resistance-in-series model analysis.

The governing equation for the fouling mechanisms for constant flow rate mode is expressed as shown in Equation (1.1) and the flux data can be plotted as d^2t/dV^2 vs. dt/dV:

$$\frac{d^2t}{dV^2} = k\left(\frac{dt}{dV}\right)^n \tag{1.1}$$

where k = fouling coefficient; V= cumulative volume [m^3]; and n = filtration constant. n represents the fouling mode, i.e., the values of 0, 1, 1.5, and 2 represent cake filtration, intermediate, standard, and complete pore blocking modes, respectively (Hermans and

Bredee, 1936; Hermia, 1982). The derivatives for both experimental flux data and the model fits are calculated as follows (Yuan and Zydney, 2000):

$$\frac{dt}{dV} = \frac{1}{JA} \tag{1.2}$$

$$\frac{d^2t}{dV^2} = -\frac{1}{J^3A^2}\frac{dJ}{dt} = \frac{1}{A}\frac{d(1/J)}{dV} \tag{1.3}$$

where A = membrane surface area [m^2].

Flux data are analyzed using the combined pore blockage-cake filtration model (the combined model hereafter) to evaluate the transition of fouling mechanisms (i.e., from initial pore blockage to cake filtration) (Ho and Zydney, 2000):

$$Q = Q_0\left[\exp\left(-\frac{\alpha\Delta pC_b}{\mu R_m}t\right) + \frac{R_m}{\left(R_m + R_{p0}\right)\sqrt{1+\frac{2f'R'\Delta pC_bt}{\mu\left(R_m+R_{p0}\right)}}}\left(1-\exp\left(-\frac{\alpha\Delta pC_b}{\mu R_m}t\right)\right)\right] \tag{1.4}$$

where Q = volumetric filtrate flow rate through the membrane [m^3/s]; Q_0 = initial value of Q; α = pore blockage parameter [m^2/kg]; Δp = applied transmembrane pressure [Pa]; μ = viscosity [Pa·s]; R_m = intrinsic membrane resistance [m^{-1}]; R_{p0} = initial resistance of the deposit [m^{-1}]; f' = fractional amount of foulant contributing to cake growth; and R' = specific cake layer resistance [m/kg]; t = filtration time [s]; and C_b = bulk concentration of the feed solution [kg/m^3]. The first term in Equation (1.4) accounts for the classic pore

blocking model and the second term the cake filtration model. Equation (1.4) can be rewritten as follows using lumped parameters, k_1 and k_2:

$$Q = Q_0\left[\exp(-k_1 t) + \frac{R_m}{(R_m + R_{p0})\sqrt{1+k_2 t}}\left(1-\exp(-k_1 t)\right)\right] \tag{1.5}$$

where

$$k_1 = \frac{\alpha \Delta p C_b}{\mu R_m} \tag{1.6}$$

$$k_2 = \frac{2 f' R' \Delta p C_b}{\mu(R_m + R_{p0})} \tag{1.7}$$

The filtration data were fitted to the above equations via non-linear optimization using a curve fitting tool in MATLAB® (The Mathworks, Inc., Natick, MA) with a trust region method to result in the greatest coefficient of determination, R^2, or the smallest sum of squared residuals.

In addition to the combined model, the conventional cake filtration model and the UMFI model are used to comparatively analyze the flux behaviors. The analysys of this study confirms that ceramic membrane fouling can be mainly described by cake formation. In the conventional cake filtration theory, the parabolic law is used to identify the fouling characteristic (Schippers and Verdouw, 1980). The rate of filtration is expressed as in Equation (1.8), and when integrated, the relationship between t/V vs. V is obtained as shown in Equation (1.9).

$$\frac{dV}{dt} = \frac{\Delta p}{\mu(R_c + R_m)} = \frac{\Delta p}{\mu(k_{RC}\frac{V}{A} + R_m)} \tag{1.8}$$

$$\frac{t}{V} = \frac{\mu R_m}{\Delta p} + \frac{\mu k_{RC}}{2A\Delta p}V \tag{1.9}$$

where R_c = cake resistance [m^{-1}]; and k_{RC} = a proportionality coefficient between R_c and V/A [m^{-2}]. The cake filtration model suggests that the linearity exists when t/V is plotted vs. V (Fig. 10a). When cake filtration is the dominant mechanism, the UMFI can be defined as follows (Huang et al., 2008; Nguyen et al., 2010):

$$\frac{J_0}{J} = 1 + (UMFI)V_s \tag{1.10}$$

where J_0 = pure water flux of clean membrane [m/s]; V_s = cumulative permeate volume per unit membrane surface area [m]; and $UMFI$ = a measure of total fouling [m^{-1}]. Therefore, the UMFI model suggests the linearity between J_0/J plot vs. V (Huang et al., 2008; Nguyen et al., 2010; Schippers and Verdouw, 1980). When the filtration data were applied to both models, a linear relationship can be found for t/V vs. V and J_0/J vs. V, respectively. Although these models have been exclusively applied for polymeric membrane filtration in the past, our results wherein the data fit to the linear models suggest that these widely used models based on cake filtration might provide an adequate approach to mathematically represent ceramic membrane fouling by NOM during surface water treatment.

The general form of the resistance-in-series model represented as Equation (1.11), was used to quantify the contribution of each fouling mechanism to overall flux decline:

$$J = \frac{\Delta p}{\mu R_t} = \frac{\Delta p}{\mu\left(R_m + R_{cp} + R_{pr} + R_{cr} + R_{if}\right)} \tag{1.11}$$

where J = flux [m/s]; R's = resistances [m^{-1}] (R_t = total resistance; R_{cp} = resistance due to concentration polarization; R_{pr} = cake and pore deposit resistance removable by backwash, *i.e.*, physically removable fouling; R_{cr} = chemically reversible resistance; and R_{if} = chemically irreversible resistance).

Past studies on polymeric membranes suggest that various factors such as solution chemistry, membrane surface properties, and operating conditions influence the membrane fouling by NOM (Childress and Elimelech, 1996; Evans et al., 2008). If the fouling mechanism were governed by differences in the membrane surface properties, different fouling behaviors might result. Of particular interest is a potentially significant difference in the interaction between solutes and membrane surface, which has been frequently correlated to NOM fouling characteristics even among polymeric membranes. These interactions between solutes/particles and membrane surface have been investigated via surface potential measurement, atomic force microscopy (AFM) analysis, and contact angle measurements in past studies (Hong and Elimelech, 1997; Lee et al., 2004; Li and Elimelech, 2004).

Another objective of this study is to comparatively examine ceramic versus polymeric membrane fouling under varying water quality conditions. Feed water pH, divalent ion concentration, and ionic strength on the membrane fouling are of primary

concern (Liang et al., 2008; Yuan and Zydney, 1999), as they are known to affect the interaction between solutes/particles and membrane surface (Chiu and James, 2007; de la Casa et al., 2007) due to acid/base speciation, electrical double layer compressions (Li and Fu, 2002; Liang et al., 2008), charge screening (Ghosh and Schnitzer, 1980; Hering and Morel, 1988), complex formation (Gao et al., 2012; Li and Elimelech, 2004), and aggregation and deposition (Costa and de Pinho, 2005; Hong and Elimelech, 1997). Ceramic membranes are made of metal oxides which are generally more hydrophilic than most polymeric materials and may assume different surface potential that originates from different surface functional moieties. Therefore, it is hypothesized that the impact of water quality on NOM fouling is different between ceramic and polymeric membranes. To test this hypothesis, filtration experiments were performed and fouling characteristics were quantitatively analyzed using a resistance-in-series model. A method of visualizing fouling using a confocal laser scanning microscopy (CLSM), which was recently employed for biofouling visualization (Meng et al., 2007; Sun et al., 2011), was newly applied to analyze fouling by colloidal foulants using carboxlyated quantum dots (QDs) as a surrogate. AFM analysis was performed for the first time to probe the interactive forces between a carboxylated latex particles and the ceramic membrane surface. Results point to critical similarities and dissimilarities between ceramic and polymeric membranes, and advantage of ceramic materials for surface water treatment application, particularly in terms of the reversibility of fouling and the effectiveness of cleaning process.

The removal of natural organic matter (NOM) is one of the primary requirements for the production of drinking water (Choi and Dempsey, 2004; Leiknes et al., 2004).

NOMs lead to membrane fouling by which the performance of membrane processes becomes sub-optimal as well as play as a precursor to of disinfection by-products (DBPs) (Mitch et al., 2011; Yang and Shang, 2004) and causes an aesthetic concern related to color. It is well know that the membrane fouling is an inevitable phenomenon and one of the greatest hurdles in membrane processes, the reduction of such fouling has been a major topic of previous studies. Among various pretreatment options applied to minimize membrane foulng, scaling and degradation of membranes, coagulation is known to be one of the most effective pretreatments for the NOM removal in drinking water production by destabilizing aquatic contaminants leading to larger particulate matters via precipitation onto coagulants (Berube et al., 2002; Fiksdal and Leiknes, 2006; Leiknes et al., 2004). Previous studies on the characteristics optimization of coagulation, however, mainly dealt with polymeric membranes and little is known about a novel hybrid ceramic membrane processes.

In this study, using selected U.S. surface waters, direct filtration of chemically treated surface water have been being evaluated. The coagulation-ceramic membrane hybrid system can be an effective process in reducing membrane fouling with a less footprint compared conventional coagulation-flocculation-sedimentation process (Huang et al., 2009). In-line coagulation with microfiltration in which destabilized contaminants and their aggregates and the hydrolytes and precipitates of coagulant are fed (Choi and Dempsey, 2004), have been studied for its performance in comparison with direct filtration of raw surface waters. Literature contains many publications regarding ceramic membranes, but the majority of them involve industrial applications instead of municipal drinking water production. Many of the drinking water publications that do involve the

use of ceramic membranes do not use the hybrid process of coagulation and ceramic membrane filtration. However, there have limited number of publications involving the hybrid process of coagulation-ceramic membrane filtration, which unfortunately, have been rather limited in scope (Kanaya et al., 2007; Lehman et al., 2008; Loi-Brugger et al., 2006). The comparison of different coagulants, lacking in the study for U.S. source waters, and the fouling mechanism study would be necessary for the implementation of the hybrid system to U.S. surface water treatment.

Additional study on other parameters which can influence the membrane performance including the effect of the intrinsic physical properties of membranes such as pore size, molecular weight cut-off (MWCO) (Howe and Clark, 2002), roughness (Evans et al., 2008) and thickness of active and support layers are necessary to understand the similarities and dissimilarities in the fouling behavior between ceramic and polymeric membranes. The design and operation of ceramic membrane processes need to be carefully tailored based on fouling characteristics of ceramic membranes, rather than assuming similar trends found with polymeric membranes. More in-depth studies on the performance of ceramic membrane processes including operating conditions, scale-up studies, and pretreatment options, are required for rapid translation of this emerging technology to the full-scale application. Various materials and configurations of ceramic membranes also need to be further tested to build knowledge comparable to the large corpus already available for polymeric counterparts.

CHAPTER 2

COMPARATIVE ANALYSIS OF FOULING CHARACTERISTICS OF CERAMIC AND POLYMERIC MICROFILTRATION MEMBRANES USING FILTRATION MODELS

2.1 Introduction

Membrane fouling by natural organic matter (NOM) is an inevitable phenomenon and one of the greatest hurdles in membrane processes to treat surface water for potable water production (Shao et al., 2011; Taniguchi et al., 2003). A great deal of effort has been made to understand the nature of the membrane fouling, develop mitigation strategies, and improve the filtration performance (Howe and Clark, 2002; Lee et al., 2001). Previous studies have provided valuable insights on the factors that affect membrane fouling including membrane types, properties of membrane materials, process configuration, operating conditions, water quality parameters, and cleaning strategies. The effect of membrane material, in particular, has been the focus of many past studies in which the surface properties of the membranes (e.g., hydrophobicity, roughness, and zeta potential) were correlated to interaction with foulants (Childress and Elimelech, 1996; Evans et al., 2008). Polymeric membranes have been almost exclusively dealt with; however, alternative membrane materials have been receiving increasing interest in recent years.

Ceramic membrane processes are a rapidly emerging technology due to many inherent advantages over the conventional polymeric membrane processes. Made of

inorganic materials, ceramic membranes exhibit far superior chemical resistivity allowing much more aggressive cleaning approaches without risk of damaging membrane integrity. The use of more aggressive chemical cleaning to remove otherwise irreversible fouling would significantly prolong the life expectancy of ceramic membranes and decrease the downtime required for routine cleaning. Ceramic membranes have much greater structural integrity and reliability, which would eliminate the repetitive testing, repair, and replacement of polymeric membranes for problems such as broken hollow fibers. Therefore, ceramic membranes have been used in many industrial applications, not only where polymeric membranes could not perform acceptably, but also where superior system integrity is required (Pendergast and Hoek, 2011). While the adoption by water industries has been limited primarily due to relatively high costs, ceramic membrane processes are now increasingly viewed as a new, viable, and cost-competitive option for drinking water treatment (Loi-Brugger et al., 2006). For example, there are approximately 50 small ceramic membrane drinking water facilities in Japan, which have all been constructed in the last decade (Kanaya et al., 2007; Loi-Brugger et al., 2007). In the US, a pilot study was conducted at a plant with a capacity of 2.5-MGD in California, and a 10-MGD plant is currently being designed in Colorado (Freeman and Shorney-Darby, 2011; McAliley and D'Adamo, 2009). Despite the potential wider application in water treatment, virtually little is known about the performance characteristics of the ceramic membranes, in particular related to membrane fouling by NOM.

This study presents one of the first in-depth studies of fouling mechanisms of ceramic membranes. Dead-end, constant-pressure filtration experiments were performed with ceramic microfiltration membranes using polyethylene glycol (PEG) and Suwannee

River Humic Acid (SRHA) solutions and a synthetic river water. PEG was chosen as a model organic matter since it has been widely used as a standard macromolecule in previous comparable studies examining polymeric membrane fouling (Ganguly and Bhattacharya, 1994; Ghose et al., 2000; Vincent-Vela et al., 2009). Flux data from ceramic membrane filtration were applied for the first time to a constant pressure filtration model taking into account the transition of fouling mechanisms from pore blocking to cake filtration, originally applied to polymeric membranes treating proteins (Ho and Zydney, 2000), and applied to identify the transitions of fouling mechanisms of NOM solutions (Taniguchi et al., 2003). The conventional cake filtration model and the recently developed unified membrane fouling index (UMFI) were used for comparison. The evaluation of mechanism(s) was further augmented by a resistance-in-series model analysis.

2.2 Experimental

2.2.1 Materials

Disc-type ceramic microfiltration membranes were obtained from Sterlitech Corp. (Kent, WA). The membranes are 2.5 mm thick and 47 mm in diameter with an effective filtration area of 14.6 cm^2 and a nominal pore size of 0.2 μm. These membranes are resistant to temperature up to 350 °C and pressure up to 4 bars, and have a pH range of operation from 0 to 14. Virgin membranes were chemically cleaned and wetted by soaking in ultrapure water (resistivity > 18.2 MΩ) for 30 min or by filtering 300 mL of

Table 2.1 Characteristics of ceramic and polymeric membranes used in this study.

Material		Pore size (μm)	Contact angle (°)	Active layer thickness (μm)
Ceramic	TiO_2 (surface) Al_2O_3, TiO_2, ZrO_2 (support)	0.2[a]	15.6 ± 3.4[b]	27.0 ± 1.7[b]
Polymeric	PVDF	0.22[a]	69.3 ± 2.9[b]	100 - 125[a]
	Polycarbonate (PC)	0.2[a]	53.5 ± 1.4[b]	25 - 30[a]

[a] reported by manufacturer
[b] measured in this study

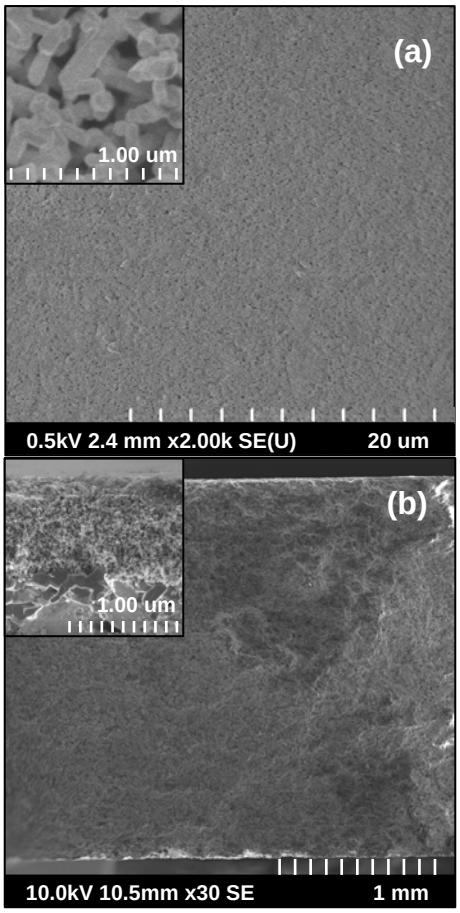

Figure 2.1 SEM images of the surface (a) and cross-section (b) of the ceramic membrane used in this study. Embedded images are the enlarged view of the surface (a) and the active surface layer of the cross-section (b).

ultrapure water before use. Polycarbonate (PC) and polyvinylidene fluoride (PVDF) microfiltration membranes with pore sizes of 0.2 and 0.22 μm, respectively, were obtained from Millipore (Bedford, MA). The polymeric membranes were prepared by soaking in ultrapure water for 2 hours, while replacing ultrapure water at least three times. Contact angles were measured for ceramic and polymeric membranes using Rame-Hart Model 250 Goniometer (Succasunna, NJ) and the thickness of the ceramic membranes was measured using a variable pressure scanning electron microscope (Hitachi, VP-SEM 3700, Japan). The characteristics of the ceramic and polymeric membranes are summarized in Table 2.1, and the SEM images of the surface and the cross section of the ceramic membrane are presented in Figure 2.1.

A model organic foulant, PEG with an average molecular weight of 20 kDa (J. T. Baker Co., Philipsburg, NJ), was used without further purification. Feed solutions (50, 100, 500, and 1,000 mg/L) were prepared by dissolving PEG pellets into ultrapure water. SRHA (International Humic Substances Society, St. Paul, MN) was used, without further purification, to prepare feed solutions (50 and 100 mg/L). The pH values of the feed solutions and ultrapure water used for filtration, rinse, and backwash were adjusted to 8.0 ± 0.1 using 0.1 N HCl or NaOH. A synthetic river water at pH 7.5 contained alkalinity of 50 mg/L as $CaCO_3$ (prepared by adding $NaHCO_3$), turbidity of 20 NTU (by adding bentonite), hardness of 100 mg/L as $CaCO_3$ (by adding $CaCl_2$) and dissolved organic carbon of 2.5 mg/L (by adding SRHA). Used ceramic membranes were cleaned by soaking in 200 mL of 0.1 N NaOH at 85 °C for 15 min, followed by neutralization and acid cleaning in 85% phosphoric acid at 50 °C for 15 minutes. Polymeric membranes were cleaned in a 0.1 N NaOH solution at room temperature overnight.

2.2.2 Filtration Experiments

A dead-end filtration system (Model HP4750 Stirred Cell, Sterlitech Corp., Kent, WA) (Figure 2.1), made of stainless steel 316, was used for all the filtration experiments. Since the cell was originally manufactured to house a thin polymeric membrane coupon, its bottom housing was carefully modified to fit much thicker ceramic membranes. In addition to 300 mL of feed inside the cell which was stirred at 200 rpm, an additional 20-liter stainless steel feed reservoir (Pressure Vessel XX6700P20, Millipore, Bedford, MA) or 1.0 L polyethylene container (GXWH04F, GE, Trevose, PA) was used as an external feed reservoir. The pressure was maintained at 2.0 psi by nitrogen gas and monitored using a digital pressure transmitter (Omegadyne Inc., Model PX319-050G5V, Sunbury, OH) and the temperature at 23 ± 1 °C. Permeate was collected on a digital balance (Sartorius, ED623S, Goettingen, Germany), and the cumulative mass of permeate was recorded in a personal computer every 1 or 10 s via a RS-232 connection to calculate the flux. The pH values of all solutions were monitored before and after each filtration. The concentration of solutions was analyzed using TOC-Vw Analyzer (Shimadzu, Columbia, MD) or spectrofluorophotometer (RF-5031PC, Shimadzu, Japan). Particle size distributions of PEG, SRHA and a synthetic river water were measured using Zetasizer Nano ZS (Malvern, UK). Schematic diagrams of experimental setup and filtration steps are shown in Figure 2.2.

2.2.3 Filtration Model Analysis

Flux data were analyzed using the combined pore blockage-cake filtration model (the combined model hereafter) to evaluate the transition of fouling mechanisms (i.e., from initial pore blockage to cake filtration) (Ho and Zydney, 2000):

$$Q = Q_0\left[\exp\left(-\frac{\alpha\Delta pC_b}{\mu R_m}t\right)+\frac{R_m}{\left(R_m+R_{p0}\right)\sqrt{1+\frac{2f'R'\Delta pC_bt}{\mu\left(R_m+R_{p0}\right)}}}\left(1-\exp\left(-\frac{\alpha\Delta pC_b}{\mu R_m}t\right)\right)\right] \tag{2.1}$$

where Q = volumetric filtrate flow rate through the membrane [m^3/s]; Q_0 = initial value of Q; α = pore blockage parameter [m^2/kg]; Δp = applied transmembrane pressure [Pa]; μ = viscosity [Pa·s]; R_m = intrinsic membrane resistance [m^{-1}]; R_{p0} = initial resistance of the deposit [m^{-1}]; f' = fractional amount of foulant contributing to cake growth; and R' = specific cake layer resistance [m/kg]; t = filtration time [s]; and C_b = bulk concentration of the feed solution [kg/m^3]. The first term in Equation (2.1) accounts for the classic pore blocking model and the second term the cake filtration model. Equation (2.1) can be rewritten as follows using lumped parameters, k_1 and k_2:

$$Q = Q_0\left[\exp\left(-k_1t\right)+\frac{R_m}{\left(R_m+R_{p0}\right)\sqrt{1+k_2t}}\left(1-\exp\left(-k_1t\right)\right)\right] \tag{2.2}$$

where

$$k_1 = \frac{\alpha\Delta pC_b}{\mu R_m} \tag{2.3}$$

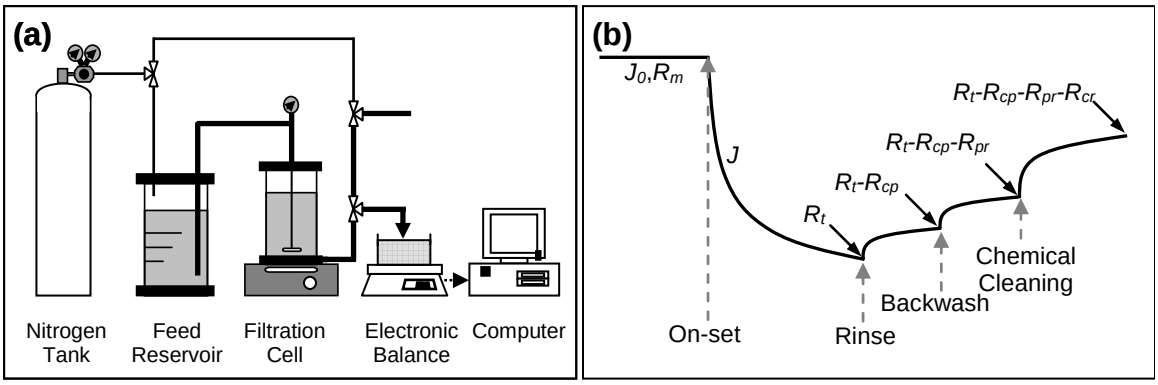

Figure 2.2 Schematic diagrams of experimental setup (a) and filtration steps (b). Intrinsic membrane resistance (R_m) was measured from initial water flux, total resistance (R_t) at the end of feed filtration, and resistance due to concentration polarization (R_{cp}), cake and pore deposit resistance removable by backwash, *i.e.*, physically removable fouling (R_{pr}), chemically reversible resistance (R_{cr}) and chemically irreversible resistance (R_{if}) after rinse, backwash, and chemical cleaning steps, respectively.

$$k_2 = \frac{2f'R'\Delta pC_b}{\mu\left(R_m + R_{p0}\right)} \tag{2.4}$$

The filtration data were fitted to the above equations via non-linear optimization using a curve fitting tool in MATLAB® (The Mathworks, Inc., Natick, MA) with a trust region method to result in the greatest coefficient of determination, R^2, or the smallest sum of squared residuals.

In addition to the combined model, the conventional cake filtration model and the UMFI model were used to comparatively analyze the flux behaviors.

2.2.4 Resistance-in-Series Model Analysis

The general form of the resistance-in-series model represented as Equation (2.5), was used to quantify the contribution of each fouling mechanism to overall flux decline:

$$J = \frac{\Delta p}{\mu R_t} = \frac{\Delta p}{\mu\left(R_m + R_{cp} + R_{pr} + R_{cr} + R_{if}\right)} \tag{2.5}$$

Where J = flux [m/s]; R's = resistances [m^{-1}] (R_t = total resistance; R_{cp} = resistance due to concentration polarization; R_{pr} = cake and pore deposit resistance removable by backwash, *i.e.*, physically removable fouling; R_{cr} = chemically reversible resistance; and R_{if} = chemically irreversible resistance).

Table 2.2 Classification of Resistances.

Resistance	Definition	Description
R_m	Intrinsic membrane resistance	Pure water resistance
R_{cp}	Concentration polarization or gel layer	Concentration polarization or gel layer exerted by the feed solution and removed by rinse
R_{pr}	Resistance removable by backwash	Cake formed on the surface or in the pore, not removable by rinsing but removable by backwash
R_{cr}	Chemically reversible resistance	Internal fouling, a portion of the total resistance removable only by chemical cleaning
R_{if}	Chemically irreversible resistance	Residual resistance after chemical cleaning
R_t	Total resistance	Measured at the end of feed filtration: $R_m+R_{cp}+R_{pr}+R_{cr}+R_{if}$

Contributing resistances accounting for the total resistance can be defined according to the specific procedure of the filtration steps, and the classification and definition of each resistance is summarized in Table 2.2.

Each resistance was obtained by designing a series of filtration experiments, measuring the flux at the end of each filtration step at a given temperature and pressure. R_{cp} term was obtained from the difference between the final feed flux and the pure water flux after rinse twice using 40 mL of ultrapure water under stirring at 300 rpm. R_{pr} was calculated after backwash when the remaining resistance is R_t-R_{cp}-R_{pr}, R_{cr} was obtained after chemical cleaning from the residual resistance R_t-R_{cp}-R_{pr}-R_{cr}, and finally R_{if} was back-calculated from the difference between R_t and the sum of resistances calculated so far, i.e., R_m, R_t, R_{cp}, R_{pr}, and R_{cr}.

2.3 Results and Discussion

2.3.1 Filtration of PEG-Containing Solution

Normalized fluxes (J/J_0) through a ceramic membrane in Figure 2.3(a) fit well to the combined model (solid lines), suggesting that ceramic membrane fouling and flux behavior can be well represented by the model that accounts for initial pore blocking followed by cake formation in polymeric membrane filtration. The parameters obtained via non-linear optimization of selected flux data using Equations (2.2) to (2.4) are summarized in Table 2.3.

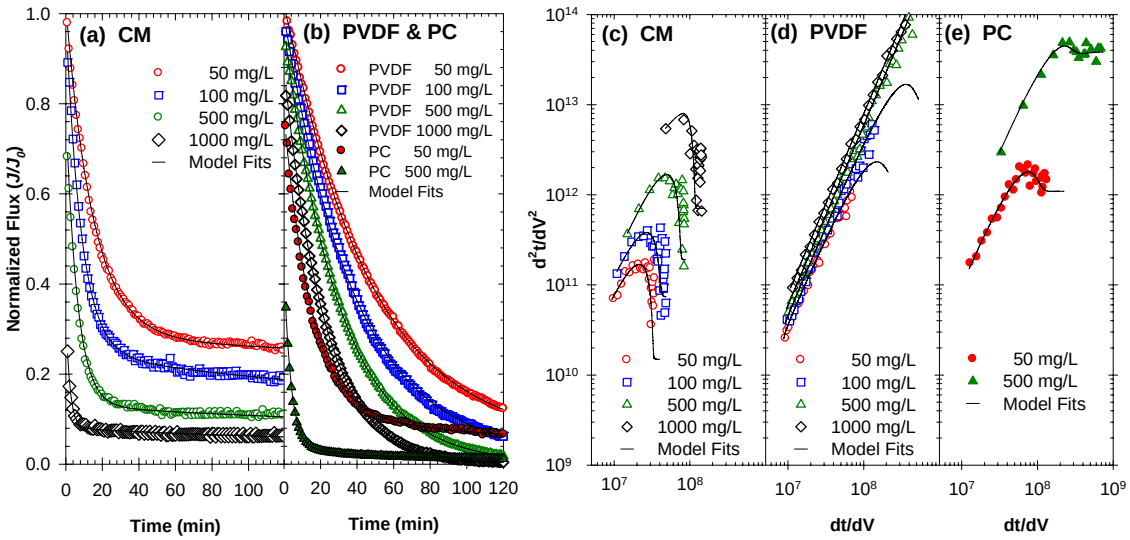

Figure 2.3 Effects of feed concentration and membrane materials on the flux decline during ceramic and polymeric membrane filtrations of PEG solutions. (a) Normalized flux (J/J_0) and the combined pore blockage-cake filtration model fits (Equations (2.2) – (2.4)). (b) Filtration power law plots (d^2t/dV^2 vs. dt/dV) using Equations (2.6) – (2.8). Solid lines are model fits using parameters obtained from the non-linear optimization.

Table 2.3 Model parameters for the effect of the feed concentration on the stirred PEG filtration.

Concn. (mg/L)	J_{wo} (LMH)	R_m (m^{-1})	R_{po} (m^{-1})	k_1	k_2	α (m^2/kg)	$f'R'$ (m/kg)	R^2	SSR
50	274.43	1.939E+11	5.15 E+11	0.0676	0.00167	799.1	2.545 E+13	0.9993	0.00422
100	252.55	2.106E+11	5.78 E+11	0.121	0.00694	286.9	2.505 E+13	0.9982	0.00578
500	233.93	2.274E+11	9.83 E+11	0.161	0.00479	76.16	8.014 E+12	0.9980	0.00436
1,000	261.41	2.035E+11	6.26 E+11	0.456	0.00679	1077	2.758 E+13	0.9798	0.00315

The flux curves were characterized by initial sharp decrease followed by gradual decrease and the plateau at the later phase, suggesting potential fouling mechanism shift during the course of filtration. As the concentration of PEG increased from 50 mg/L to 100 mg/L, the permeate flux declined faster. The flux behaviors and overall trend were similar to those reported with polymeric membranes filtering similar suspensions (Bhattacharjee et al., 1996; Ghose et al., 2000). For the same concentration of PEG, for example 500 mg/L, the normalized permeate flux through ceramic membrane was in between those of PVDF and PC membranes (Figure 2.3(b)). Direct comparison of absolute values of permeate flux might not be valid considering the difference in clean water flux that results from difference in membrane active layer thickness and porosity. The ceramic membrane with an active layer of 27.0±1.7 μm measured by SEM in this study and a porosity of 23.6% calculated from the clean water flux, showed lower clean water flux. In comparison, the PVDF membrane has much higher porosity (75%) although the active layer is thicker (100-125 μm), and the PC membrane has much thinner skin layer (25-30 μm) despite low porosity (13.8%).

However, clearly observed was higher normalized flux by ceramic membranes at the latter phase of filtration when the flux reached the plateau (Ho and Zydney, 2000; Taniguchi et al., 2003). Solute rejections (results not shown) were low and did not provide meaningful information to discern fouling characteristics between these membranes (Nguyen et al., 2010; Taniguchi et al., 2003). Flux data shown in Figure 2.3(a) can be alternatively plotted as total resistance (R_t) vs. filtration time (t) (Figure 2.4), which also fit well to the model.

These flux data were replotted as d^2t/dV^2 vs. dt/dV based on the following equation (Yuan et al., 2002; Yuan and Zydney, 2000) to further examine the shift in fouling mechanisms from initial pore blockage to cake filtration during the filtration:

$$\frac{d^2t}{dV^2} = k\left(\frac{dt}{dV}\right)^n \tag{2.6}$$

where k = fouling coefficient; V= cumulative volume [m^3]; and n = filtration constant (n = 0, 1, 1.5, and 2 represent cake filtration, intermediate, standard, and complete pore blocking modes, respectively) (Hermans and Bredee, 1936; Hermia, 1982). The derivatives for both experimental flux data and the model fits were calculated as follows (Yuan and Zydney, 2000):

$$\frac{dt}{dV} = \frac{1}{JA} \tag{2.7}$$

$$\frac{d^2t}{dV^2} = -\frac{1}{J^3A^2}\frac{dJ}{dt} = \frac{1}{A}\frac{d(1/J)}{dV} \tag{2.8}$$

where A = membrane surface area [m^2].

A few features are noteworthy in Figure 2.3(c). First, the plots for higher feed concentrations appeared at larger values of both dt/dV and d^2t/dV^2, resulting from the lower initial flux measured during the initial phase of filtration yielded by the fast declining flux when the PEG loading was higher (Duclos-Orsello et al., 2006). Second,

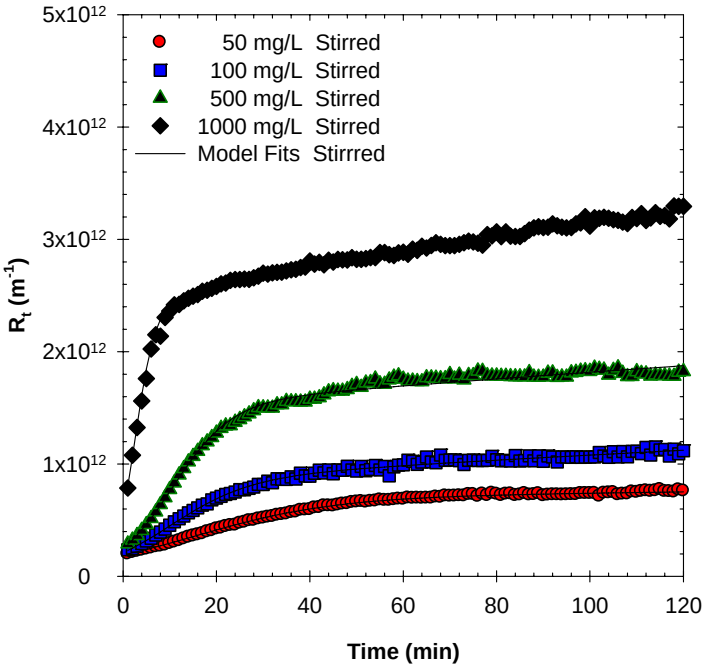

Figure 2.4 Effect of feed concentration on the total resistance (R_t) during the filtration of PEG solutions at various feed loadings using ceramic membranes. Solid and dotted lines are the model fits obtained using the parameters obtained from the non-linear optimization using the combined pore blockage-cake filtration model (Equations (2.2) – (2.4)).

negative slopes appeared after the maxima, which is counterintuitive to the mechanistic interpretation and is not clearly understood so far but is not uncommon (Duclos-Orsello et al., 2006). The second derivative (d^2t/dV^2) in Equation (2.8) is the product of $1/J^3$ and dJ/dt (Yuan and Zydney, 2000). Therefore, the decrease in d^2t/dV^2 implies the reduction in flux decline (dJ/dt), and d^2t/dV^2 would decrease when dJ/dt decreases faster than J itself. For example, a similar phenomenon was observed when the ratio of the resistance exerted by the initial deposit of foulant (i.e., PEG) to the intrinsic membrane resistance, (R_{p0}/R_m), was relatively small (Duclos-Orsello et al., 2006). As the negative slopes always appeared after d^2t/dV^2 reached a peak followed by a zero slope (Duclos-Orsello et al., 2006; Ho and Zydney, 2000; Taniguchi et al., 2003), it is believed that the negative slopes are caused by the transition of filtration mechanism to cake filtration. Finally, the transitions were smooth, continuous and concave down. Such transitions were observed in the past studies as either smooth and continuous (Ho and Zydney, 2000; Taniguchi et al., 2003), or not smooth and continuous (Hwang et al., 2007). Our results were consistent with the findings in previous works (Taniguchi et al., 2003; Yuan et al., 2002), wherein multiple mechanisms are involved during the transitions.

All the curves in Figure 2.3(c) were characterized by initial slopes close to 1.5 to 2, which indicate the dominance of standard or complete blocking mechanisms for the early flux decline. It is noteworthy that the pore blocking occurred during the initial phase of filtration, even though PEG particles are generally smaller than the pore size (Figure 2.5). Similar results were observed in the NOM filtration with 300, 500 and 1000 kDa membranes and the microfiltration of BSA giving slopes close to 2 (Ho and Zydney, 2000; Taniguchi et al., 2003).

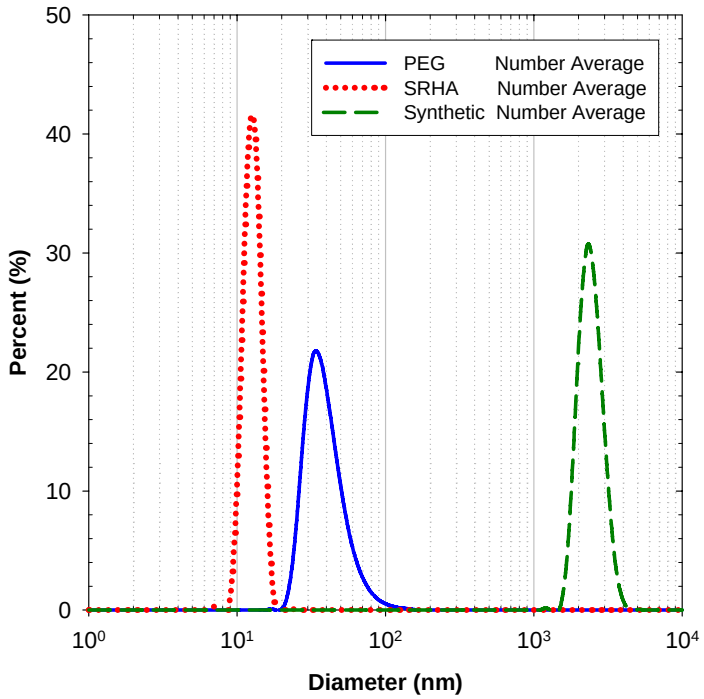

Figure 2.5 Particle size distributions of PEG, SRHA and synthetic river water.

Overall, it is noteworthy that fast transition to cake filtration, with pore blocking dominance only for very short period during the early phase of filtration, was characteristic of ceramic membrane filtration, when compared to polymeric membranes (Figures 2.3(d) and 3(e)). In the case of PVDF, such transitions were hardly observed and most flux decline was attributed to blocking mechanisms.

2.3.2 Filtration of SRHA-Containing Solution

Figure 2.6 shows the results of parallel filtration experiments performed using SRHA (50 and 100 mg/L) with ceramic and polymeric membranes. The flux data and the filtration power law plots were again in excellent agreement with the combined model. Flux decline was faster and greater for all types of membranes as SRHA concentration increased from 50 to 100 mg/L (Figure 2.6(a)). The normalized fluxes were higher with ceramic membranes than polymeric membranes at different concentrations, indicating less fouling by SRHA with the former, although direct comparison is not valid as discussed above. Noteworthy is the difference in mechanism transition during the course of filtration as shown in Figure 2.6(b), where the initial pore blocking was nearly absent with earlier transition to cake filtration in the ceramic membrane as indicated by the curve maxima and negative slopes and clearly different from polymeric membranes. This is in particularly interesting because ceramic membrane flux was still in the decline phase (*i.e.*, far from reaching plateau), since the onset of negative slope and occurrence of cake filtration mode are typically observed after the flux curve passes the initial fast decline. Alternatively, this analysis suggests that ceramic membrane filtration of SRHA seems less governed by blocking mechanisms with earlier development of cake formation compared to polymeric membranes.

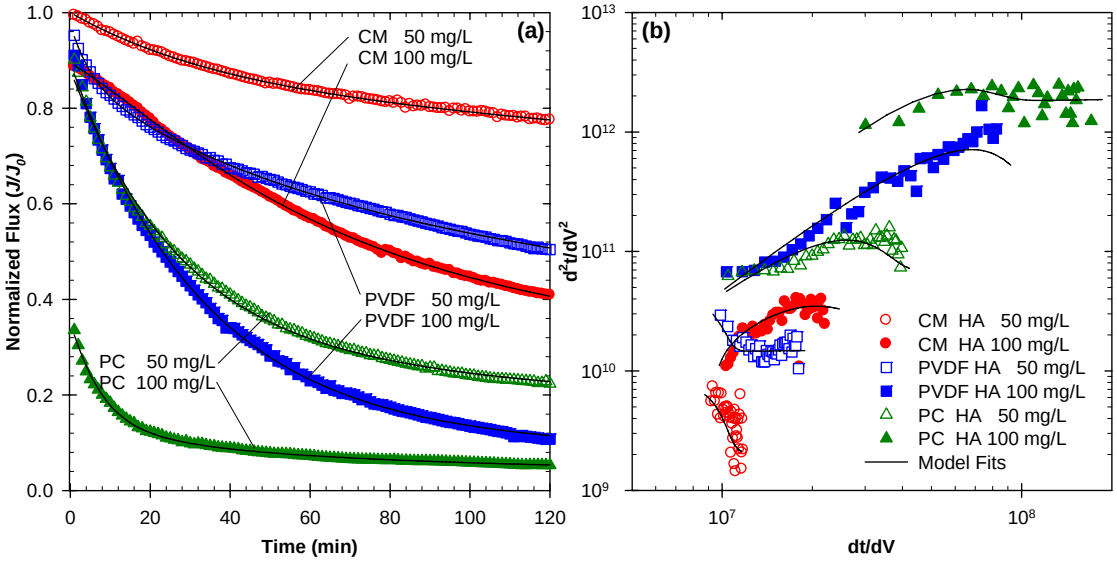

Figure 2.6 Ceramic and polymeric membrane filtrations of SRHA solutions. (a) Normalized flux (J/J_0) and the combined pore blockage-cake filtration model fits (Equations (2.2) – (2.4)). (b) Filtration power law plots using Equations (2.6) – (2.8). Solid lines are model fits using parameters obtained from the non-linear optimization.

Selected experiments were performed without feed stirring, which has been the condition in some past studies performed with polymeric membranes (Bhattacharjee and Datta, 2003; Taniguchi et al., 2003), and the results are shown in Figure 2.7. The fluxes were generally lower than those with stirring, indicating enhanced concentration polarization and greater membrane fouling in the absence of stirring. Filtration power law analysis suggests that pore blocking mechanism extends to later phase of filtration without stirring; for instance, pore blocking phase was not observed at 50 mg/L with stirring (Figure 2.6(b)) but observed without stirring for ceramic and PVDF membranes (Figure 2.7).

For the PC membrane, the pore blocking mode was extended even further. At 100 mg/L, pore blocking accounted for a longer period of filtration with ceramic and PVDF membranes. Therefore, it is postulated that the higher concentration near the membrane surface, either by the increased feed concentration or the denser concentration polarization layer, would contribute significantly not only to the cake layer growth but also to the aggravated pore blocking (Ho and Zydney, 2000; Taniguchi et al., 2003). Consistent with the filtration of PEG solutions, SRHA rejections were very low (<5%) except only at the initial phase of filtration where the adsorption of solutes takes place most (Howe and Clark, 2002; Nguyen et al., 2010; Taniguchi et al., 2003).

2.3.3 Resistance-In-Series Model Analysis

Figure 2.8(a) shows results of resistance-in-series model analysis for the PEG solution filtration. Since the membranes had pore sizes of 0.2 or 0.22 μm, the intrinsic

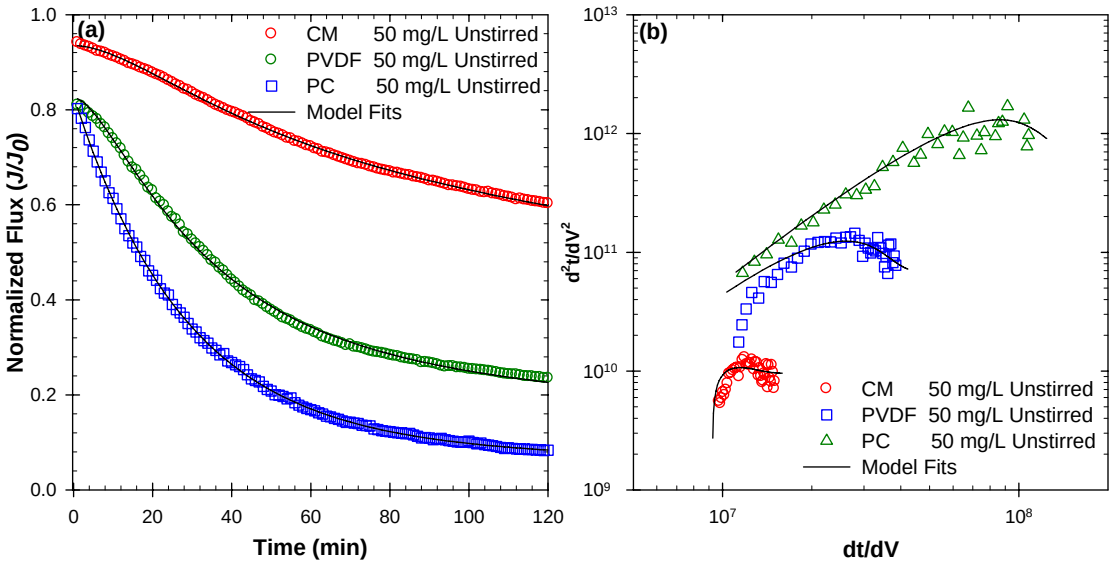

Figure 2.7 Unstirred filtration of SRHA solutions using ceramic and polymeric membranes. (a) Normalized flux (J/J_0) and model fits using the combined pore blockage-cake filtration model (Equations (2.2) – (2.4)). (b) Filtration power law plots (d^2t/dV^2 vs. dt/dV) using Equations (2.6) – (2.8). Solid lines are model fits using parameters obtained from the non-linear optimization.

membrane resistance, R_m, did not account for a large portion of the total resistance. The initial pure water flux was smaller for the ceramic membrane, which resulted in the relatively larger contribution of R_m to R_t, compared to that for polymeric membranes. In all cases, R_{cp} contributed to a significant portion of the resistance such that a large portion of flux would be recovered by simply replacing the feed with clean water. Physically removable resistance, R_{pr}, also contributed significantly to the ceramic and PVDF membrane.

The difference between ceramic and polymeric membranes was evident when the relative contribution of the resistances was examined. First, chemically removable resistance, R_{cr}, was much less for the ceramic membrane, while it constituted a significant portion of R_t for PVDF and PC membranes. For the PC membrane, R_{cr} was the major contributor to the membrane fouling. Second, irreversible fouling, R_{if}, was negligible for the ceramic membrane; the original pure water flux was almost fully recovered after chemical cleaning. In contrast, R_{if} was significant in particular with PC membrane, which would be detrimental to long term operation. It should be noted that it was possible to apply a harsher chemical cleaning condition to ceramic membrane than polymeric membranes. However, such a difference most likely resulted from stronger organic foulants adsorption to polymeric membrane surface via hydrophobic interactions compared to ceramic membranes. Even though PVDF and PC membranes are known to be relatively hydrophilic, the contact angle measurement showed that these materials are less hydrophilic than the ceramic surface (Table 2.1). Overall, the above results suggest that physical cleaning such as rinse and backwash would be much more effective for the

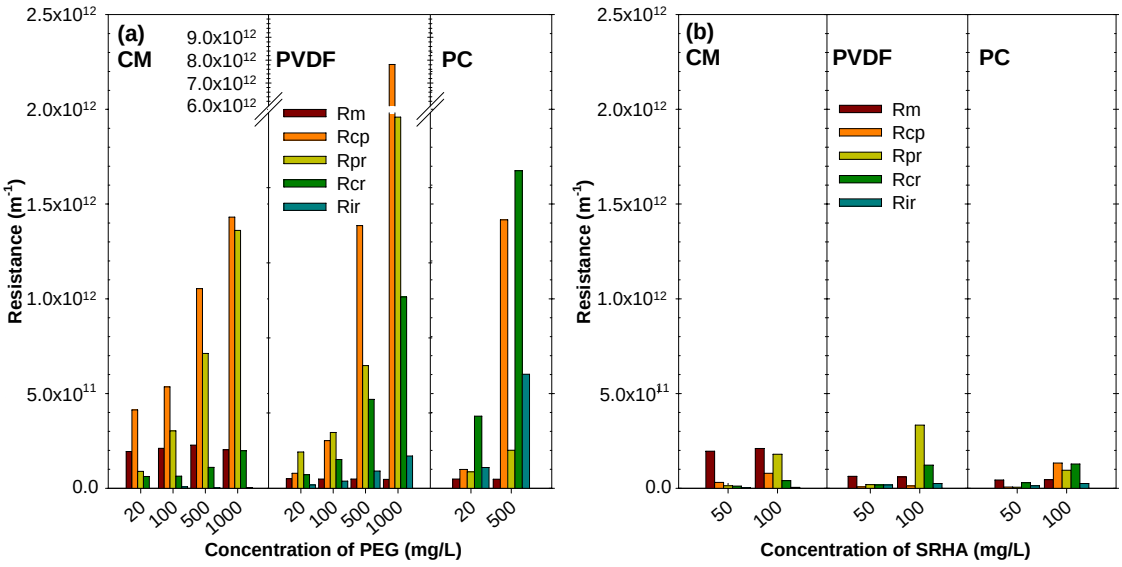

Figure 2.8 Resistance-in-series model analysis for the filtration of (a) PEG and (b) SRHA solutions by ceramic and polymeric membranes.

ceramic membrane than polymeric membranes, which is critical information for the application of the ceramic membrane for water treatment.

All the resistance terms increased monotonically as the feed concentration increased for all three membranes (Figure 2.8). The higher organic matter loading and the enhanced concentration polarization would contribute to greater cake growth as well as increased pore blocking. At higher feed concentration, the initial slope in the d^2t/dV^2 vs. dt/dV plot gradually changed from 2 to near 1.5 (Figure 2.3(c)), suggesting that the relative significance of the deposition in the inner pores (*i.e.*, standard blocking) might become more significant when the feed concentration increased. However, the complete blocking mechanism should not be excluded because the slope change might simply mean a more dominant role of standard blocking (Cogan and Chellam, 2009). It is also noteworthy that a greater blocking was followed by a more rapid transition to cake filtration.

It should be noted that the definition of each resistance term might not directly correlate to fouling mechanisms defined in filtration models. For example, the fouling from pore blocking might lead not only to R_{cr} and R_{if} but also to R_{pr} which can be physically removed by backwash. Likewise, cake formation in filtration model might contribute to fouling that cannot be readily removed by physical means. Nonetheless, the comparative analysis of these two models collectively suggests earlier transition to cake formation and dominating role of cake filtration throughout most of the filtration duration in case of the ceramic membrane.

The parallel results from the filtration of SRHA are shown in Figure 2.8(b). Compared to the filtration of PEG solutions, the resistances caused by SRHA were

smaller due to the smaller size than that of PEG (Figure 2.5), which made R_m more significantly contributing to R_t. Nonetheless, the increasing trend of each resistance term with the increase of concentration was consistent with that for PEG. Again, the physically removable resistances (R_{cp} and R_{pr}) constituted the most of R_t for ceramic membranes, whereas R_{cr} accounted for a much greater portion for polymeric membranes. Also consistent with PEG results, R_{cr} and R_{if} were much larger with polymeric membranes than the ceramic membrane, suggesting more favorable interaction between SRHA and polymeric surfaces. When physical cleaning alone is applied, ceramic membranes would recover 76 and 85 % of reduced flux due to fouling for 50 and 100 mg /L SRHA solution filtration, while only 43 and 70 % would be recovered for PVDF and 21 and 60 % for PC membranes, respectively, once again suggesting the critical operational advantage of the ceramic membrane.

2.3.4 Filtration of Synthetic River Water

Figure 2.9(a) shows the flux decline curves for the filtration of a synthetic river water. The flux of the ceramic membrane showed a rapid decrease followed by a gradual slowing of the flux. In contrast, flux curves for both polymeric membranes kept decreasing over the whole range of the filtration. These patterns were the same as in the filtration of PEG (Figure 2.3) and SRHA (Figure 2.6). As shown in Figure 2.9(b), the shift of mechanism to cake filtration from the onset of the filtration was evident for the ceramic membrane, while initial pore blocking mechanism followed by later transition to cake filtration mode was apparent with polymeric membranes. These results were also

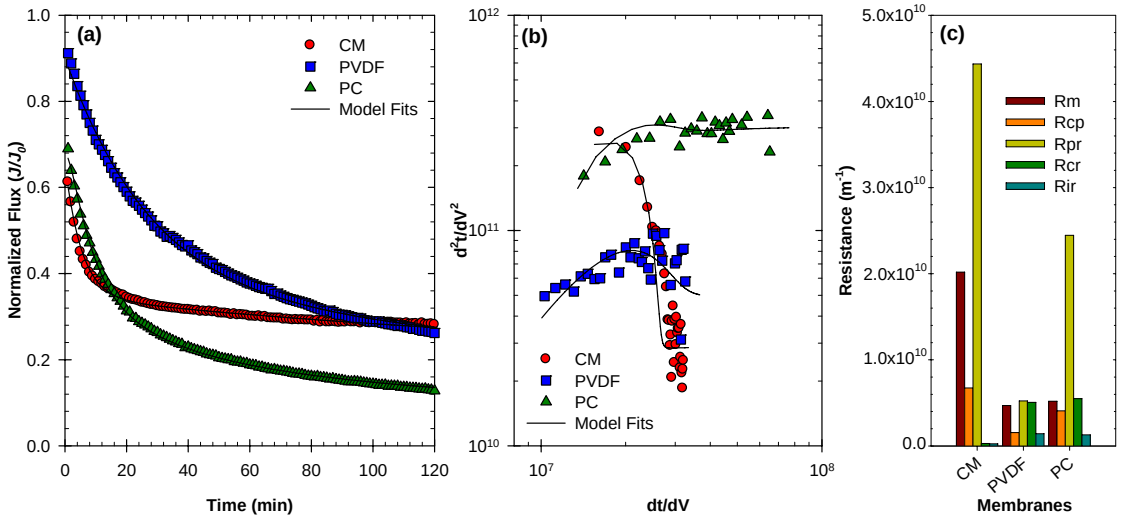

Figure 2.9 Fouling behavior during the filtration of a synthetic river water. (a) Normalized flux (J/J_0) and the combined pore blockage-cake filtration model fit (Equations (2.2) – (2.4)). (b) Filtration power law plots using Equations (2.6) – (2.8). (c) Resistance-in-series model analysis.

consistent with the filtration results for PEG and SRHA. The resistance-in-series model analysis results (Figure 2.9(c)) also confirmed that R_{pr} was dominant in the ceramic membrane fouling. In the case of PVDF membrane, R_{pr} and R_{cr} were mostly responsible for the fouling, with R_{if} noticeable. There was a significant level of R_{pr} for the PC membrane but the other contributing resistances, R_{cr} and R_{if}, were also responsible for R_t. Collectively, ceramic membrane filtration was characterized by earlier occurrence of cake formation which accounted for the large portion of overall membrane fouling, whereas polymeric membrane filtrations would be strongly influenced by blocking mechanisms and the resulting presence of fouling components that are not readily removed by physical cleaning methods.

2.3.5 Comparison of Fouling Models

Analysis presented in Figure 2.10 confirms that ceramic membrane fouling can be mainly described by cake formation. In the conventional cake filtration theory, the parabolic law is used to identify the fouling characteristic (Schippers and Verdouw, 1980). The rate of filtration is expressed as in Equation (2.9), and when integrated, the relationship between t/V vs. V is obtained as shown in Equation (2.10).

$$\frac{dV}{dt} = \frac{\Delta p}{\mu(R_c + R_m)} = \frac{\Delta p}{\mu(k_{RC}\frac{V}{A} + R_m)} \tag{2.9}$$

$$\frac{t}{V} = \frac{\mu R_m}{\Delta p} + \frac{\mu k_{RC}}{2A\Delta p}V \tag{2.10}$$

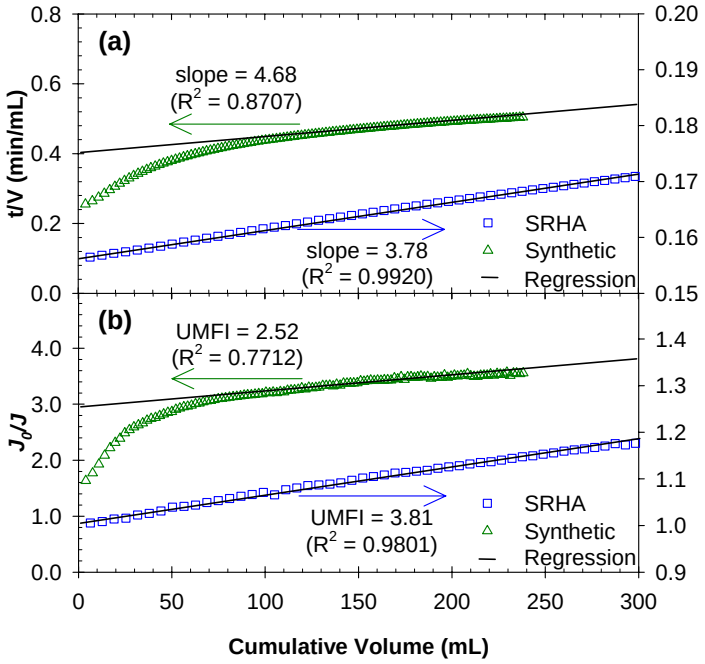

Figure 2.10 Analysis of fouling mechanisms for the ceramic membrane filtration of SRHA (50 mg/L) and a synthetic river water using the (a) conventional cake filtration and (b) unified membrane fouling index (UMFI) model.

where R_c = cake resistance [m^{-1}]; and k_{RC} = a proportionality coefficient between R_c and V/A [m^{-2}]. The cake filtration model suggests that the linearity exists when t/V is plotted vs. V (Figure 2.10(a)).

When cake filtration is the dominant mechanism, the UMFI can be defined as follows (Huang et al., 2008; Nguyen et al., 2010):

$$\frac{J_0}{J} = 1 + (UMFI)V_s \tag{2.11}$$

where J_0 = pure water flux of clean membrane [m/s]; V_s = cumulative permeate volume per unit membrane surface area [m]; and $UMFI$ = a measure of total fouling [m^{-1}]. Therefore, the UMFI model suggests the linearity between J_0/J plot vs. V (Huang et al., 2008; Nguyen et al., 2010; Schippers and Verdouw, 1980). When the filtration data were applied to both models, a linear relationship was found between t/V vs. V (Figure 2.10(a)) and J_0/J vs. V (Figure 2.10(b)), respectively. The linear correlation became more evident as the filtration time or cumulative volume increased. Although these models have been exclusively applied for polymeric membrane filtration in the past, our results wherein the data fit to the linear models suggest that these widely used models based on cake filtration might provide an adequate approach to mathematically represent ceramic membrane fouling by NOM during surface water treatment.

2.4 Conclusions

The present study is one of the first successful attempts to apply filtration and fouling models which have been applied to polymeric membranes to analyze the flux and fouling characteristics of ceramic microfiltration membranes. Considering that these models have been extensively studied for polymeric membranes, this study provides a foundation for further application and enhancement of the models for this emerging technology. More importantly, the results presented herein suggest some critical differences between ceramic and polymeric membrane filtration. Ceramic membranes appeared to have a much less irreversible fouling than polymeric membranes. This was due to weaker interaction of the foulant with ceramic membranes than with polymeric membranes, presumably due to the more hydrophilic nature of the ceramic membranes. The majority of total resistance in ceramic membrane filtration of PEG, SRHA solutions and a synthetic river water could be removed by physical cleaning methods, and irreversible fouling was negligible for all types of feed solutions tested. These results are noteworthy when compared to the polymeric membranes in which irreversible fouling is one of the major reasons for process efficiency deterioration during long term operation. Fouling in polymeric membranes can only be removed by chemical cleaning (R_{cr}) or sometimes cannot be even removed by chemical cleaning (R_{if}). Presence of such fouling requires extensive cleaning which requires increased process downtime as well as potential damage to membrane integrity.

Compared to the vast number of reports dealing with polymeric membrane filtration of surface waters, the study on ceramic membrane filtration as well as full-scale application in water treatment is only at an embryonic stage. Additional research is necessary to understand many factors that affect the filtration behavior and fouling

mechanisms of ceramic membranes based on the understanding of polymeric counterparts. Effects of water quality parameters (i.e., types and concentration of NOM, concentration of multivalent ions, ionic strength, pH, presence of colloidal matter), types of ceramic membranes, and pretreatment processes such as coagulation are of particular importance to develop guidelines for the application of this emerging technology and are the subjects of our current study. More in-depth study on surface properties of ceramic membranes in comparison to polymeric membranes and their impact on interactions with foulant are also required.

CHAPTER 3

DIFFERENTIAL NATURAL ORGANIC MATTER FOULING OF CERAMIC VERSUS POLYMERIC ULTRAFILTRATION MEMBRANES

3.1 Introduction

Ceramic ultrafiltration membranes are drawing an increasing attention in drinking water treatment sectors as a cost-effective alternative to traditional polymeric counterparts (Freeman and Shorney-Darby, 2011). This emerging technology takes advantage of superior chemical resistivity that enables aggressive chemical cleaning and structural rigidity that alleviates problems associated with repetitive testing, repair, and replacement which are typical of polymeric membranes. However, virtually little is known about the characteristics of ceramic membrane fouling by natural organic matter (NOM), preventing a rapid translation into full-scale surface water treatment practices (Freeman and Shorney-Darby, 2011; Loi-Brugger et al., 2006). Insights on the membrane fouling by NOM are critical for design and operation of membrane processes (Howe and Clark, 2002; Lee et al., 2001), but they are limited to polymeric membranes.

Past studies on polymeric membranes suggest that various factors such as solution chemistry, membrane surface properties, and operating conditions influence the membrane fouling by NOM (Childress and Elimelech, 1996; Evans et al., 2008). One can conjecture that some of these factors have similar effects on ceramic membrane fouling,

as the filtration in both cases is based on the same physical mechanism of size exclusion, Donnan exclusion, and water permeation through pores. Alternatively, different fouling behaviors might result, if the fouling mechanism were governed by differences in the membrane surface properties. Of particular interest is a potentially significant difference in the interaction between solutes and membrane surface, which has been frequently correlated to NOM fouling characteristics even among polymeric membranes. These interactions between solutes/particles and membrane surface have been investigated via surface potential measurement, atomic force microscopy (AFM) analysis, and contact angle measurements in past studies (Hong and Elimelech, 1997; Lee et al., 2004; Li and Elimelech, 2004).

The objective of this study is to comparatively examine ceramic versus polymeric membrane fouling under varying water quality conditions. Feed water pH, divalent ion concentration, and ionic strength on the membrane fouling (Liang et al., 2008; Yuan and Zydney, 1999) are of primary concern, as they are known to affect the interaction between solutes/particles and membrane surface (Chiu and James, 2007; de la Casa et al., 2007) due to acid/base speciation, electrical double layer compressions (Li and Fu, 2002; Liang et al., 2008), charge screening (Ghosh and Schnitzer, 1980; Hering and Morel, 1988), complex formation (Gao et al., 2012; Li and Elimelech, 2004), and aggregation and deposition (Costa and de Pinho, 2005; Hong and Elimelech, 1997). Ceramic membranes are made of metal oxides which are generally more hydrophilic than most polymeric materials and may assume different surface potential that originates from different surface functional moieties. Therefore, it is hypothesized that the impact of water quality on NOM fouling is different between ceramic and polymeric membranes.

To test this hypothesis, filtration experiments were performed and fouling characteristics were quantitatively analyzed using a resistance-in-series model. A method of visualizing fouling using a confocal laser scanning microscopy (CLSM), which was recently employed for biofouling visualization (Meng et al., 2007; Sun et al., 2011), was newly applied to analyze fouling by colloidal foulants using carboxlyated quantum dots (QDs) as a surrogate. AFM analysis was performed for the first time to probe the interactive forces between a carboxylated latex particles and the ceramic membrane surface. Results point to critical similarities and dissimilarities between ceramic and polymeric membranes, and advantage of ceramic materials for surface water treatment application, particularly in terms of the reversibility of fouling and the effectiveness of cleaning process.

3.2 Experimental

3.2.1 Materials

A disc-type ceramic ultrafiltration membrane, CM50 with a molecular weight cut off (MWCO) of 50 kDa (Sterlitech, Kent, WA), was selected as a representative ceramic membrane. The CM50 has a ZrO_2 surface with an Al_2O_3-TiO_2-ZrO_2 support layer, a thickness of 2.5 mm, and a diameter of 47 mm, and is resistant to temperature up to 350 °C, pressure up to 4 bars, and pH of 0 to 14. Two types of polymeric membranes with MWCO of 100 kDa made of polyethersulfone (PES100) and regenerated cellulose (RC100) (Millipore, Bedford, MA) were comparatively tested. The PES100 membrane

has a polyethersulfone surface with a nonwoven polyolefin support layer and a thickness of 280 μm, and RC100 has a regenerated cellulose surface with a nonwoven polypropylene layer and a thickness of 230 μm. All membrane samples had an effective surface area of 13.9 cm^2 for testing. Virgin ceramic membranes were chemically cleaned and wetted by soaking in ultrapure water (resistivity > 18.2 MΩ) for 30 min or by filtering 300 mL of ultrapure water before use, and PES100 and RC100 by soaking in ultrapure water for 2 h, while replacing ultrapure water at least three times.

Feed solutions contained Suwannee River humic acid (SRHA) standard (International Humic Substances Society, St. Paul, MN) at 20 mg/L as a model natural organic foulant. Ionic strength and calcium ion concentrations were adjusted using NaCl and $CaCl_2$. Carboxylate modified latex (CML) particles with an average diameter of 4 μm (Interfacial Dynamics, Portland, OR) and water soluble CdSe/ZnS red QDs with surface carboxyl groups (NN-Labs, Fayetteville, AZ) with an average diameter of 8 nm were also used as model foulants in selected experiments. The QDs have a CdSe/ZnS core/shell structure, and the terminal carboxyl groups of an organic surface layer (mercaptoundecanoic acid) render the quantum dots water-soluble. The emission peak was at 622-623 nm.

3.2.2 Filtration Experiments

Filtration with flat ceramic (CM50) and polymeric (PES100 and RC100) membranes was conducted using dead-end filtration cells (HP4750, Sterlitech, Kent, WA). The bottom housing of one of the cells was modified to hold a thicker ceramic

membrane. Pressure was maintained at 14.7 psi by nitrogen gas and monitored by a pressure transducer (Omegadyne, PX319-050G5V, Sunbury, OH). Fluxes were measured as the cumulative mass of permeate collected on a digital balance (Sartorius, ED623S, Goettingen, Germany), connected to a computer via an RS-232 interface. Stirring was provided at 200 rpm, and temperature (23 ± 1°C) and pH were monitored before and after each filtration step. Detailed procedures for pure water filtration, feed solution filtration, rinsing, backwashing, and chemical cleaning, were identical as in the previous report (Lee et al., 2013). Backwashing was conducted at 22.1 psi, 1.5 times the operating pressure, and chemical cleaning by soaking fouled polymeric membranes in a 0.1 N NaOH at room temperature overnight or fouled ceramic membranes in 0.1 N NaOH at 85 °C for 15 min followed by acid cleaning in 0.375 % H_3PO_4 at 50 °C for 15 min. After each cleaning step, pure water flux was measured.

3.2.3 Analyses

SRHA concentrations were measured using a TOC-Vw Analyzer (Shimadzu, Columbia, MD) and a UV/VIS spectrofluorophotometer (RF-5031PC, Shimadzu, Japan). Contact angles were measured for clean and fouled membranes by a sessile drop method using a goniometer (Ramé-Hart Model 250, Succasunna, NJ). A 2 μL of Milli-Q water drop was deposited on a membrane surface, and the contact angles were measured consistently after 5 s. Fifteen measurements (five for each of three coupons) were averaged. Fluorescence microscopy images were obtained using a CLSM (Eclipse 90*i*, Nikon Instruments, Melville, NY) at an excitation of 488 nm. Zeta potentials were

obtained using Zetasizer Nano ZS (Malvern, UK), for which the surface layer of ceramic membranes were ground using 600-mesh sand paper and equilibrated in Milli-Q water for 2 h. The size of the QDs was measured using a transmission electron microscope (TEM, Hitachi, H9500, Japan).

An AFM (Veeco Metrology Group, Dimension 3100, Santa Barbara, CA) analysis was performed in a tapping mode using a modified probe (a tipless SiN cantilever loaded with a CML particle, Bruker AFM Probes, CA). The ionic strength was adjusted identical to relevant solution chemistry, and fifteen measurements were conducted (five for each of three sampling spots). The normalized adhesion force, F/R, (Equation 3.1) between the particle and the membrane surface was obtained from the deflection of a cantilever (Li and Elimelech, 2004; Stawikowska and Livingston, 2013).

$$F/R = 2\pi W = -H/6Z^2 \tag{3.1}$$

where F = interaction force between a CML particle and membrane surface [N]; R = radius of the CML particle [m]; W = interaction energy per unit area between a particle and membrane surface [J/m^2]; H = Hamaker constant [J]; and Z = the total deflection or the sum of the cantilever deflection and the piezo position [m] (Li and Elimelech, 2004; Stawikowska and Livingston, 2013; Zhang et al., 2011).

3.2.4 Model Analyses

Rejections at the end of filtration were calculated as (1 – permeate concentration/feed concentration) × 100 (%). The following resistance-in-series model was used to quantify each contributing resistance as detailed in our previous work (Lee et al., 2013):

$$J = \frac{\Delta p}{\mu R_t} = \frac{\Delta p}{\mu\left(R_m + R_{cp} + R_{pr} + R_{cr} + R_{if}\right)} \quad (2)$$

where J = flux [m/s]; Δp = applied transmembrane pressure [Pa]; R_t = total resistance; R_m = intrinsic membrane resistance (pure water resistance) [m^{-1}]; R_{cp} = resistance removable by rinsing (concentration polarization exerted by the feed solution and removed by rinsing) [m^{-1}]; R_{pr} = resistance removable by backwashing (cake formed on the surface or in the pore, not removable by rinsing but removable by backwashing) [m^{-1}]; R_{cr} = chemically reversible resistance (internal fouling, a portion of the total resistance removable only by chemical cleaning) [m^{-1}]; and R_{if} = chemically irreversible resistance (residual resistance after chemical cleaning) [m^{-1}].

Each resistance was obtained by designing a series of filtration experiments, measuring the flux at the end of each filtration step at a given temperature and pressure. R_{cp} term was obtained from the difference between the final feed flux and the pure water flux after rinse twice using 50 mL of ultrapure water under stirring at 200 rpm. R_{pr} was calculated after backwashing at 1.5 times the operating pressure when the remaining resistance is R_t-R_{cp}-R_{pr}, R_{cr} was obtained after chemical cleaning from the residual resistance (R_t-R_{cp}-R_{pr}-R_{cr}), and finally R_{if} was back-calculated from the difference between R_t and the sum of resistances calculated so far, i.e., R_m, R_t, R_{cp}, R_{pr}, and R_{cr}.

3.3 Results and Discussion

3.3.1 Effect of pH

Figure 3.1 shows the effect of pH on the filtration of SRHA-containing water by ceramic (CM50) and polymeric (PES100) membranes. As the feed solution pH increased, flux decline gradually mitigated for both CM50 and PES100. Similar trends have been observed in previous studies performed with other polymeric membranes (PVDF (Liang et al., 2008), PES (Yuan and Zydney, 1999), and polysulfone (Li and Fu, 2002)). This pH dependency has been attributed to the fact that, as pH increase, membrane surface becomes more negatively charged, although the isoelectric point (IEP) of PES100 is at around 3 (Chiu and James, 2007; Huisman et al., 1998; Ricq et al., 1997). Consequently, membrane surface is less prone to be fouled by negatively charged humic acids due to greater electrostatic repulsion (de la Casa et al., 2007).

However, the magnitude of pH effect was noticeably different. When the pH changed from 4 to 6, 8 and 10, the normalized fluxes (J/J_0) at the conclusion of filtration increased by 17, 30 and 34 %, respectively, from the flux at pH 4 for CM50 (Figure 3.1(a)), while the increase was 6, 14, and 19 % for PES100 (Figure 3.1(b)). Also noticeable with CM50 was the fact that flux changed significantly when pH changed around 6. This resulted as the IEP of CM50 is at around 6.5 (Figure 3.1(c)) at which point the surface charge of the membrane inverses (Rao et al., 2007; Renger et al., 2006). At lower pHs, the CM50 surface is positively charged and favorably interacts with negatively charged solutes. It is

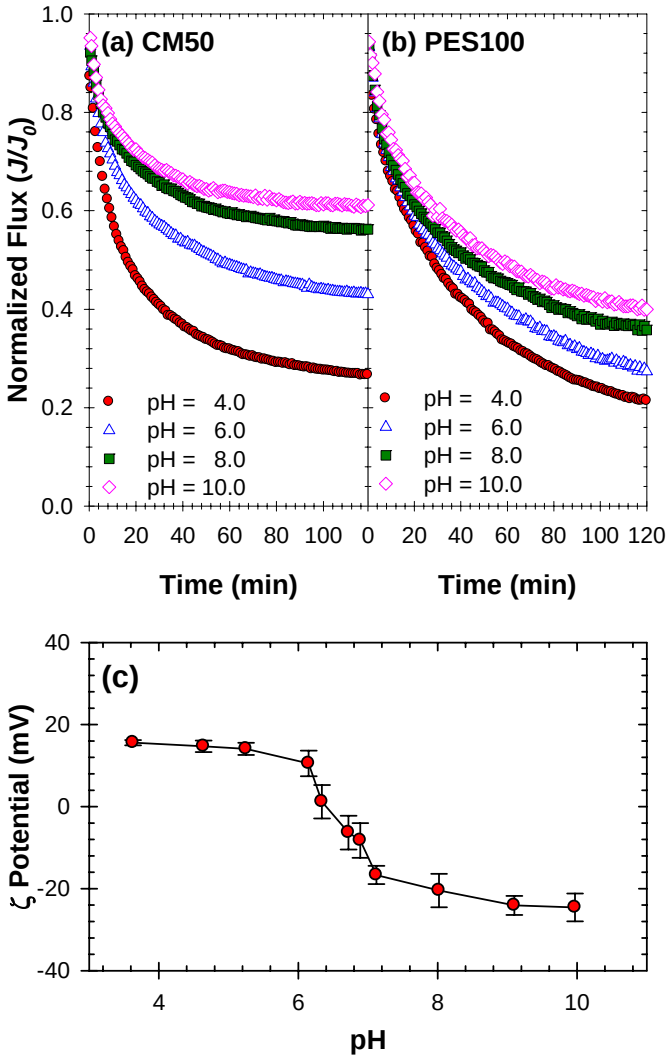

Figure 3.1 The effect of solution pH on the filtration of SRHA with (a) CM50 and (b) PES100 ([SRHA] = 20 mg/L; pH 8.0; stirring at 200 rpm), and (c) the zeta potential of CM50 (ionic strength = 10 mM adjusted by NaCl).

noted that, even at this pH, CM50's flux is no less than that of PES100. As pH increases beyond IEP, electrostatic interaction becomes repulsive and contributes to decreased fouling tendency. At higher pH, pH dependency of CM50 was somewhat comparable to that of PES100, as both membranes are negatively charged.

It is worth further attention that not only the electrostatic interaction but also the amphipathic nature of humic acids would influence the foulant affinity to membrane surfaces. The hydrophobic interaction, in particular, has been identified as one of factors that are responsible for the adsorption onto metal oxide surfaces (Childress and Elimelech, 1996; Elimelech et al., 1994; Kleijn and Norde, 1995), which is further discussed later.

3.3.2 Effect of Calcium Ions

The effect of calcium ions on the fouling also exhibited both similarity and dissimilarity between ceramic and polymeric membranes as shown in Figure 3.2. In all cases, the presence of calcium ions significantly reduced the flux. It is well established that divalent ions adversely affect the membrane fouling by complex formation between negatively charged membrane and negatively charged foulants (Gao et al., 2012; Hering and Morel, 1988; Kim et al., 2009; Li and Elimelech, 2004) as well as double layer compression, charge screening and conformational change in humic substances (Ghosh and Schnitzer, 1980; Hering and Morel, 1988; Hong and Elimelech, 1997). The dependency of J/J_0 of CM50 on calcium concentration was negative exponential (R^2 = 0.988) rather than linear (R^2 = 0.830); i.e., as more calcium was added, flux further

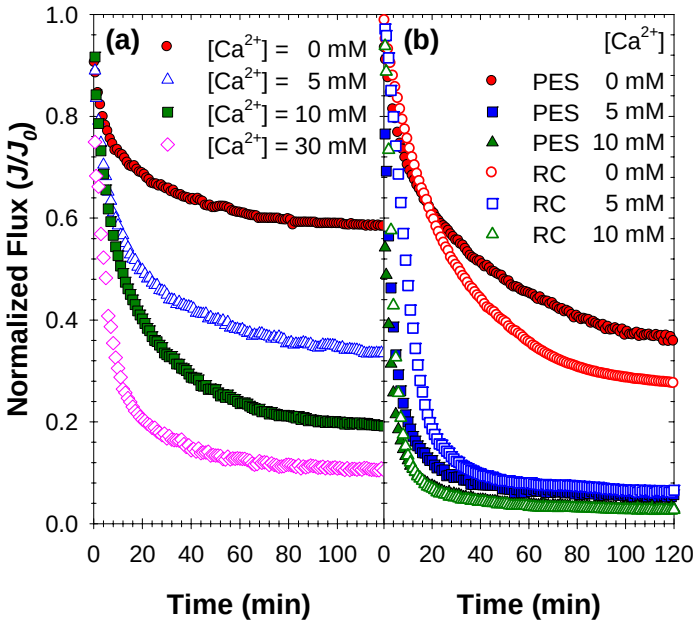

Figure 3.2 The effect of calcium ion concentration on the SRHA fouling with (a) CM50 and (b) PES100 and RC100 membranes. [SRHA] = 20 mg/L; pH 8.0; stirring at 200 rpm.

declined but to a lesser extent. A similar trend was observed with PES100 and RC100 polymeric membranes, and also reported in the literature (e.g., filtration of DOM using PVDF microfiltration membranes) (Hong and Elimelech, 1997; Liang et al., 2008).

It is interesting to note that the calcium ion effect was considerably less with CM50 (Figure 3.2(a) vs. 2(b)). As the concentration of calcium ions increased from 0 to 5, 10 and 30 mM, J/J_0 at the end of the filtration decreased by 43, 67 and 82 % for CM50 (Figure 3.2(a)). In contrast, the reduction in J/J_0 at 5 mM of calcium ions was up to 92 and 90 % for PES100 and RC100, respectively, which was even greater than that with CM50 at the maximum concentration tested (30 mM). The reason why the calcium ion has more negative effect with polymeric membranes is currently not known and further study is required. Regardless, this is a potentially important finding for the application of ceramic membranes for surface water treatment, considering prevalence of divalent ions and associated fouling problems.

3.3.3 Effect of Ionic Strength

The effect of the ionic strength on the filtration of SRHA-containing solution with ceramic and polymeric membranes is shown in Figure 3.3. As the ionic strength increased from 0 to 50 mM, J/J_0 monotonically decreased for CM50 (Figure 3.3(a)). J/J_0 with CM50 at the end of the filtration (120 min) further decreased by 9.3 and 9.6 % at 30 and 50 mM, respectively, compared to J/J_0 at 0 mM. Previous studies reported a similar trend in the NOM filtration; severer fouling and lower fluxes were observed with

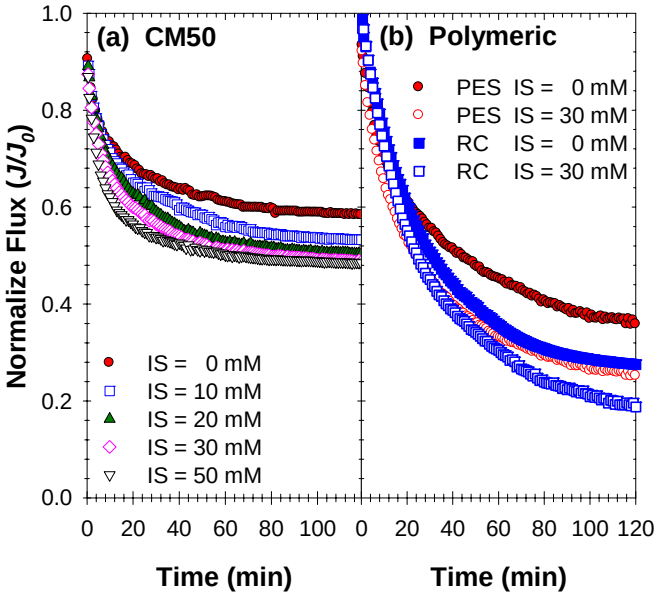

Figure 3.3 The effect to ionic strength on the SRHA fouling with (a) CM50 and (b) PES100 and RC100 membranes. [SRHA] = 20 mg/L; pH 8.0; stirring at 200 rpm.

polymeric membranes (aromatic polyamide thin-film composite(Hong and Elimelech, 1997) or cellulose acetate asymmetric membranes (Costa and de Pinho, 2005)) and ceramic (α-alumina) membranes as well (Nazzal and Wiesner, 1994). This phenomenon has been claimed to result from the decrease in the electrostatic repulsion between organic foulant and the membrane surface caused by electrical double layer compression and charge screening as well as conformational change of humic macromolecules and consequent formation of a denser fouling layer as ionic strength increases (Ghosh and Schnitzer, 1980; Hering and Morel, 1988; Hong and Elimelech, 1997).

It should be noted that there was little difference between ceramic and polymeric membranes in the tendency and the magnitude of the additional decrease due to increased ionic strength; the dependency on the ionic strength showed similarity compared to other solution chemistry parameters such as pH and divalent ions. As shown in Figure 3.3(b), the reduction in J/J_0 with polymeric membranes at 30 mM of ionic strength was 10.7 and 8.8 % for PES100 and RC100, respectively, which was comparable to the result for CM50.

3.3.4 CLSM Analysis

Filtration experimental results presented above consistently suggested that ceramic membranes are less fouled than polymeric membranes under the identical water chemistry. This difference is herein visually examined using CLSM analysis. As membrane was fouled by 20 mg/L NOM at pH = 8.0 and [Ca^{2+}] = 10 mM, we introduced 12.5 nM of QDs of size 8 nm (Figure 3.4(a)). For this size and with this concentration,

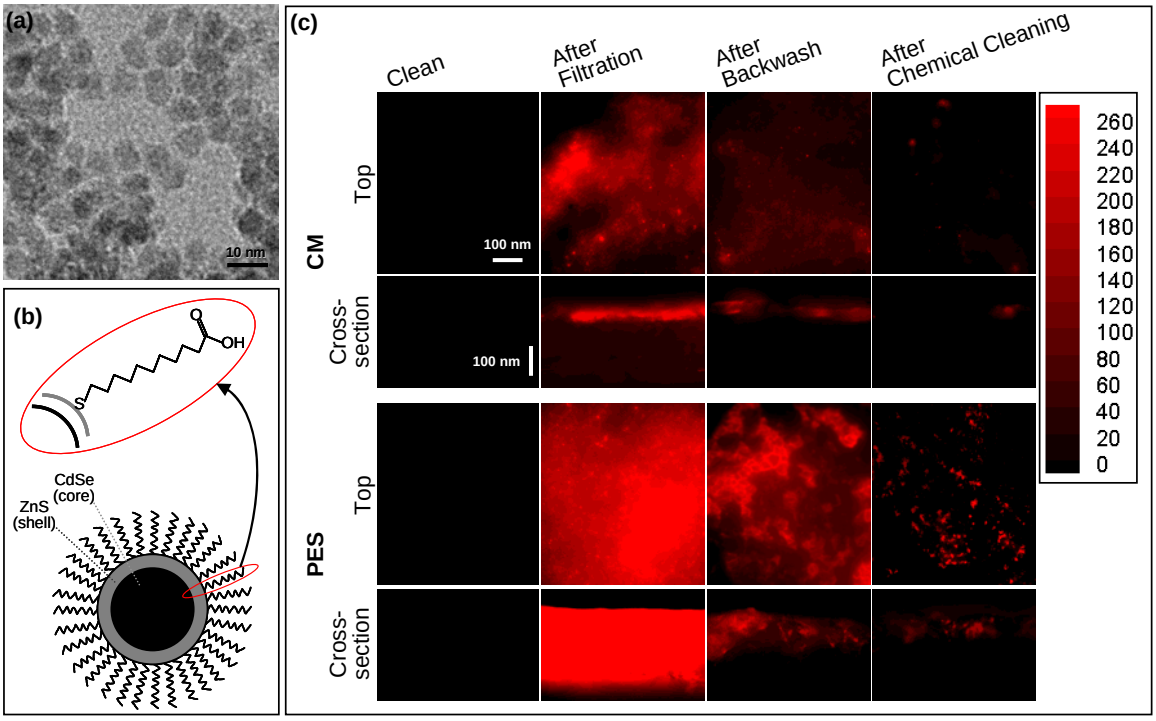

Figure 3.4 (a) TEM image of water soluble CdSe/ZnS QDs obtained with 200 kV, (b) a schematic diagram of the QD showing its core, shell and surface, and (c) CLSM images of the surface and the cross-sections of CM50 and PES100, before filtration and after filtration and subsequent cleaning steps.

QDs did not contribute to membrane fouling nor alter the overall fouling behavior, but became effectively embedded in NOM fouling layers and enabled fluorescence visualization of fouling structures. Surfaces of these QDs are carboxylated with mercaptoundecanoic acid ligands (i.e., mercapto groups are bound to the QD's surface and the carboxyl groups are towards the aqueous phase; Figure 3.4(b)), similarly to the CML particles that are widely used as surrogates for natural colloidal particles (Ang et al., 2011; Li and Elimelech, 2004). Similar CLSM techniques have previously been applied, but only to biofouling visualization using fluorescence-tagged molecules.

Shown in Figure 4.4(c) are CLSM images of the clean and fouled surfaces and cross-sections of CM50 and PES100. These images were taken using a water dipping lens at a magnification of 40 and at an excitation wavelength of 488 nm. Red colors in each pixel of 0.56 μm resolution represent QD fluorescence in an arbitrary scale of 0 to 255. After the filtration, fouling was 76% more significant with PES100 than CM50 based on the fluorescence intensity integrated over the surface. Fouling on PES100 was more uniform across the surface and deeper through the cross-section of the membrane. Physical cleaning via backwashing removed 36 % and 26 % of this fouling in CM50 and PES100, respectively. The residual fouling after chemical cleaning was only 8 % for CM50 (compared to fouling after the filtration), while it was 19 % for PES100. Although a direct correlation of these values to the flux decline is not possible and analysis is semi-quantitative, these images provide visual evidences not only for the critical differences between CM50 and PES100 membranes during fouling but also for the effectiveness of cleaning.

3.3.5 Resistance and Rejection

The resistance-in-series model analysis shown in Figure 3.5(a) provides further quantitative insights into differential filtration and cleaning behaviors observed above. When NaCl (30 mM) or Ca^{2+} (10 mM) was added to the SRHA solution, most resistance terms increased regardless of membrane type, with greater effect by calcium ions than ionic strength. However, a relative contribution of each resistance varied for different membranes. For CM50 at 10 mM of Ca^{2+}, physically removable resistances (R_{cp} and R_{pr}) dominantly contributed to the overall fouling resistance, i.e., 61 % of R_t - R_m, and irreversible resistance (R_{if}) was negligible. It contrast, R_{cp} + R_{pr} was 44 and 45 %, and R_{if} was significant (12 and 8 %) for PES100 and RC100, respectively. Even though the same ionic strength was achieved by 10 mM $CaCl_2$ or 30 mM NaCl, R_{cr} and R_{if} were significantly greater with Ca^{2+} addition; the increase in R_{cr} by $CaCl_2$ and NaCl was 15 and 1 % for CM50, 25 and 0 % for PES100, 35 and 3 % for RC100, respectively; and the increase in R_{if} was 3 and 1 %, 12 and 4 %, and 8 and 6 % for CM50, PES100 and RC100, respectively. This analysis confirms that ceramic membrane fouling is much less subject to Ca^{2+} effect (Costa and de Pinho, 2005; Ghosh and Schnitzer, 1980; Hering and Morel, 1988; Hong and Elimelech, 1997).

Higher efficiencies of physical and chemical cleaning for CM50 are also consistent with the aforementioned CLSM image analyses. Backwashing removed 36 and 26 % of R_t for CM50 and PES100, while 49 and 42 % based on fluorescence intensities. Likewise, R_{if} was 3 and 12 % for CM50 and PES100 from the resistance analysis, while 8 and 19 % based on CLSM analysis. The absolute values obtained from resistance-in-

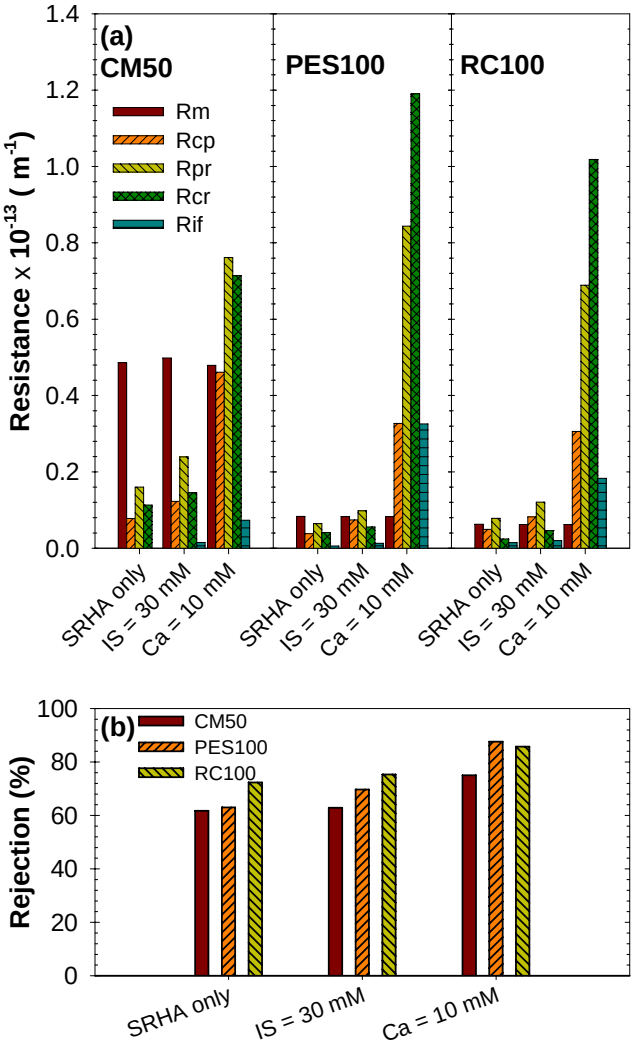

Figure 3.5 (a) Resistance and (b) rejection data for selected set of the filtration of SRHA using ceramic and polymeric membranes. [SRHA] = 20 mg/L; pH 8.0; stirring at 200 rpm.

series and CLSM analyses cannot be directly compared, since the accumulation of foulants on the surface and inside the pores contribute differently to the overall flux decline depending on the mode of accumulation. Yet, they provide complementary evidence as to the critical difference between ceramic and polymeric membranes.

Rejection data shown in Figure 3.5(b) echo the findings in the flux and resistance data. Rejection increased due to more fouling when ionic strength and Ca^{2+} concentration were higher. The higher rejection of SRHA by polymeric membranes, even with a greater MWCO, is mostly likely due to the greater level of fouling on the surface and in the pores, which would function as an additional barrier for the solute transport through the pores.

3.3.6 Adsorption Tests and Contact Angle Measurements

Varying tendencies of foulant adsorption to membrane material due to different surface properties would contribute to unique fouling behaviors and cleaning efficiencies. Results shown in Figure 3.6 were obtained through batch adsorption tests which were conducted by soaking membrane coupons with the same active filtration area (4.5 cm^2) into 20 mg/L SRHA solutions (200 mL) and shaking for 24 h at room temperature. The amount of adsorbed SRHA was calculated from the difference between the concentrations before and after adsorption. As shown in Figure 3.6, a much less amount of SRHA was adsorbed onto CM50 compared to PES100 and RC100. For example, the adsorbed amount on CM50 at pH 8 was 36 and 37 % less than on PES100 and 43 and 38 % less than on RC100, respectively, with or without 10 mM Ca^{2+}. Difference was much

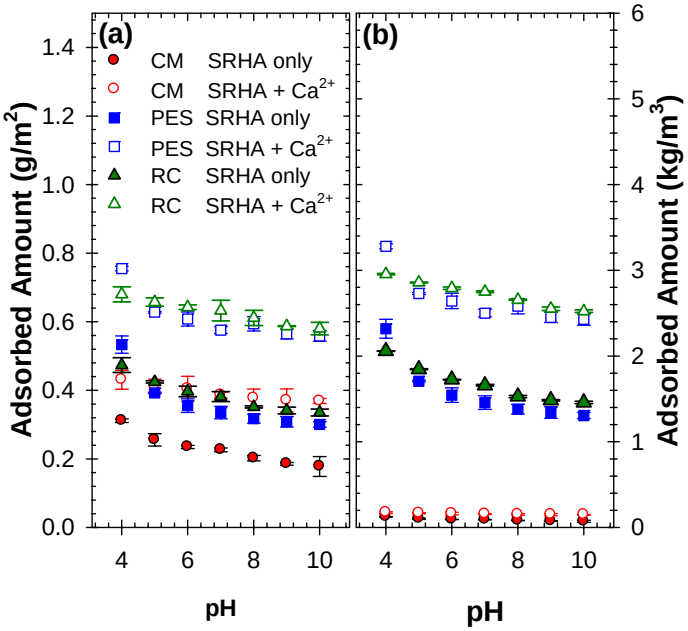

Figure 3.6 Adsorption of SRHA onto ceramic and polymeric membranes. Adsorbed amount of SRHA normalized by (a) the active surface area and (b) the volume of membrane submerged in the SRHA solution after 24 h of shaking. [SRHA] = 20 mg/L; [Ca^{2+}] = 10 mM.

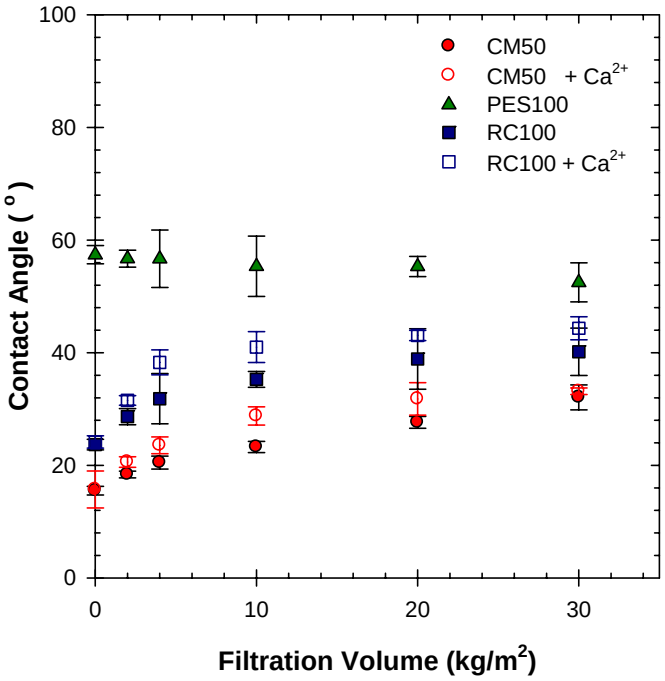

Figure 3.7 Effect of SRHA adsorption on the contact angles as a function of filtration volume. [SRHA] = 20 mg/L; ionic strength = 10 mM; pH 8.0; stirring at 200 rpm.

more pronounced when data were volume-normalized to reflect difference in thickness (i.e., CM50 is nearly thousand times thicker than polymeric membranes). Volume-normalized adsorption data suggest that ceramic materials are significantly less prone to SRHA adsorption and that, when compared to filtration-area normalized data, foulant adsorption inside the pores should contribute much less to overall fouling of CM50 compared to polymeric membranes. Finally, more SRHA adsorbed as pH and Ca^{2+} concentration increased, consistent with the observation made on the flux behaviors. Changes in contact angle through the course of filtration are shown in Figure 3.7. CM50 was the most hydrophilic (15.5 °), RC100 relatively hydrophilic (23.7 °), and PES100 hydrophobic (57.4 °) when clean. As filtration proceeded, the contact angles of CM50 as well as RC100 increased (i.e., became more hydrophobic), while hydrophobic PES100 showed a slight decrease. Although RC100's contact angle trend resembled that of CM50, it showed greater and initially faster increase with overall higher contact angle throughout the filtration. Similar increase in hydrophobicity due to organic matter adsorption has been reported with regenerated cellulose membranes (Lee et al., 2004), and inorganic surfaces (e.g. montmorillonite clay (Lopez-Duran et al., 2003)). Also observed was increased contact angle in the presence of 10 mM Ca^{2+}, which accounted for the aggravated fouling with Ca^{2+} (Figure 3.2). Overall, the ceramic material exhibited more hydrophilic properties than polymeric membranes, even taking into account of surface coverage by the same foulant during filtration, which contribute to less adsorption and less fouling than polymers (Yuan and Zydney, 2000).

2.3.7 Adhesion force measurement using AFM

The adhesion force between foulants and membrane surface was estimated using an AFM probe modified with a CML particle (Figure 3.8, insets A and B) (Ang et al., 2011; Li and Elimelech, 2004). The spring constant of the modified probe (0.151 N/m) was slightly higher than that of unmodified one (0.12 N/m), since the CML particle added to the total mass of the probe. In the absence of Ca^{2+}, the force profiles did not show any measurable interactive forces for both clean (results not shown) and fouled membranes, consistent with the literature reports (Chiu and James, 2007). When the membrane was fouled and 10 mM Ca^{2+} was present, negative (net attractive) forces were observed in both approach and retraction curves for all the membranes. The slight left-shift of the deflection curves for polymeric membranes was likely due to the indentation of soft surface caused by compression (Xu et al., 2007; Zhang et al., 2011).

A couple of differences in force profiles were noteworthy. First, the absolute value of *F/R* for CM50 (-0.26 mN/m) were always smaller than those for polymeric membranes (-0.39 and -0.46 mN/m for PES100 and RC100, respectively). Second, the range of interaction, denoted as a piezo position, was shorter for CM50 (25.2 – 30.1 nm) than for PES100 and RC100 (23.4 – 60.3 nm and 23.6 – 56.4 nm, respectively), under the same experimental conditions. The greater negative force and longer range of interactions have been correlated to the increased likelihood of foulant accumulation on membrane surfaces (Li and Elimelech, 2004; Stawikowska and Livingston, 2013), as well as increased difficulty of removing the adsorbed foulant from the surface. The results collectively suggest that the weaker attractive forces observed with ceramic materials are

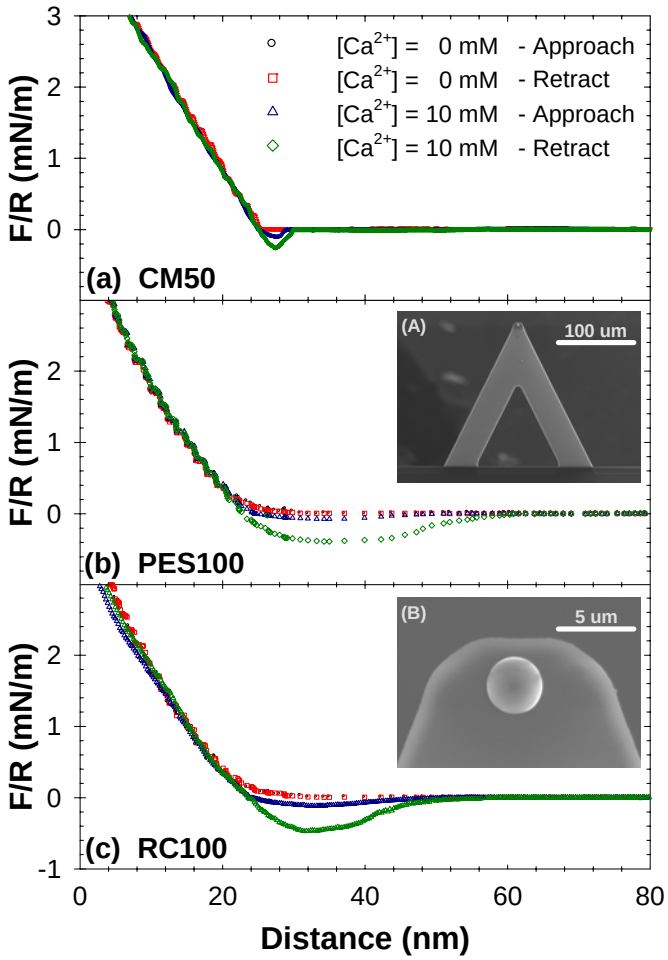

Figure 3.8 Normalized adhesion forces (*F/R*) of a CML particle to (a) CM50, (b) PES100 and (c) RC100. Inset (A) is SEM image of the modified probe and inset (at 10.0 kV 10.4 mm ×300 SE) and (B) is the enlarged SEM image of the end of the probe showing the attached CML particle (at 10.0 kV 10.4 mm ×8.00k SE).

related to less adsorption (Figure 3.6); consequently less fouling (Figures 3.1 – 3.3), lower resistances (Figure 3.5) and greater cleaning efficiency (Figures 3.4 and 3.5).

3.4 Significance and Future Studies

The design and operation of ceramic membrane processes need to be carefully tailored based on fouling characteristics of ceramic membranes and the effect of solution chemistry parameters, rather than assuming similar trends found with polymeric membranes. The similarities and dissimilarities in the fouling behavior between ceramic and polymeric membranes, clearly demonstrated in this study, will provide important guidelines for cleaning strategies and framework upon which further studies can be built. Results presented in this study particularly point to overall less NOM fouling and more effective physical and chemical cleaning after fouling in the ceramic membrane than polymeric membranes, which will add to increasing interests of water industries. More in-depth studies on the performance of ceramic membrane processes including operating conditions, scale-up studies, and pretreatment options, are required for rapid translation of this emerging technology to the full-scale application. Various materials and configurations of ceramic membranes also need to be further tested to build knowledge comparable to the large corpus already available for polymeric counterparts.

CHAPTER 4

EFFECTS OF COAGULATION ON THE CERAMIC MEMBRANE FOULING DURING THE FILTRATION OF SURFACE WATERS

4.1 Introduction

As many advantages of ceramic membranes over conventional polymeric membranes have drawn attention and ceramic membranes becomes a cost-competitive alternative to polymeric membranes (Pendergast and Hoek, 2011), the questions related to the effective implementation of ceramic membranes for U.S. drinking water production remains unanswered. Since membrane fouling is an inevitable phenomenon and one of the greatest hurdles in membrane processes leading poor production efficiency (Shao et al., 2011; Taniguchi et al., 2003), the reduction of such fouling has been a major topic of previous studies (Carroll et al., 2000; Cho et al., 2000). The removal of natural organic matter (NOM) is one of the primary requirements for the production of drinking water (Shao et al., 2011; Taniguchi et al., 2003; Zhang et al., 2003). NOMs lead to membrane fouling by which the performance of membrane processes becomes sub-optimal (Howe and Clark, 2006; Judd and Hillis, 2001) as well as play as a precursor to disinfection by-products (DBPs) (Hu et al., 2010; Kwon et al., 2005; Shah et al., 2011). The evaluation of the pretreatment conditions is prerequisite for the implementation of membrane processes for surface water treatment for drinking water production. Various pretreatment strategies, i.e., adsorption by powdered activated carbon (Berube et al., 2002; Karanfil et al., 1996), irradiation of ozone or ultraviolet (Brown et al., 2008; Huang

et al., 2001; Song et al., 2004), or coagulation (Bagga et al., 2008; Jones and O'Melia, 2000; Lee et al., 2000), have been employed to increase the efficiency and life expectance of membrane processes and make the feed water compatible with membranes by minimizing fouling, scaling and degradation of membranes (Huang et al., 2009; Sondhi and Bhave, 2001). Among those, coagulation is known to be one of the most effective pretreatments for the removal of humic substances in surface waters by destabilizing aquatic colloids including dissolved organic carbon (DOC) and other substances and leading to larger particulate matters via precipitation onto coagulants (Jones and O'Melia, 2000; Kennedy et al., 2003).

Previous studies on the characteristics and the optimization of coagulation pretreatment and membrane filtration processes, however, mainly dealt with polymeric membranes (Guo and Hu, 2012; Mo and Huang, 2003), and little is known about those in a novel hybrid ceramic membrane process. As done with polymeric membranes, the suitability, performance and optimization of coagulation-ceramic membrane hybrid processes remain necessary to be elucidated to meet the quality water production (Howe et al., 2006; Huang et al., 2009). Only limited number of studies are available in the literature on the performance of the hybrid system, especially for the US surface waters for drinking water production and comparative studies between ceramic and polymeric membranes are highly needed (Lehman et al., 2008).

The objectives of studies are to evaluate the performance of a coagulation-ceramic membrane process, which can be a robust option for surface water treatment through the utilization of the intrinsic mechanical durability and chemical resistivity of ceramic membranes and the optimization of coagulation pretreatment. The effects of

coagulants and coagulation conditions on the fouling behavior was systematically investigated during the filtration of selected US surface waters, and the comparison of fouling characteristics between ceramic and polymeric membranes systems are presented in terms of fouling characteristics, cleaning efficiency and NOM removal. The results of this study provide critical information to guide the industry practitioners, consultants, and regulatory agents considering early adoption of this new technology as well as fundamental knowledge upon which further in-depth studies can be built.

4.2 Experimental

4.2.1 Natural raw waters

Natural surface waters from GA and NC were tested in a lab-scale. Two river waters and two lake waters were collected from local water treatment plants, transported and stored in a refrigerator at 4 °C. The characteristics of the source waters are shown in Table 4.1. The source waters had low Turbidity (0.67 – 5.14) and DOC (1.08 – 2.21). The Chattahoochee river water had high SUVA value of 5.26 with the other sources at low range (1.90 – 2.24).

4.2.2 Coagulation

Three coagulants, ferric chloride ($FeCl_3 \cdot 6H_2O$, Fisher Scientific, NJ), aluminum sulfate ($Al_2O_3 \cdot 18H_2O$, Acros Organics, NJ) and polyaluminum chloride (PACl, 23%

Table 4.1 Characteristics of raw surface waters sources.

	Chattahoochee River, GA	**Catawba River, NC**	**Lake Lanier, GA**	**Lake Norman, NC**
Notation	GR	NR	GL	NL
pH	7.3	6.9	7.2	7.1
Alkalinity (mg/L)	20	27	18	17
Hardness (mg/L)	15	27	16	20
Turbidity (NTU)	3.77	5.14	0.67	1.59
TOC (mg/L)	1.94	2.65	1.45	1.80
DOC (mg/L)	1.39	2.21	1.08	1.53
UV_{254} (m^{-1})	7.31	4.73	2.42	2.90
SUVA (L/mg·m)	5.26	2.14	2.24	1.90

Table 4.2 Conditions of coagulation.

Feed Water	Coagulant	Dose (mg/L)	pH	Final Condition	Operation Mode
Chattahoochee River, GA **GR**	Ferric chloride Aluminum sulfate PACl	0.5-2.6	4.5–7.5	Alum 1.3 mg/L as Al, pH 6.5 Ferric 2.6 mg/L as Fe, pH 6.0 PACl 1.3 mg/L as Al, pH 6.0	Constant flow Constant pressure
Catawba River, NC **NR**	Ferric chloride			(Equimolar comparison) Ferric 2.6 mg/L as Fe, pH 6.0	Constant flow
Lake Lanier, GA **GL**	Ferric chloride Aluminum sulfate			(Equimolar comparison) Alum 1.3 mg/L as Al, pH 6.5 Ferric 2.6 mg/L as Fe, pH 6.0	Constant flow Constant pressure
Lake Norman, NC **NL**	Ferric chloride			(Equimolar comparison) Ferric 2.6 mg/L as Fe, pH 6.0	Constant flow

Al_2O_3, 80-83% basic, PAX-XL19, Kemira, GA) were tested for each source water. These coagulants tested in previous studies were adopted in this study as representative coagulants. The doses of coagulants and pHs for aluminum sulfate were selected from common ranges available in the literature (Hofs et al., 2011; Matsui et al., 2003; Yonekawa et al., 2004), and a final set of the dose and pH were chosen based on a series of in-line coagulation followed by membrane filtration. The coagulation condition for ferric chloride was on equimolar basis relative to aluminum. Table 4.2 lists the conditions used in this study.

4.2.3 Membranes and Filtration

Ceramic and polymeric microfiltration membranes were tested. Hollow fiber ceramic membranes, CM01, are made α-alumina and have a pore size of 0.1 μm with the following dimension. Outer diameter is 2.2 mm, internal diameter 2.1 mm, and the membrane thickness 0.05 mm. Polymeric hollow fiber membranes, PS01, made of polysulfone with an outer diameter of 0.04 cm and a pore size of 0.1 μm (Minntech, Fiberflo HF 100, Minneapolis, MN) were comparatively tested. The direction of the filtration was inside-out for CM01 and outside-in for PS01. Lab-scale filtration modules was made to hold one ceramic membrane with a length of 19 cm and an effective surface area of 12.5 cm^2 for CM01 or seven thinner polymeric membrane fibers with a length of 5.0 cm and a total effective surface area of 13.2 cm^2 for PS01 (Figure 4.1). The active layer of the disc membranes is ZrO_2, and the support layer consists of alumina, titania and zirconia. Virgin membranes were either cleaned or wetted before use. Ceramic

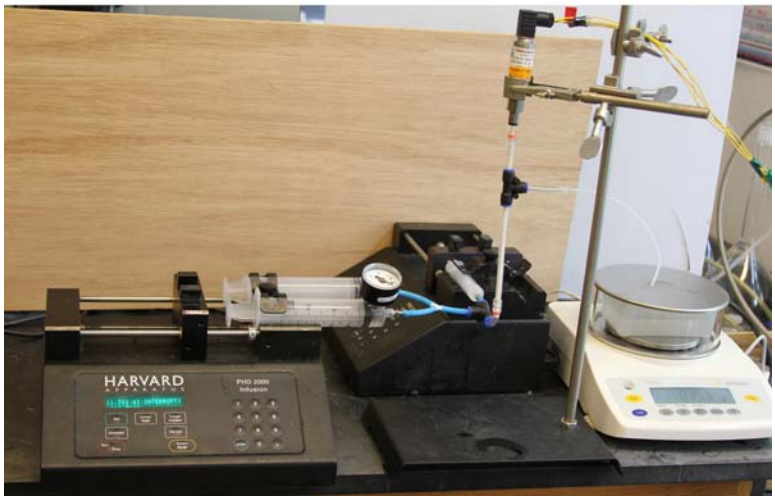

Figure 4.1 Experimental setup for constant flow filtration

membranes were chemically cleaned and soaked in ultrapure water (resistivity > 18.2 MΩ) for 30 min, and PS01 membranes were wetted by filtering 300 mL of ultrapure water.

Filtration experiments were conducted in a constant flow rate mode using syringe pumps (PHD 2000 Infusion, MA, Harvard Apparatus, MA). The modules and the experimental setup are shown in Figure 4.1. Feed surface water and coagulant solution were fed using respective syringe pump and mixed in-line to give the desired final concentration of the coagulant. The flow rate was 100 LMH and the retention time after mixing before the coagulated feed water reach the membrane was 1 minute. The pressure was monitored using pressure transducers connected to a computer via a data acquisition module and LabView software. The pH of the feed solution was adjusted to give the final target pH after coagulation. Selective sets of filtration experiments were also conducted in constant pressure mode to evaluate the efficiency of coagulation and the fouling. The pressure was maintained at 5 psi and the permeate flux was calculated from the difference between two adjacent readings of mass with a specific time interval used for the filtration using a digital balance (Sartorius, ED623S, Goettingen, Germany) with a resolution of 0.001g communicating with a personal computer via an RS-232 connection.

Backwashing was conducted using ultrapure water for 30 s at 25 psi after 30 min filtration of feed solutions for all experiments. Chemical cleaning procedure were as follows: backwashing using ultrapure water for 30 s at 25 psi followed by backwashing for 30 s using 350 mg/L sodium hypochlorite and soaking for 30 min, then acid backwashing using 1,300 mg/L phosphoric acid for 30 s and soaking for 10 min 350 mg/L, and lastly backwashing using ultrapure water for 30 s at 25 psi. These procedures

were applied to both types of membranes commonly in constant flow rate and constant pressure modes.

TOC and DOC were measured using a TOC-Vw Analyzer (Shimadzu, Columbia, MD) and a UV absorbance using a UV/VIS spectrofluorophotometer (RF-5031PC, Shimadzu, Japan). Water samples were filtered through 0.45 μm cellulose acetate cartridge filter (GD/X, Whatman, NJ) for DOC and UV absorbance measurements. Turbidity was measured using a turbidimeter (2100N, Hach Company, Loveland, CO).

4.2.4 Model Analysis

The general form of the resistance-in-series model represented as Equation 4.1, was used to quantify the contribution of each fouling mechanism to overall flux decline:

$$J = \frac{\Delta p}{\mu R_t} = \frac{\Delta p}{\mu\left(R_m + R_p + R_c + R_i\right)} \tag{4.1}$$

where J = flux [m/s]; R's = resistances [m^{-1}] (R_t = total resistance; R_p = cake and pore deposit resistance removable by backwash, *i.e.*, physically removable fouling; R_c = chemically reversible resistance; and R_i = chemically irreversible resistance). Each resistance was obtained by designing a series of filtration experiments, measuring the flux at the end of each filtration step at a given temperature and pressure. R_p term was obtained from the difference between the final feed flux and the pure water flux after backwash, R_c was obtained after chemical cleaning from the residual resistance R_t-R_p-R_c,

and finally R_i was back-calculated from the difference between R_t and the sum of resistances calculated so far, i.e., R_m, R_t, R_p, and R_c.

4.3 Results and Discussion

4.3.1 Effect of the type of Coagulant on the Fouling Behavior

Figure 4.2 shows the results of the filtration of Chattahoochee River with CM01 and PS01 using three types of coagulants, ferric chloride, alum, and PACl. The effects of types of coagulants on the fouling and backwashing were observed. The performance was evaluated in terms of pressure fouling reduction as resultant pressure and the ease with which backwashing was conducted, and the rejection of NOM measured as DOC and UV_{254}. Among the coagulants, ferric chloride showed the best performance with CM01 in the reduction of fouling, and the pressure was reduced by 25.7, 29.8 and 30.8 % after first, second and third cycle, respectively (Figure 4.2(a)). Aluminum sulfate also reduced the pressure, however, to a lesser degree, i.e., 18.9, 17.9 and 15.2 % after each cycle. PACl resulted in poor performance giving increase in the pressure at the end of each cycle by 0.9 to 3.2 %.

Not only the terminal pressure but also the profile of the pressure during the course of filtration need to be considered since the area swept by the pressure curves relates to the energy consumption or the cost of water production. The fouling models for constant flow rate mode depict the shape of fouling behavior, standard, intermediate, complete blocking and cake filtration (Table 4.3). Linear increase of pressure as a

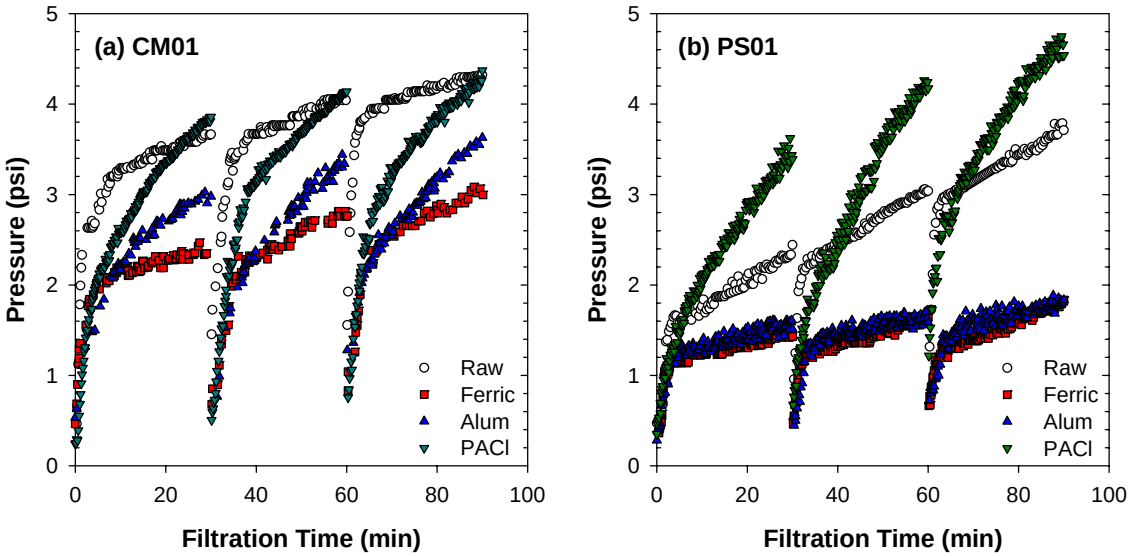

Figure 4.2 Effect of type of coagulants during the filtration of Chattahoochee River with ceramic (CM01) and polymeric (PS01) membranes.

function of time is characterized as cake filtration in most of filtration runs in this study. Gradual and continuous concave-up increase can be interpreted as either complete blocking or standard blocking, and intermediate blocking is observed when there is fast and steep increase in pressure in the initial phase of filtration. Distinctive shapes of pressure profiles were observed in the filtration runs in each cycle of filtration and with different coagulants. At the beginning of each cycle, the fast increase in pressure could have resulted either from the pressurization of the filtration system after onset of filtration or intermediate blocking of pores, which was not clearly understood. The transition of the fouling to cake filtration mechanism differed with coagulants. The coagulation with ferric chloride resulted in lower pressure with similar pressure profile while aluminum sulfate and PACl showed relatively slower transition with less decrease in pressure. Most of the pressure profiles in each cycle transitioned into a linear increase, i.e., proportional to filtration volume or time and is described as cake filtration. Faster transition to cake filtration was favorable when ferric chloride was used while more pore blocking seemed to be involved with aluminum sulfate and PACl. The performance in terms of rejections and resistances will be discussed later.

The parallel results using PS01 are shown in Figure 4.2(b). The lower pressure for relevant coagulants was due to higher initial water flux of PS01. It was noteworthy that the slope of pressure increase in the filtration of raw water was greater with PS01 compared to that with CM01, which indicates higher fouling potential onto polymeric membranes than ceramic membranes as found in previous sections. Considering the higher porosity of PS01 with about 3.3 times the pure water flux, the fouling was severer with PS01, i.e., the final pressure of the first cycle with each membrane was 2.8 and 5.6

Table 4.3 Fouling models for constant flow rate filtration (Bolton et al., 2006).

Models	Linear Equation
Cake Filtration	$\frac{P}{P_0} = 1 + K_c J_0^2 t$
Intermediate Blocking	$\ln\left(\frac{P}{P_0}\right) = K_i J_0 t$
Complete Blocking	$\frac{P}{P_0} = \frac{1}{(1 - K_b t)}$
Standard Blocking	$\frac{P}{P_0} = \left(1 - \frac{K_s J_0 t}{2}\right)^{-2}$

times the initial flux for CM01 and PS01, respectively. Subsequent cycles showed similar trend resulting in 2.1 – 2.9 and 3.7 – 8.6 times with coagulation for CM01 and PS01, respectively. The effectiveness among coagulants was similar but there were difference in the fouling reduction with CM01 and PS01. Greater efficiency was obtained in the order of ferric chloride, aluminum sulfate and PACl with both types of membranes, and the difference in pressure between ferric chloride and aluminum sulfate was more pronounced with CM01. The slope of pressure increase was influenced to a greater extent with PS01. Achieved pressure reduction was over 50 % with PS01 while 15 – 31 % with CM01, relative to the pressure for the filtration of raw water. When ferric chloride or aluminum chloride was used, however, the levels of pressure based on the initial pressure for pure water were 2.1 – 3.2 times for CM01 and 3.7 – 9.2 times for PS01 at the end of filtration cycles.

4.3.2 Effect of Coagulation on Various Surface Waters

Other US surface waters were tested using ferric chloride which showed best performance for GR. The results of the filtration of Catawba River (NR), Lake Lanier (GL) and Lake Norman (NL) waters are shown in Figure 4.3. When the natural waters were filtered with in-line coagulation at 2.6 mg/L as Fe and pH 6.0, slight different fouling behavior was observed for varying source waters. As the fouling was severe with NR and slightly less with GL and NL, the pressure reduction was greatest with NR (3.7 – 4.5 psi at the end of respective cycles) followed by NL (3.0 – 3.7 psi) and GL (3.2 – 3.5 psi) at the end of the first cycle. The performance of coagulation was, however, not

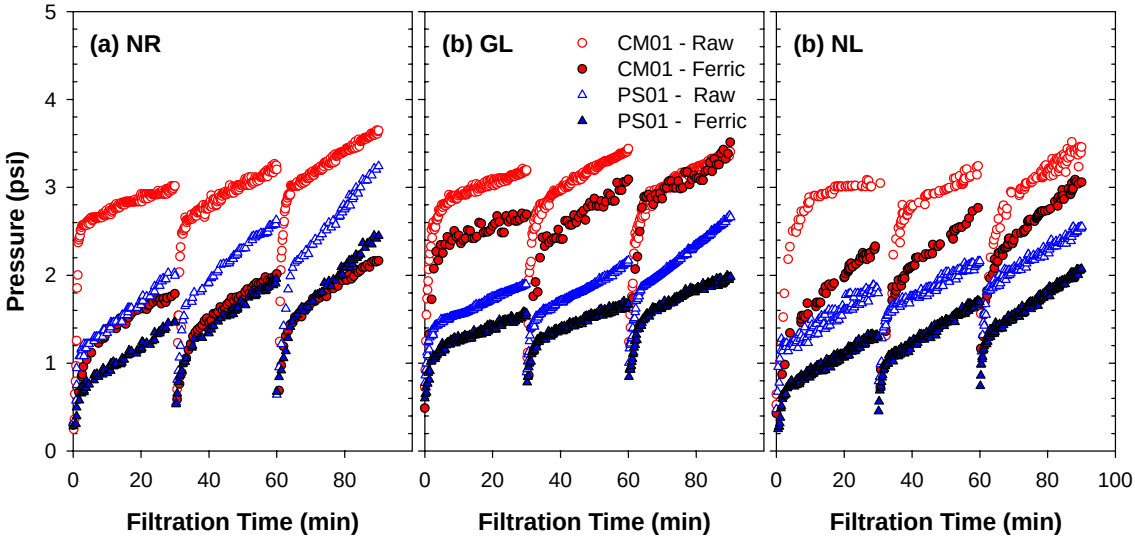

Figure 4.3 Effect of ferric chloride on the fouling of different source waters with ceramic (CM01) and polymeric (PS01) membranes.

parallel with the results of the raw water filtration. The pressure reduction achieved by coagulation was 40.2, 16.5 and 24.4 %, respectively for NR, GL and NL at the end of the first cycle. In subsequent cycles of filtration, the pressure reduction was achieved consistently at around 40 % with NR while the difference in the pressure between raw water and coagulated feed solution became gradually less meaningful with river waters (GL and NL) at the end of second and third cycles. Compared with the results for GR shown in Figure 4.3, NR was treated best with ferric chloride.

On the other hand, filtration with PS01 resulted in difference level of pressure reduction for other surface waters. The pressure was reduced by 19 – 29 % for varying source waters and the absolute pressure values were lowest with NL. Combined with the results for GR, ferric chloride performed best with GR in terms of operating pressure and its reduction. Any significant relationship between the fouling behavior and the characteristics of different surface waters and this is not unexpected from the finding in the literature. The coagulation conditions need to be optimized for each source water since the interplay of constituent of a surface water may not be simply correlated to the performance of a coagulation-filtration system. An optimal condition of coagulation could be different even with the same source water when filtered with membranes with different properties, which was the case in this study comparing the fouling behavior using ceramic and polymeric membranes. Usually, jar tests are conducted for a specific feed solution to find the optimal condition for that reason.

4.3.3 Resistances and Rejections

The performance of coagulation-filtration systems was evaluated in terms of resistances and rejections (Figures 4.4 – 4.7). The total resistances were consistent with pressure monitored during the filtration experiments. CM01 had a relatively large intrinsic membrane resistance, R_m, which constituted the largest portion of the total resistance, R_t. The results for the first cycles of filtration of GR with various coagulants are shown in Figure 4.4(a). Among the additional resistances, physically removable resistance, R_p, i.e., the resistance removable by backwash, was the greatest of R_t except in the filtration with poor coagulation with PACl. Ferric chloride and aluminum sulfate reduced each portion of R_p, chemically removable resistance, R_c, and irreversible fouling remaining after chemical cleaning, R_i. Such decrease in the resistances were greatest with ferric chloride which performed best with GR when filtered with CM01.

Figure 4.4(b) shows the relevant results for parallel experiments with polymeric counterpart (PS01). The lower R_m value was 1.02×10^{-11} m^{-1} for PS01 while that of CM01 was 3.34×10^{-11} m^{-1} which is 3.3 times larger and results from the difference in the initial pure water flux or porosity. Unlike with CM01, R_p and R_c values were similar to or greater that R_m, and the R_p's were not the greatest contributor to the total resistances with PS01. Filtration of raw water without coagulation using PS01resulted in very high resistance values comparable to those with CM01 and PACl seemed to aggravate the filterability. The resistances, R_p's and R_c's, were commensurate with ferric chloride and aluminum sulfate. Coagulation with these coagulants reduced the resistances significantly resulting in 35.1 and 30.7 % for ferric chloride and aluminum sulfate, respectively.

Even with the difference in R_m's by 3.3 times, that in R_t's became marginal at the end of the first filtration cycles. The R_t's for CM01 were only 1.1 – 1.9 times those for

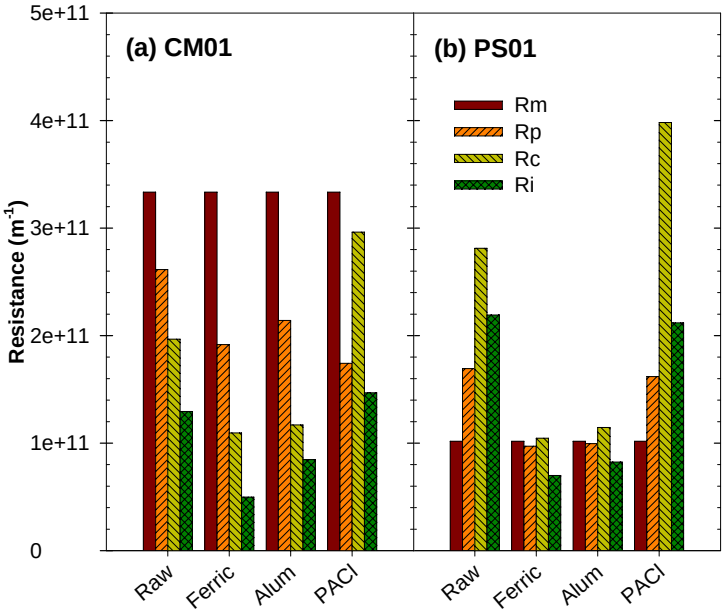

Figure 4.4 Results of resistance-in-series model analysis for the filtration of Chattahoochee River (GR) using various coagulants.

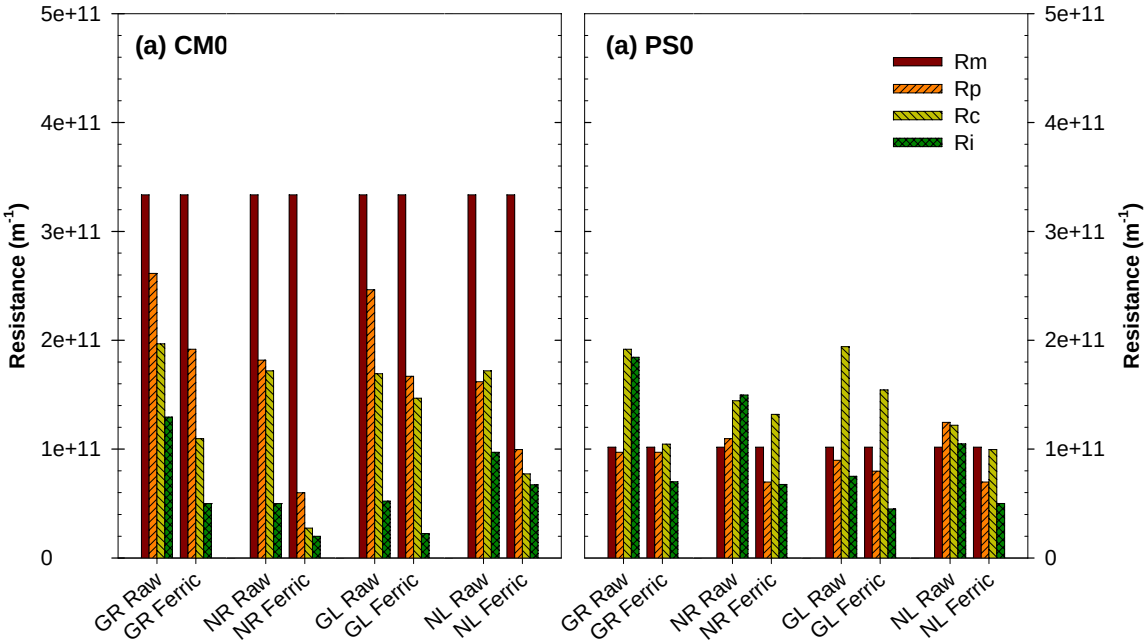

Figure 4.5 Results of resistance-in-series model analysis for the filtration of various natural water sources coagulated with ferric chloride.

PS01. Again, this indicates the fouling was predominant onto polymeric membranes. Therefore, 25.7 and 18.5 % pressure reduction for ferric chloride and aluminum sulfate with CM01 should not be underestimated. For CM01, the physically removable resistance, R_p, was the greatest for the raw water and two coagulants (ferric chloride and alum) while chemically removable resistance, R_c, was greatest for PACl which showed worst performance and even increased the pressure after coagulation. R_p accounted for around 28 % of R_t and relatively small portion of irreversible fouling remained after chemical cleaning (7-14 %). On the other hand, R_p values were 17 – 26 % for PS01 and 19 – 32 % was still responsible for R_t for PS01. It should be noted that these values are based on R_t which includes R_m. Since there is more than three-fold difference in the initial pressure, the comparison of the resistances caused only by fouling can be more relevant. When each resistance component was based on R_t–R_m, R_p's were 45 – 52 and 25 – 36 % for raw water and successfully coagulated feeds with CM01 and PS01, respectively. Similarly, R_c's ranged 28 – 34 and 39 – 42 % and R_i's 14 – 22 and for 26 – 39 % for CM01 and PS01, respectively. This observation was consistent with previous reports elucidating the fouling characteristics of ceramic microfiltration and ultrafiltration membranes utilizing representative model compounds including polyethylene glycol (PEG) and Suwannee River humic acid (SRHA) and synthetic river water (Lee et al., 2013).

Using the same coagulation condition, the resistance-in-series model analysis was extended to the filtration of other surface waters, and Figure 4.5 provides the comparison of resistance components. As seen above for different river and lake waters, NR (Catawba River) was most efficiently treated in terms of pressure reduction regardless of

water sources and membrane types, and there was a positive correlation between the flux reduction and $R_p/(R_t - R_m)$ In other words, the efficiency of physical cleaning or backwashing is likely to relate to the flux reduction. This improved membrane performance could have resulted from the formation of flocs capable of forming porous cakes on the surface of membranes and cake layer physically removable with ease. Such flocs, formed optimally for the pore size of membranes, would allow greater flow through the cake, thereby minimizing further blocking of membrane pores (Kennedy et al., 2003).

Even with greater efficiency of physical cleaning with ceramic membranes, the pressure reduction was not exactly proportional to the R_p values. For instance, the final pressure values at the end of the second cycle in the filtration of GR was greater than those at the end of the first cycle by 4.7 % with the reduction in R_p by 28.0 % while by 10.2 % with the reduction in R_p by 28.4 % when coagulated with ferric chloride. For NR, the reduction in R_p's by 24.7 and 13.6 % resulted in 9.5 and 14.1 % increase in pressure for raw and coagulated feed waters, respectively. Therefore, not only R_p's but also the effect of remaining resistances, R_c and R_i, should be taken into account for the fouling subsequent cycles.

The removal of NOM was evaluated in terms of DOC, UV_{254} and SUVA for each set of filtration (Figure 4.6). The rejections of DOC and UV_{254} for the filtration of GR with CM01 were 5.8 and 12.2 %, respectively, which can be intuitively understood from the relative size of NOM molecules to the pores of microfiltration membranes. When the coagulated GR was filtered the removal of DOC and UV_{254} increased to 41.7 and 70.6 % for ferric chloride and 25.9 and 62.8 % with aluminum sulfate. These results led to the

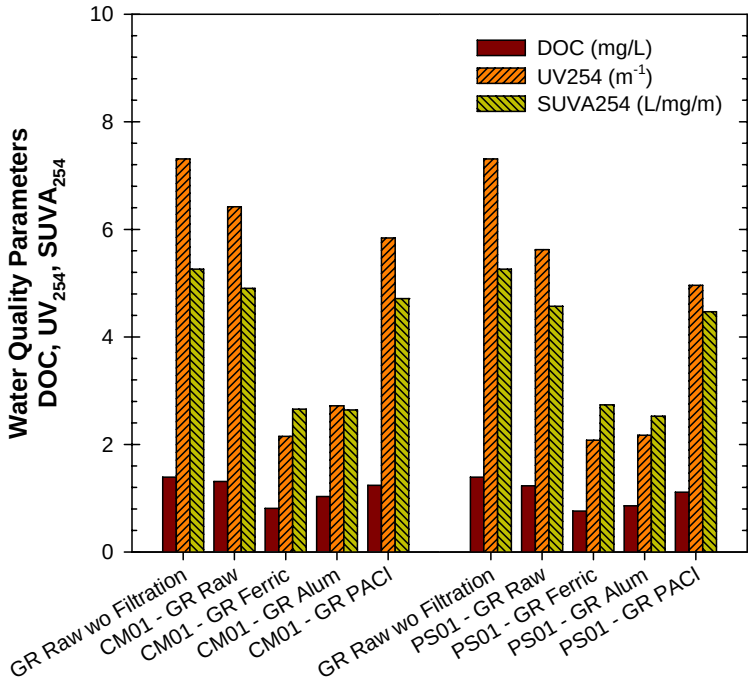

Figure 4.6 The Effect of coagulants on the NOM removal during the filtration of Chattahoochee River.

SUVA removal of 49.5 and 49.7 % with ferric chloride and aluminum sulfate, respectively while it was merely 10.4 % with PACl which was not efficient for the reduction of pressure and resistances. As shown in Figure 4.6(b), PS01 was slightly more efficient than CM01 for the filtration of raw water. DOC and UV_{254} values after filtration were 11.5 and 23.1 %, respectively, which is likely due to preferential adsorption of NOMs and severer fouling onto polymeric membranes (Lee et al., 2013). The SUVA value of the raw water, GR, was 4.90 and implies high hydrophobicity and molecular weight of NOM in the water (Edzwald, 1993). Therefore, 13.1 % of SUVA could be achieved without coagulation. When coagulant was added, the SUVA removal increased significantly to 48.0 and 52.0 % for ferric chloride and aluminum sulfate, respectively, with increases in both the rejections of DOC and UV_{254}. As with CM01, PACl did not performed well for PS01 with a SUVA removal of 15.0 %.

When the other natural waters were tested under the same coagulation conditions with ferric chloride, the rejections of all parameters, DOC, UV_{254} and SUVA, were not as high as for GR (Figure 4.6). The SUVA removals for NR, GL and NL were 33.5, 28.8 and 20.9 % for CM01 and 37.7, 33.4 and 47.2 % for PS01, respectively (Figure 4.7). This was as expected from the characteristics of the surface waters tested in this study. The SUVA values of source waters were 5.26 for GR and 1.94 – 2.24 for the other waters. It was demonstrated that low final SUVA values results from poor DOC removal when the SUVA value of the raw water is lower than 2 while it was high when the SUVA value is greater than 4. The removals of DOC, UV254 and SUVA for NL were unexpectedly higher than for NR and GR was presumably by severe fouling onto PS01 resulting in higher particle removal and poor pressure reduction (Figures 4.2 and 4.3). In summary,

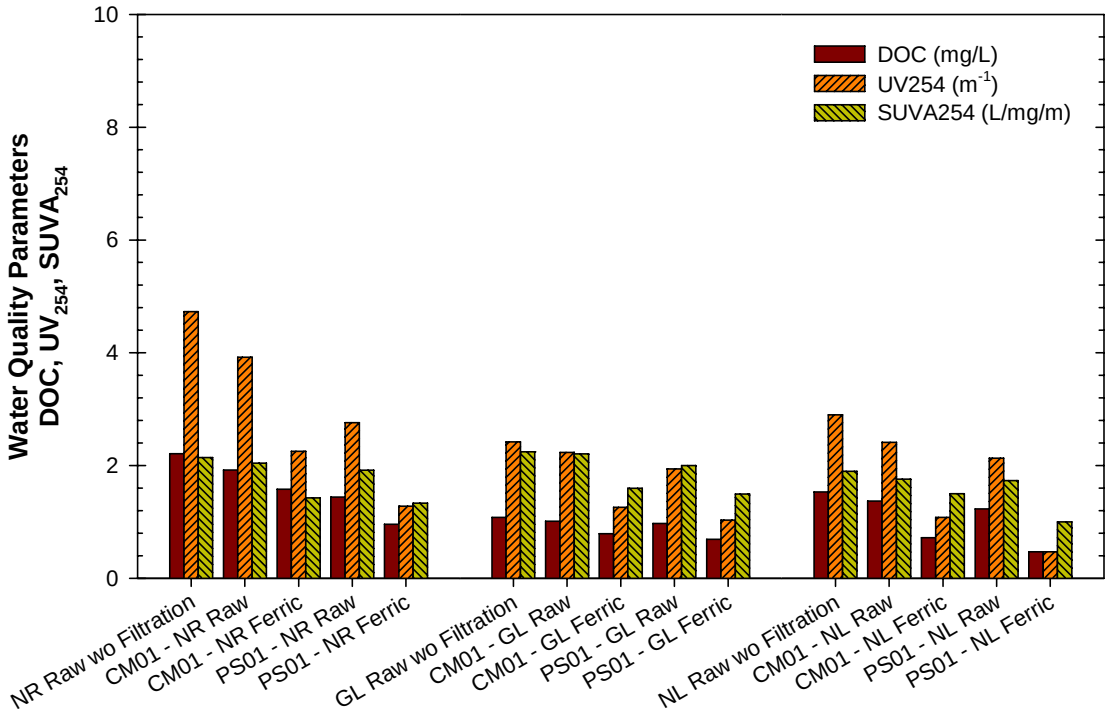

Figure 4.7 NOM removals during the filtration of natural surface waters with coagulation using ferric chloride.

the rejection of NOM was more efficient with polymeric membranes (PS01) than ceramic membranes for all types of source waters and the removal and correlated well with the pressure and resistance data.

4.3.4 Effect of backwashing and coagulation

Comparison of the effect of backwashing and coagulation for five cycles of filtration of GR with or without coagulation was provided in Figure 4.8. Raw water was filtered with CM01 without coagulation and backwash, but the filtration was stopped after 30 min and resumed with pressure release between cycles to compare the effect of backwashing on the pressure change. The pressure increased monotonically as the filtration time increased. At the beginning of each filtration cycle, the pressure was low since the membrane module started to be pressurized. After a short period of pressure build-up, linear increase of the pressure was observed. The low pressure between each cycle was due the pressure release. The pressure profile in successive filtration cycles resembled the pressure increase observed in the first cycle. The results showed that the fouling took place continuously and that there was little effect of pressure release on the fouling.

The results for the same filtration except with backwash after each filtration cycle using the product water shows a linear increase in the pressure during the filtration similar to that in the previous experiment. The second and the following cycles, however, showed lower pressure than those obtained without backwashing. These results clearly showed that the backwashing had influence on the pressure by removing a portion of

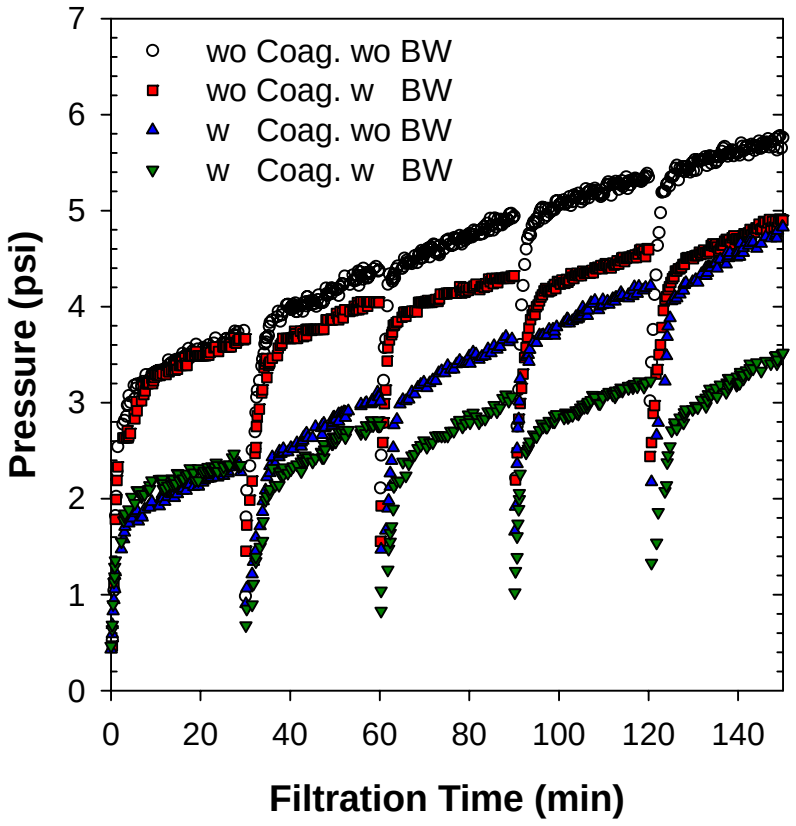

Figure 4.8 The effect of coagulation and backwashing on the filtration of Chattahoochee River water with CM01.

resistance exerted by the fouling during the previous fouling steps. After each filtration cycle, the pressure increased to 3.7, 4.0, 4.3, 4.6, and 4.9 when backwashing was performed while the pressure reached 3.8 4.4, 4.9, 5.4, and 5.8 when any backwash was not performed between filtration cycles. The difference between the terminal pressures at the end of each cycle kept increasing by 9.1 to 15.5 % for the first and fifth cycles. On the other hand, when coagulation was conducted with ferric chloride and filtered without backwashing, the pressure was reduced up to 38.2 % with decreasing the effect of the coagulation, i.e., 17.2 % for the fifth cycle. Finally, when both the coagulation and backwashing were performed, the pressure reduction became greater and the individual effect seemed to be additive. The slopes for the filtrations of raw water and coagulated water were similar as 0.017 and 0.020 psi/min, and those obtained only by backwashing and by the combination of coagulation and backwashing were close to each other, i.e., 0.010 and 0.009 psi/min, respectively. Even though these results may not be used to generalize the effects of such operations, it can be concluded that membrane fouling takes place continuously and the effect of pressure release is negligible in a dead-end mode. In addition, coagulation alone might not be enough for the fouling reduction for extended filtration and needs to be accompanied by proper cleaning procedures for better performance.

4.3.5 Fouling Behavior in a Constant Pressure Mode

The fouling behavior under different operational conditions was examined by conducting filtration experiments in a constant pressure mode. The results showed that

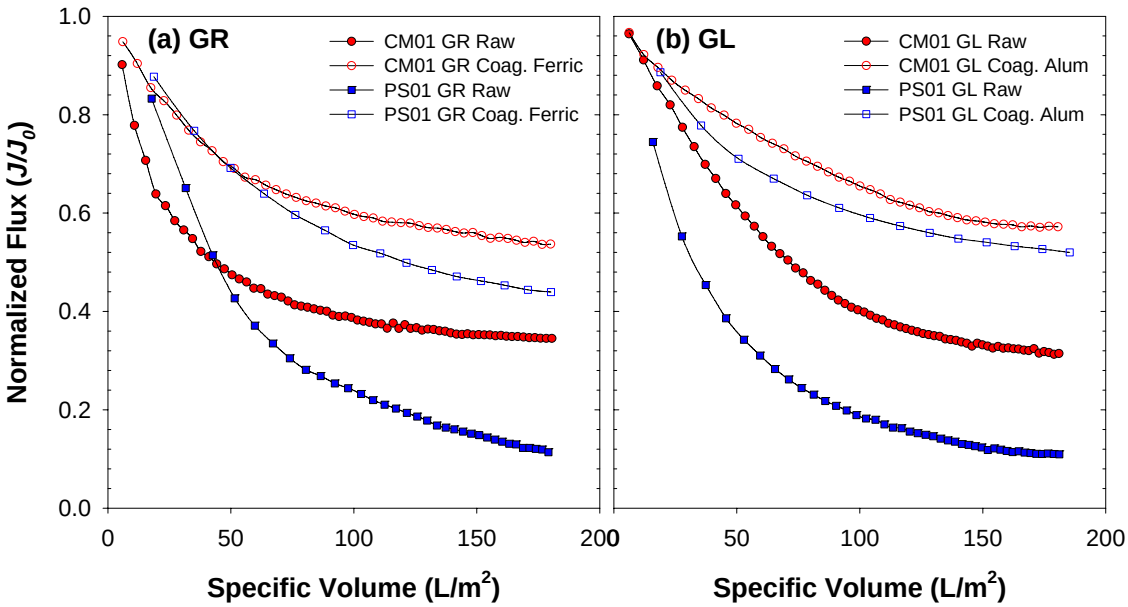

Figure 4.9 Filtration of Chattahoochee River with in-line coagulation in a constant pressure mode using ceramic (CM01) and polymeric (PS01) membranes.

the fouling was severer with polymeric membranes by far as observed in a constant flow rate mode (Figure 4.9). The fouling mechanisms involved in distinctive operational modes, i.e., constant flow or pressure modes and cross-flow or dead-end modes, could be different (Arnot et al., 2000; Bowen and Mukhtar, 1993; Lee et al., 2008), and the examination of performance of a filtration system in different conditions would help understand the fouling characteristics of the system.

First of all, the filtration of GR with or without coagulation resulted in aggravated fouling with polymeric membranes (PS01) in terms of normalized flux. The normalized flux (J/J_0) at the end of the filtration of raw water was 0.345 and 0.116 for CM01 and PS01, respectively. When ferric chloride was added, the flux was recovered by 19.2 and 32.2 % for CM01 and PS01, respectively. At 50 min of filtration that is equivalent by specific permeate volume (50 L/m^2) to the end of the first cycle of the filtration in a constant flux mode, J/J_0 values with CM01 were 0.485 and 0.703 with raw and coagulated waters and those with PS01 were 0.444 and 0.691. These results were consistent in trend with the results of the filtration in a constant flux mode where the relative pressure reduction after coagulation was 25.7 and 35.1 % for CM01 and PS01, respectively. Figure 4.9(b) shows a parallel set of data obtained from the filtration of GL with or without coagulation with aluminum sulfate. The flux recovery after coagulation was slightly more efficient than was observed in the filtration of GR (Figure 4.9(a)) for both types of membranes, CM01 and PS01.

Secondly, the flux with CM01 seemed to reach a plateau at higher levels of J/J_0, which should be advantageous in an extended operation. Even with higher flux recovery with PS01, the fouling was severer and remained increasing with PS01. This observation

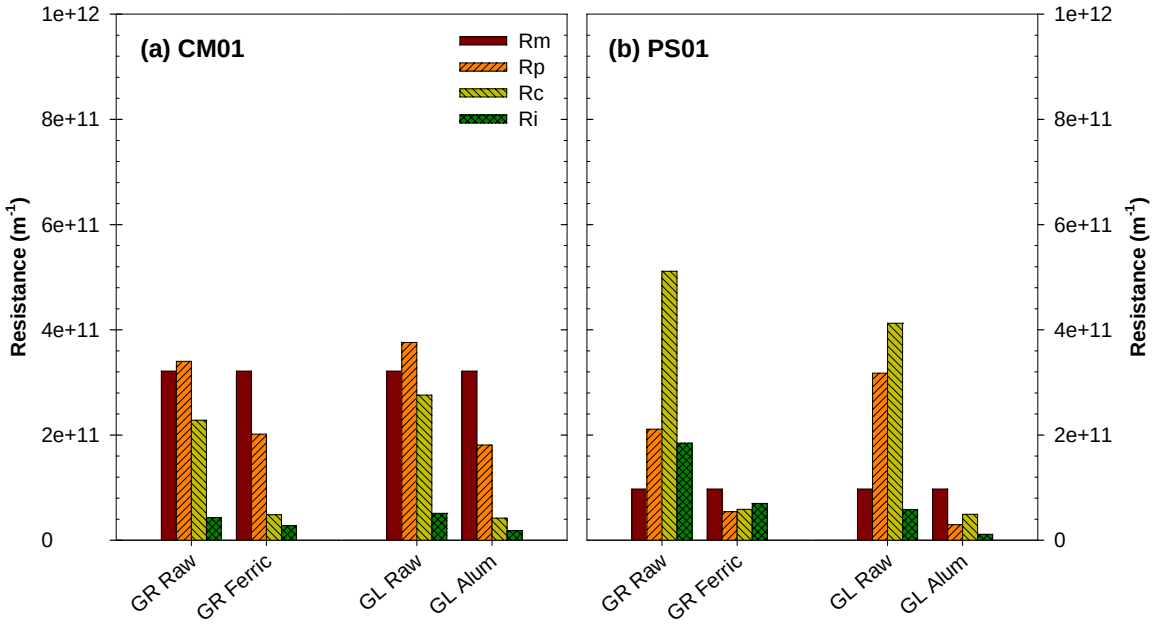

Figure 4.10 Resistance-in-series model analysis for the filtration of Chattahoochee River water and Lake Lanier water with in-line coagulation in a constant pressure mode using ceramic (CM01) and polymeric (PS01) membranes.

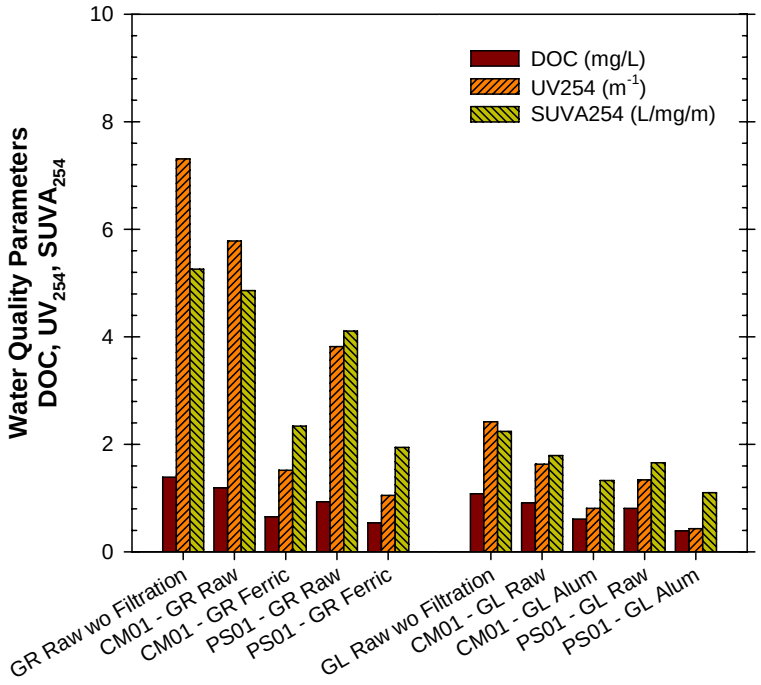

Figure 4.11 NOM removal during the filtration of natural surface waters with coagulation in a constant pressure mode

was consistent with a finding that ceramic membranes led to a earlier appearance of a plateau while gradual decrease in the flux and reaching a plateau at a later phase of the filtration of PEG with polymeric membranes (Lee et al., 2013).

The results of resistance-in-series model analysis are shown in Figure 4.10. R_p was the predominant contributor to R_t for both source waters when CM01 was used while the filtration with PS01 resulted in greater R_c's than R_p's in all cases. Irreversible fouling, R_i, was less with CM01 than with PS01 except for the filtration of GL with coagulation. Physical cleaning was more efficient with CM01, and coagulation could successfully remove R_p's and R_c's. In the filtration in a constant pressure mode, the specific volume at the end of each run was 180 L/m^2 while it was 50 L/m^2 for each filtration cycle in a constant flow rate mode. Therefore, direct comparison of the resistance values may not be quantitatively relevant. The trend in the fouling in terms of flux or pressure and the relative comparison between different membrane materials, however, can shed a light on the fouling behavior.

For the filtration experiments in a constant pressure mode, DOC removals were evaluated (Figure 4.11). As expected from the SUVA values of source waters (GR and GL) (Table 4.1) and the larger specific volume at the end of filtration, higher DOC and SUVA rejections were observed with GR. With the SUVA rejections of 7.6 and 20.1 % with CM01 and 21.9 and 20.1 with PS01 for GR and GL without coagulation, increased SUVA values were obtained with coagulation. The results that the SUVA removals were 55.5 and 63.0 % with CM01 and PS01 for raw waters, respectively, and 40.7 and 50.8 % for coagulated waters, consistently parallel with the finding correlating the SUVA values of raw waters with the final removal efficiency of coagulated waters (Edzwald and

Tobiason, 1999). DOC and SUVA rejections were greater with PS01 than CM01 and support the flux behavior and resistance analysis data observed from the filtration in a constant pressure mode, which is also consistent in trend with the results obtained in a constant flow rate mode. As membrane fouling involves various phenomena including adsorption and cake formation, and is influenced by coagulation, it would not be simply predicted from flux, resistances or rejection data. The surface properties which seemed to influence the fouling behavior and mechanism (Causserand et al., 1994; Combe et al., 1999) could have affected the interactions between NOMs or flocs formed by coagulation and membrane surface. Since the materials of ceramic membranes differ by composition and consequently the surface properties, the interactions need to be clearly understood for better understanding the fouling characteristics of coagulation-ceramic membrane systems.

4.4 Conclusions

Various coagulants and surface waters were tested in a coagulation-membrane filtration system. The effects of coagulants, source waters, and operational modes were evaluated and comparison of the performance of the system was made between ceramic and polymeric membranes. The effectiveness of coagulants was dependent on the type of source waters. Ferric chloride was most effective for the treatment of surface waters tested in this study and aluminum sulfate also performed competitively. It was observed that same coagulation condition did not result in the same efficiency with ceramic and polymeric membranes. The optimal condition needs to be determined not only from the

coagulation test but also by filtration experiments for a specific water source. Materials effect on the fouling characteristics was distinctive. Physically removable fouling was dominant form of the fouling with ceramic membranes while the fouling removable by chemical cleaning and irreversible fouling were more significant with polymeric membranes. The effect of backwashing and coagulation on the pressure was additive and best performance was achieved with physical cleaning and coagulation. As severe fouling took place onto polymeric membranes, the rejections of NOM was slightly higher with polymeric membranes in terms of DOC and SUVA. The removal efficiency was correlated well with the SUVA values of source waters both with polymeric ceramic membranes. Operational modes provided similarity between pressure reduction in a constant flow rate and flux decline in a constant pressure mode. Resistance and rejections data in two modes were parallel for the same source water and coagulation condition.
It is likely that the advantage of the coagulation-ceramic membrane system over polymeric counterpart results from the surface properties leading to relatively less severe fouling and more effective cleaning efficiency.

CHAPTER 5

EFFECTS OF PORE SIZE ON THE FOULING BEHAVIOR OF CERAMIC MEMBRANES

5.1 Introduction

The intrinsic physical properties of membranes such as pore size, molecular weight cut-off (MWCO) (Howe and Clark, 2002), roughness (Evans et al., 2008), and thickness of active and support layers, are known to have influence on the performance of membrane filtration. Such effects have been widely studied for polymeric membranes (Bottino et al., 1991; Cao et al., 2007; Gupta et al., 1999; Howe and Clark, 2002) while relevant information has not been accumulated for ceramic membranes. The understanding of the similarities and dissimilarities in the effects for the fouling behavior of ceramic and polymeric membranes will help tailor the design and operation of ceramic membrane processes based on fouling characteristics of ceramic membranes, rather than assuming similar trends found with polymeric membranes.

Literature shows that there are effects of membrane pore size. Membranes with larger pore size experience initial internal pore fouling while those with smaller pores led to cake growth on the membrane surface (Tracey and Davis, 1994). The rate of fouling was influenced by the pore size in a manner that faster fouling was observed with the membranes with larger pore size (Ando et al., 2012; Zarate-Rodriguez et al., 2001). In

addition, the roughness had an effect on the fouling with rougher membrane surface being fouled faster than its smoother counterpart (Evans et al., 2008; Hoek et al., 2003; Jin et al., 2009). It was also reported that the pore size distribution had a significant influence on the separation of solutes.(Gupta et al., 1999).

It was noted that ceramic membranes available in the commercial market were significantly thicker than polymeric membranes. Several hundred microns are typical of polymeric membranes while over 1 mm thickness is not uncommon for ceramic membranes. Not only the overall thickness of the membranes but the active filtration layers were found to be thinker on ceramic membranes. As the membrane filtration flux is proportional to the total resistance which includes intrinsic membrane resistance. Pore blocking and cake resistances have been the target for reduction by optimizing filtration conditions and using various cleaning strategies.

Among the properties, MWCO is one of the fundamental parameters to investigate for ceramic membranes as literature shows that there are effects of membrane pore size (Howe and Clark, 2002; Ohya et al., 1998; Taniguchi et al., 2003) and pore size distribution (Bottino et al., 1991; Munson-McGee, 2002; Urase et al., 1994). Therefore, the effect of the pore size of ceramic membranes on the fouling behavior was investigated using a various range of pore sizes or MWCOs in this study. The results can be utilized for composition between ceramic and polymeric membranes to better understand the fouling characteristics of ceramic membranes.

5.2 Experimental

5.2.1 Materials

Disc-type ceramic membranes with different pore size or molecular weight cut-off (MWCO) were selected. The disc membranes are 2.5 mm thick and 47 mm in diameter with effective filtration area of 14.6 or 13.9 cm^2 depending on O-rings used. The active layer of microfiltration and ultrafiltration membranes is TiO_2 and ZrO_2, respectively, and the support layer for both membranes consists of alumina, titania and zirconia. The membranes are resistant to high temperature up to 350 ^oC and high pressure up to 4 bars, and have the pH range of operation between 0 and 14. the pore sizes or MWCOs were 3, 8, 15, 50, 150 and 300 kDa, and 0.14 and 0.2 μm.

Hollow fiber ceramic membranes were also tested and the pore sizes were 20, 40, 100 and 200 nm. The outer diameter is 2.2 mm, internal diameter 2.1 mm, and the membrane thickness 0.05 mm. A filtration module was made to hold one hollow fiber membrane with a length of 19 or 21 cm and an effective surface area of 12.5 or 13.9 cm^2. The flow direction is inside-out and the materials for skin and support layers are α-alumina. Disc type ceramic membranes with the MWCO of 300 kDa was used to test the effect of the thickness of active and support layer. The thickness of the membranes were changed by grinding either the active or support layer using 600-mech sand paper.

5.2.2 Membrane filtration systems and experiments

A dead-end filtration experiments aim at elucidating fundamental mechanisms of ceramic membrane fouling. A schematic and photograph of the membrane filtration

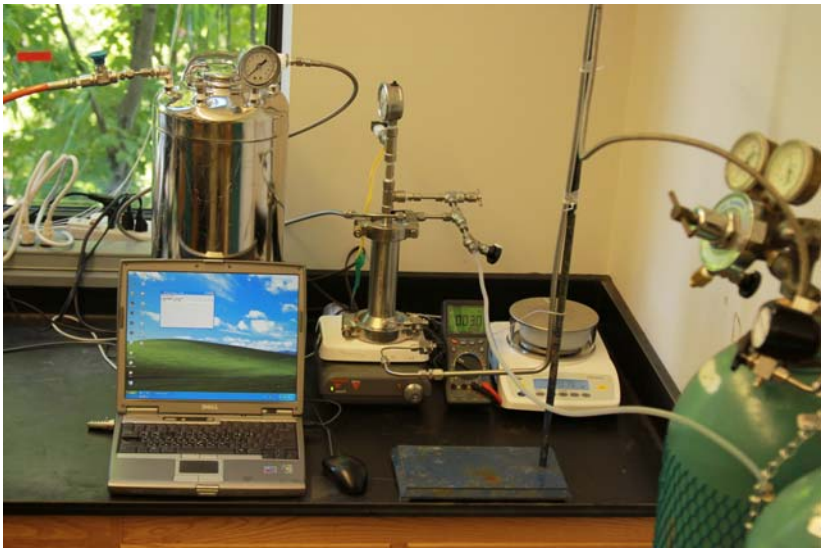

Figure 5.1 Photograph of a lab-scale ceramic membrane system for dead-end filtration with backwashing capability.

equipment assembled are shown in Figures 5.1 and 5.2, respectively. The equipment can be operated under constant pressure maintained by pressurized nitrogen gas. A 20-liter stainless steel feed reservoir (Millipore, Dispensing Pressure Vessel XX6700P20, Bedford, MA) is used to hold ultra pure water and feed water. Pressure is monitored with analog pressure gauges and a digital pressure transmitter (Omegadyne Inc., Model PX319-050G5V, Sunbury, OH). The values are recorded manually. Permeate is collected on a digital balance (Sartorius, ED623S, Goettingen, Germany) with a resolution of 0.001g, and the cumulative mass of permeate is recorded to a personal computer communicating with the balance via an RS-232 connection. The time interval between data acquisition can be programmed and the flux is calculated from the difference between two adjacent readings of mass with a specific time interval used for the filtration.

The rejection data were obtained by analyzing the concentrations of feed solution and permeate using a total organic carbon (TOC) analyzer (Shimadzu, TOC Vws, Japan). Lab-scale experiments under constant pressure so that the constant pressure filtration laws can be used to evaluate the fouling characteristics. Stirring was provided at 200 rpm, and temperature (23 ± 1°C) and pH were monitored before and after each filtration step. Detailed procedures for pure water filtration, feed solution filtration, rinse, backwash, and chemical cleaning. Backwash was conducted at 22.1 psi, 1.5 times the operating pressure, and chemical cleaning by soaking fouled polymeric membranes in a 0.1 N NaOH at room temperature overnight or fouled ceramic membranes in 0.1 N NaOH at 85 °C for 15 min followed by acid cleaning in 85% H_3PO_4 at 50 °C for 15 min. After each cleaning step, pure water flux was measured. The filtration experiments were conducted in a constant

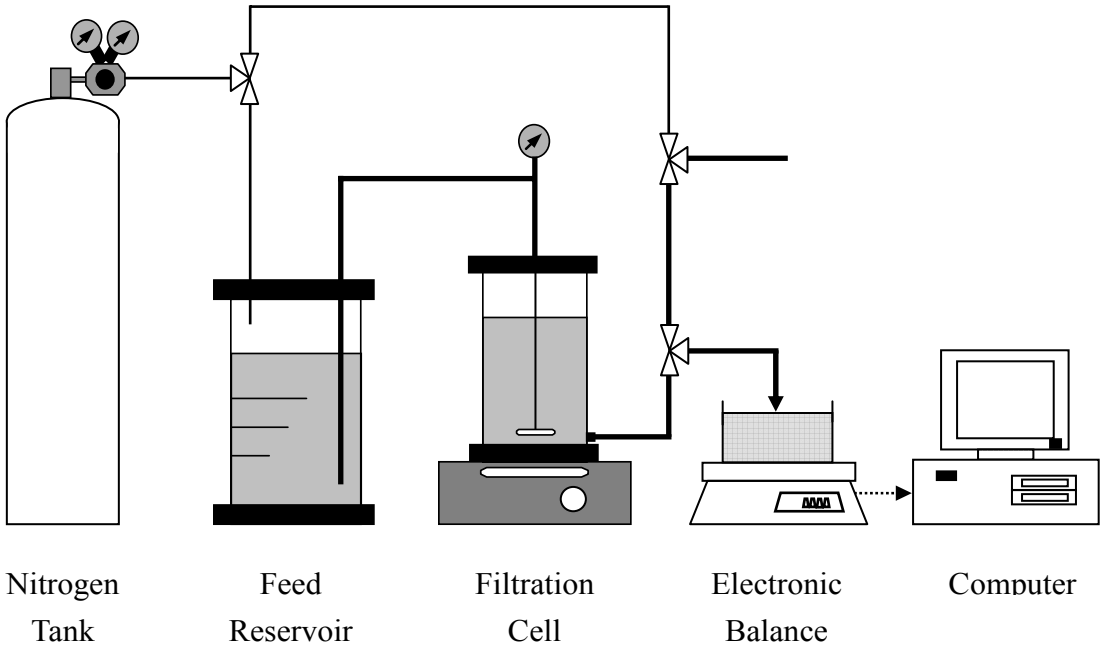

Figure 5.2 Setup of membrane filtration equipment.

flow rate mode as well using Harvard Apparatus syringe pumps (PHD 2000 Infusion, MA, Harvard Apparatus, MA). The pressure was monitored using pressure transducers connected to a computer via a data acquisition module and LabView software.

5.2.3 Feed solutions

A series of filtration experiments were conducted to investigate the fouling behavior of a model compound. The PEG filtration experiments were performed at the PEG concentration of 1.0 g/L using disc-type ceramic membranes with different MWCOs: 3, 8, 15, 50, 150, and 300 kDa for ultrafiltration membranes and 0.14 and 0.2 mm for microfiltration membranes. Suwannee river humic acid (SRHA, International Humic Substances Society, St. Paul, MN) was used, without further purification, to prepare feed solutions (50 and 100 mg/L). The pH values of the feed solutions and ultrapure water used for filtration, rinse, and backwash were adjusted to 8.0 ± 0.1 using 0.1 N HCl or NaOH. River water from the Charlotte-Mecklenburg Utilities, NC, is being tested and other source waters including Chattahoochee River and Lake Lanier will be tested.

5.2.4 Model analysis

The general form of the resistance-in-series model represented as Equation (5.1), was used to quantify the contribution of each fouling mechanism to overall flux decline:

$$J = \frac{\Delta p}{\mu R_t} = \frac{\Delta p}{\mu\left(R_m + R_{cp} + R_{pr} + R_{cr} + R_{if}\right)} \tag{5.1}$$

where J = flux [m/s]; R's = resistances [m^{-1}] (R_t = total resistance; R_{cp} = resistance due to concentration polarization; R_{pr} = cake and pore deposit resistance removable by backwash, *i.e.*, physically removable fouling; R_{cr} = chemically reversible resistance; and R_{if} = chemically irreversible resistance). Table 5.1 provides the classification and description of each resistance.

Flux data were analyzed using the combined pore blockage-cake filtration model (the combined model hereafter) to evaluate the transition of fouling mechanisms (i.e., from initial pore blockage to cake filtration) (Ho and Zydney, 2000):

$$Q = Q_0\left[\exp\left(-\frac{\alpha\Delta p C_b}{\mu R_m}t\right) + \frac{R_m}{\left(R_m + R_{p0}\right)\sqrt{1 + \frac{2f'R'\Delta p C_b t}{\mu\left(R_m + R_{p0}\right)}}}\left(1 - \exp\left(-\frac{\alpha\Delta p C_b}{\mu R_m}t\right)\right)\right] \tag{5.2}$$

where Q = volumetric filtrate flow rate through the membrane [m^3/s]; Q_0 = initial value of Q; α = pore blockage parameter [m^2/kg]; Δp = applied transmembrane pressure [Pa]; μ = viscosity [Pa·s]; R_m = intrinsic membrane resistance [m^{-1}]; R_{p0} = initial resistance of the deposit [m^{-1}]; f' = fractional amount of foulant contributing to cake growth; and R' = specific cake layer resistance [m/kg]; t = filtration time [min]; and C_b = bulk concentration of the feed solution [kg/m^3]. The first term in Equation (5.2) accounts for

Table 5.1 Classification of Resistances

Resistance	Definition	Description
R_m	Intrinsic membrane resistance	Pure water resistance
R_{cp}	Surface cake resistance	Cake formed on the surface, removable by rinsing
R_{pr}	Cake and pore resistance	Cake formed on the surface or in the pore, not removable by rinsing but removable by backwashing
R_{cr}	Chemically reversible resistance	Internal fouling, a portion of the total resistance removable only by chemical cleaning
R_{if}	Chemically irreversible resistance	Residual resistance after chemical cleaning not removable by chemical cleaning
R_t	Total resistance	Measured at the end of feed filtration: $R_m+R_{c1}+R_{c2}+R_{rf}+R_{if}$

the classic pore blocking model and the second term the cake filtration model. Equation (5.2) can be rewritten as follows using lumped parameters, k_1 and k_2:

$$Q = Q_0\left[\exp(-k_1 t) + \frac{R_m}{(R_m + R_{p0})\sqrt{1+k_2 t}}\left(1-\exp(-k_1 t)\right)\right] \tag{5.3}$$

where

$$k_1 = \frac{\alpha \Delta p C_b}{\mu R_m} \tag{5.4}$$

$$k_2 = \frac{2 f' R' \Delta p C_b}{\mu(R_m + R_{p0})} \tag{5.5}$$

The filtration data were fitted to the above equations via non-linear optimization using a curve fitting tool in MATLAB® (The Mathworks, Inc., Natick, MA) with a trust region method to result in the greatest coefficient of determination, R^2, or the smallest sum of squared residuals.

5.3 Results and Discussion

5.3.1 Effect of membrane MWCO on the Flux

A series of filtration experiments were conducted to investigate the fouling behavior of a model compound, PEG. The ceramic membranes used in this study had

different pore sizes as denoted either by MWCOs or pore diameters in μm. As the primary goal of the filtration experiments was to identify any differences in the fouling mechanisms depending on the pore sizes of ceramic membranes ranging over nano-, ultra- and microfiltration.

As shown in Figure 5.3, when the absolute flux data of each filtration set are plotted, greater and faster flux decline was observed as the MWCO of membrane increased. Since the initial flux would depend on the pore sizes of the membrane employed in a specific filtration set, it was as expected that the flux with a larger pore size was higher for membranes with a larger pore size. The highest initial flux was for the microfiltration membranes with 0.2 μm and followed by a microfiltration membrane with 0.14 μm and then by an ultrafiltration membrane with 300 kDa. In contrast, the other membranes in ultrafiltration and nanofiltration regimes showed very low initial flux with marginal difference among the membranes. For membranes with 300 kDa or higher pore sizes, initial flux declined very fast and reduced below 10 % of the initial flux within 10 minutes from the beginning of the filtration. At lower MWCOs near or below 150 kDa, the reduction in permeate flux was minimal and slower compared to that using larger pore sizes (Howe and Clark, 2002), and the permeation rate almost converged around at 20 LMH for the this range of MWCOs while the flux for larger pores kept approaching close to that value. This can be viewed intuitively as the involved fouling mechanism arising form the relative pore size to the molecular size of PEG particles. When the pore size is smaller than that of foulants, the particles are simply rejected on the membrane surface by simple sieve mechanism as is the case in the results with smaller pore sizes

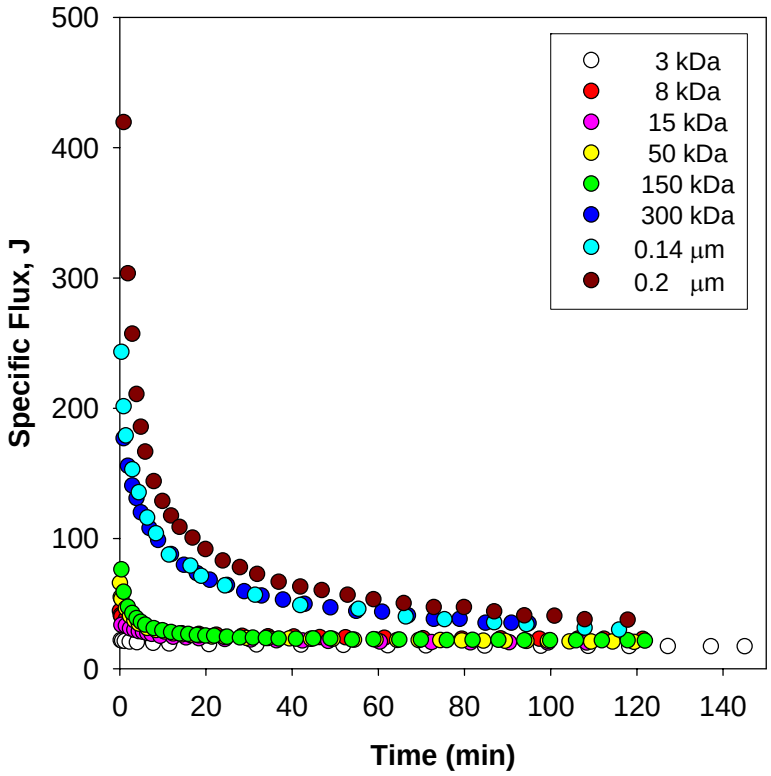

Figure 5.3 Permeation flux during the filtration of PEG solution using ceramic membranes with different MWCOs. The concentration of PEG feed solution was 1.0 g/L, the molecular weight of PEG was 20 kDa, the applied transmembrane pressure was 14.7 psi, and the temperature during all filtration was at 23±1 ^{o}C.

and cake layer starts to form from the beginning of the filtration exerting dominant form of resistance while the PEG particles can penetrate into internal pores inducing pore constriction or standard blocking for the membranes with a pore size similar or greater than the particle size. Therefore, internal fouling did not play a role when the filtration is performed using the membranes with smaller pore sizes as described above.

5.3.2 Effect of membrane MWCO on the Resistance

Through the analysis of resistances using resistance-in-series model, the information about each component and its relative contribution to total resistance can be obtained. In addition, the comparison of resistances among the membranes with different MWCOs can be made. The results of the analyses are shown in Figure 5.4. Each type of resistance defined in a previous section and measured carefully following the experimental sequence is calculated using Equations (5.2) - (5.5) and the results are shown in Figure 5.4(a). It is clearly seen that the R_m or the intrinsic resistance of a membrane decreases as the pore size or MWCO increases. The contributions of R_{pr}, the cake and pore resistance were negligible over the whole range of pore sizes and this implies that the cake layer formed on the membrane surface or in the pores is readily removed by a simple rinse step and only negligible fouling is additionally removed by a physical backwashing step. Depending on specific cleaning procedures, the calculated values of resistances could be different. At least, however, physical cleaning including rinsing and backwashing was considerably effective.

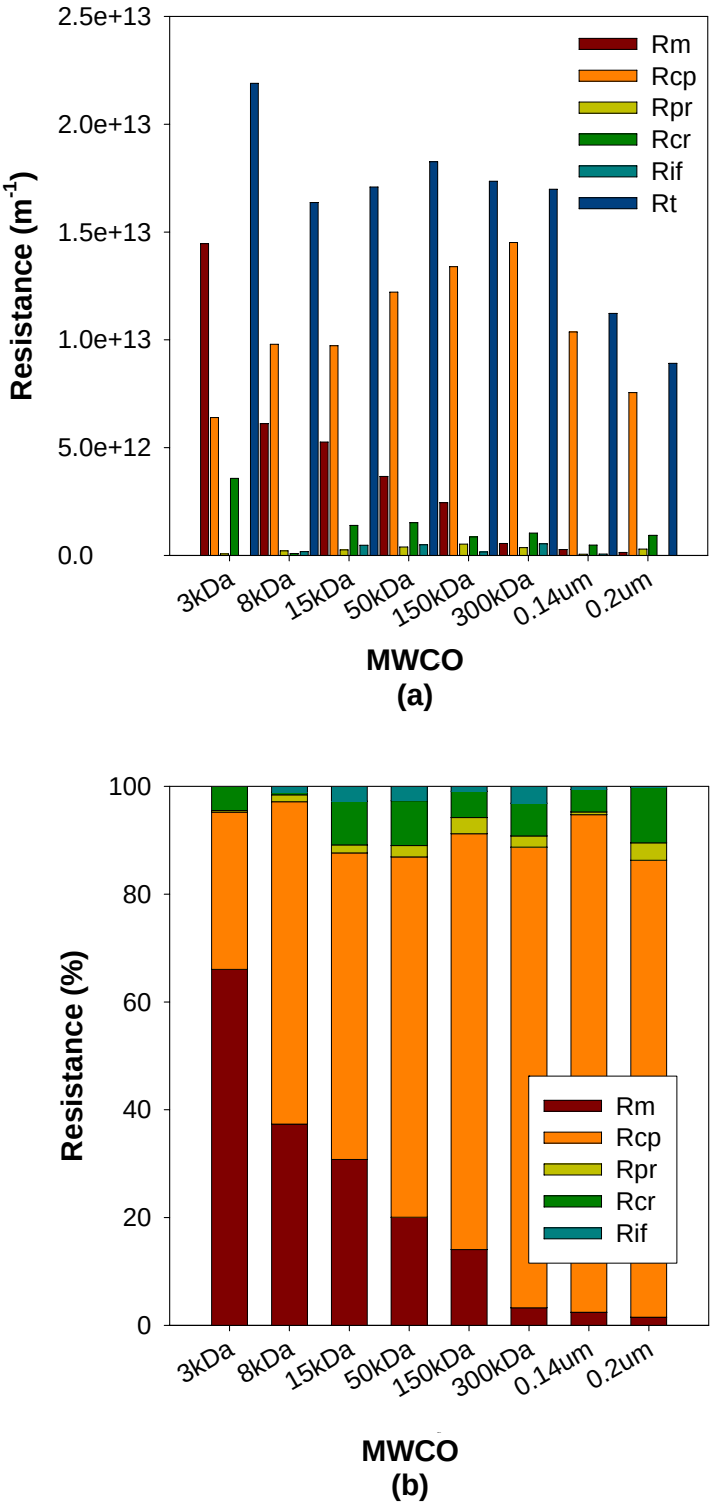

Figure 5.4 Effect of Pore Size on the Resistances: (a) Absolute and (b) Relative contribution of each resistance.

It should be noted that the total resistance from the filtration data is composed mainly of R_m and R_{cp}. The sum of these two terms determined the extent of ultimate fouling at the end of the filtration. As shown in Figure 5.4(a), the surface cake resistance, R_{pr} increases as the MWCO increases up to 300 kDa. However, when the pore size increased further to microfiltration range, the total resistance decreased and this effect was more apparent for 0.2 μm than for 0.14 μm. These results are consistence with the experimental results in a previous work (Yuan and Zydney, 1999). When the pore size increased from 30 kDa to 100 kDa and 300 kDa for the filtration of humic acids, the resistance exerted by the deposit increased. However, when a microfiltration membrane with 0.16 μm was used, the deposit resistance decreased below the resistances for ultrafiltration membranes for the pore size range from 30 kDa to 300 kDa. This resulted in the wedge shaped distribution of the surface cake resistance and in the total resistance as shown. The highest total resistance for 3 kDa is due to the highest intrinsic membrane resistance arising from the finest pore size and it outweighs the values of R_m for other membrane resistances since unlike the relative difference in R_{pr} values, the R_m for 3 kDa membrane was more than double the value of the second largest one, 8 kDa.

The effect of MWCOs on the construction of the total resistance for each filtration set is shown in Figure 5.4(b). The chemically removable fouling accounted for 10 % of the total resistance or less, and the irreversible portion of the fouling at the end of the chemical cleaning was negligible as did the R_{cp}, the cake and pore resistance after rinsing step, a physical cleaning step. With a little fluctuation, the relative contribution of cake layer was greater for the membranes with larger pores. This can be explained that even though the formation of the cake layer starts to begin from the onset of the filtration when

the pore size is very small compared to the foulant particles, the total amount of cake deposit at the end of each filtration experiment was greater for the membranes with larger pore sizes. Although the values of R_{pr} for the microfiltration membranes showed decreasing tendency with increasing pore size, the relative portion comprising the total resistance resulted in similar values as shown in Figure 5.4(b). In all cases, the reversible portions removed by physical and chemical cleaning were greater than those remaining irreversible. In other words, physical cleaning steps including rinse and backwashing removed the majority of fouling leaving only small residual resistances and the chemical cleaning was effective to get rid of the physically irreversible fouling and the pure water flux for the virgin membrane was almost recovered by the chemical cleaning step.

5.3.3 Specific Flux Analysis

When the flux data is presented in another way as shown in Figure 5.5, other important aspects of the fouling mechanisms can be retrieved. When the flux of each run was normalized by its pure water flux, the normalized specific flux was inverted in the opposite order of the absolute flux with the highest normalized specific flux being for the smallest pore size even though there were larger differences in the pure water flux suggested by the manufacturer and in the initial flux for each MWCO as shown in Figure 5.5. This can be observed when the difference in the flux for different membranes during the filtration of feed solutions is smaller than that in the pure water flux or initial flux of filtration. Instantaneous decreases of the flux were observed at the beginning of all

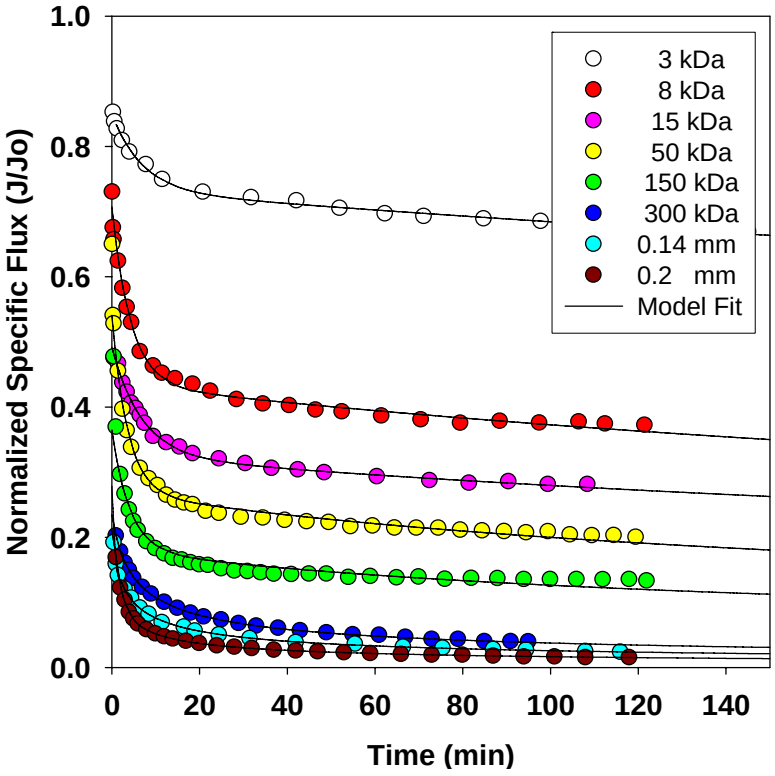

Figure 5.5 Normalized specific flux and model predictions using the combined pore blockage-cake filtration model. Solid lines are model fits of combined pore blockage-cake filtration model.

filtration sets. This implies that PEG particles cause resistance form the early stage of filtration regardless of MWCOs of membranes. However, the extent of decrease for each MWCO appeared different and this phenomenon can be clearly seen in both Figures 5.3 and 5.4.

5.3.4 Model Analysis

According to Hermia's power law of filtration (Hermia, 1982), when second derivative of filtration time to cumulative permeate volume, d^2t/dV^2 is plotted against its first derivative, dt/dV, in logarithmic scale, the slope n gives specific meaning about the mode of filtration. The values of d^2t/dV^2 and dt/dV for selected sets were calculated from experimental data and put in logarithmic scale in Figure 5.6. The values of these values for the model fits were also calculated in the same manner from the model predictions for permeation flux using Equations (5.2) – (5.5). For lower MWCOs, the maxima were reached from the very early time of filtration and could be vaguely seen, or did not even appear, followed by rapid decrease to constant values. This is not unexpected since for the range of the MWCOs, pore blocking is not expected to happen but the particles reaching the membrane surface can deposit. Since by the sieving mechanism, any molecules bigger than the size of the membrane is excluded, relatively small pore sizes with respect to the molecules or aggregates of PEG, does not allow for the introduction of PEG particles into the pores which rules out the incidence of standard blocking mode. And it is noted that the maximum value of d^2t/dV^2 and subsequent rapid decline to a

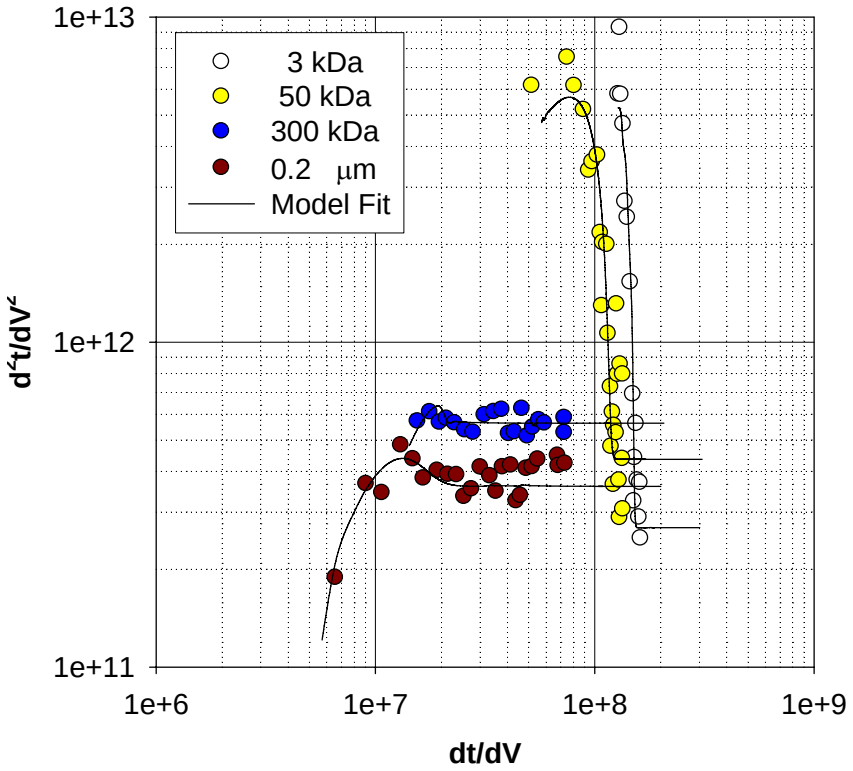

Figure 5.6 Analysis of filtration data for the effect of MWCO on the filtration modes using combined pore blockage-cake filtration model. Model fits are in solid lines using Equations (5.2) – (5.5).

constant after the apex values imply that the mode of filtration is at the stage of cake filtration.

In contrast, for the microfiltration membrane with a 0.2 μm pore size, the region before the maximum value was distinctively observed. This implies that there was the transition of the filtration mode during the filtration of PEG from pore blocking to cake filtration (Cogan and Chellam, 2009; Ho and Zydney, 2000). In case of an ultrafiltration with an MWCO of 300 kDa, a marginal transition but still more apparent than for lower MOWCs was observed and the difference between the maximum value and the asymptotical value of d^2t/dV^2 was not as big as in the filtration using the pore size of 0. 2 μm. Therefore, it can bee seen from the spans of the model fits before the maxima that the larger the pore size was, the later the transition occurred.

5.4 Conclusions

As the initial flux depended on the pore size of MWCOs, the flux decline was faster with membranes with smaller pore sizes. The flux converged to around 20 LHM at the later phase of filtration, which resulted from the formation of cake on the surface of membranes. Pore size had effect on the fouling mechanism in a manner that the relative size of foulant and the pore size led to different modes of fouling. Consequently, the contribution of each resistance component of total resistance varied with the pore size. Under the experimental condition tested in this study, the resistance caused by concentration polarization was predominant, which is favorable for the reduction of membrane fouling. Specific flux analysis showed that the flux reached plateaus at an

early stage of filtration, which in turn reflects the possible dominant cake filtration modes. According to the analyses using the filtration power laws and the combined pore blockage-cake filtration model, cake filtration was the fouling mechanism of PEG filtration with ceramic membranes with various pore sizes.

CHAPTER 6

CONCLUSIONS AND FUTURE WORK

6.1 Conclusions

6.1.1 Introduction

For the implementation of the novel processes utilizing ceramic membranes for the production of drinking water, the establishment of fundamental knowledge and reliable parameters applicable to the water industry is absolutely necessary. As polymeric membranes have been widely and almost exclusively used in drinking water production over the past few decades, various issues have been encountered and efforts have been made to address the issues. On the other hand, the superior intrinsic properties of ceramic membranes, i.e., intrinsic properties such as thermal stability, mechanical strength and chemical resistivity, have been taken advantage of and used in applications in industries where polymeric membranes could not perform satisfactorily. The lack of the research on the application of ceramic membranes in the water industry was economical rather than technical. Recent advancements in manufacturing technologies and increasing production of ceramic membranes has led to greater cost effectiveness, such that a new stance has been made toward the utilization of ceramic membranes by researchers and relevant industry. The questions, already answered for polymeric membranes but remaining unanswered for ceramic membranes, in the context of their applications in surface water treatment, were the motivation of this research.

The main approach made throughout this study was to provide a systematically comparative view of ceramic membranes against polymeric membranes. Thereby, a clearer understanding of ceramic membrane processes could be achieved. Rather than assuming similar trends found with polymeric membranes, the design and operation of ceramic membrane processes needs to be carefully tailored based on concrete data. The similarities and dissimilarities in the fouling behavior between ceramic and polymeric membranes were clearly demonstrated in this study.

The fouling characteristics were investigated by adopting existing methodologies found useful in polymeric membrane studies, as well as introducing new techniques for quantitative evaluation of ceramic membrane processes. Extensive evaluation of fouling characteristics was successfully made from various points of view: a wide range of filtration experiments paralleling ceramic and polymeric membranes, comprehensive analyses using various mathematical models including the power law of filtration, combined pore blockage-cake filtration model, resistance-in-series model and the unified membrane fouling index, and investigation of major parameters including ionic strength, pH, divalent ions, contact angles, feed loading, membrane configuration, operational mode, pore size and surface charge. Successfully demonstrated was the visualization and quantification of fouling, made possible by adopting quantum dots, confocal laser scanning microscopy, and atomic force microscopy. Further, the performance of the hybrid system of coagulation pretreatment and ceramic membrane microfiltration was evaluated for four U.S. surface water sources and three types of coagulants.

This study presents one of the first successful applications of filtration and fouling models to ceramic membrane systems and side-by-side evaluation of similarities and

dissimilarities in the effects of membrane materials and solution chemistry. As the first work comparing the coagulation-membrane filtration systems between ceramic and polymeric membranes under the same conditions, this study includes the performance of the coagulation-ceramic membrane system during the treatment of U.S. surface waters. The results of this study provide critical information to guide the industry practitioners, consultants, and regulatory agents considering early adoption of this new technology as well as fundamental knowledge upon which further in-depth studies can be built.

6.1.2 Key Findings

This chapter describes the key findings drawn from the results of this study.

A. The fouling of ceramic membranes was more easily cleaned by physical cleaning, ether rinse or backwash, than that of polymeric membranes. The resistance removable only by chemical cleaning and the remaining irreversible resistance were relatively insignificant. Higher cleaning efficiency with ceramic membranes was an optimistic finding and a different cleaning strategy for ceramic membrane fouling needs to be adopted.

B. The dominant fouling mechanism of ceramic membranes was cake filtration. Cake filtration mode was apparent in the filtration of simple model compound, natural organic matter standard, synthetic river water and U.S. surface waters. Fouling models that have been applied to polymeric membranes served as a

feasible tool for the analysis of ceramic membrane fouling and supported the observation of dominant cake filtration mechanism.

C. Less fouling and greater cleaning efficiency can be attributed to the surface property of ceramic membranes. Made of metal oxide, the surface of ceramic membranes is more hydrophilic than polymeric counterparts. The hydrophilicity was verified by contact angle measurements, adsorption tests, and solute-membrane surface interaction force measurements.

D. The effects of solution chemistry on ceramic membrane fouling were similar in trend while the extent varied depending on water quality parameters. Divalent ions had a less adverse effect on the NOM fouling of ceramic membranes than of polymeric membranes. The isoelectric points of membranes of different materials influenced the fouling as a function of pH. The surface charge inversion of ceramic membranes requires additional consideration for operation conditions.

E. Visualization and quantification of fouling utilizing quantum dots and confocal laser scanning microscopy served as a useful tool and provided evaluation of the fouling parallel to resistance-in-series model analysis. The formation and the easier removal of cake layer from ceramic membrane were verified and the fluorescence provided quantitative estimation of the extent of fouling and cleaning efficiency.

F. The coagulation-ceramic microfiltration system performed better than the polymeric counterpart in terms of relative pressure reduction and normalized flux in constant flow rate and pressure modes, respectively. Fouling was alleviated with ceramic membrane under the same experimental conditions. The optimal coagulation pretreatment condition may not be identical for ceramic and polymeric membranes. The removal efficiency of NOM was slightly higher with polymeric membranes presumably due to more severe fouling. Source surface waters had influence on the performance of the hybrid system and SUVA values correlated with the NOM rejection. Less severe fouling and higher cleaning efficiency in the hybrid system was consistent with the findings obtained using simple model compounds.

6.2 Future Work

Based on the finding of this study along with the literature review, the following research is recommended.

A. A fundamental level of guidelines should be provided to the water industry via studies on the intrinsic difference resulting from the ceramic membrane properties. The affinity of foulants to ceramic membranes could be different from that to polymeric membranes and the difference may have crucial influence on the performance of water treatment processes. The investigation

of the affinities needs to be conducted utilizing model compounds with different functional groups and performing fractionation of NOMs to elucidate molecular-level interaction of foulants and ceramic membranes.

B. Extension of the comparative research between ceramic and polymeric membrane systems on a pilot scale is highly recommended. Fundamental understanding of fouling characteristics of ceramic membranes can be reinforced through verification of the findings in a larger scale, close to real application of such processes.

C. Other sources of U.S. surface waters need to be tested. This study covered four major water sources located in the southeastern region of the U.S. and the accumulation of parallel knowledge for various water sources with different characteristics will provide general guidelines for the application of ceramic membranes.

D. Reflecting the current cost of membranes, the overall cost analysis should follow. For this, site-specific optimization is required and subsequent cost evaluation can be achieved.

E. Testing of ceramic membranes calls for diversification. One type of hollow fiber ceramic membranes made of α-alumina and disc-type membranes with TiO_2 or ZrO_2 surface were tested in this study. Other types of membranes

including monolithic ceramic membranes are available on an industry scale in the market and comparison among ceramic membranes will provide guidelines for selection of ceramic membranes.

F. Evaluation of the effects of other parameters not covered in this study will complement the finding from this work. Information about other pretreatment options, ceramic membrane specific cleaning strategy and different operational modes such as cross-flow configuration is still necessary to meet the needs of research and industry.

REFERENCES

Ando, T., Akamatsu, K., Nakao, S., Fujita, M., 2012. Simulation of fouling and backwash dynamics in dead-end microfiltration: Effect of pore size. Journal of Membrane Science 392, 48-57.

Ang, W.S., Tiraferri, A., Chen, K.L., Elimelech, M., 2011. Fouling and cleaning of RO membranes fouled by mixtures of organic foulants simulating wastewater effluent. Journal of Membrane Science 376 (1-2), 196-206.

Arnot, T.C., Field, R.W., Koltuniewicz, A.B., 2000. Cross-flow and dead-end microfiltration of oily-water emulsions: Part II. Mechanisms and modelling of flux decline. Journal of Membrane Science 169 (1), 1-15.

Bagga, A., Chellam, S., Clifford, D.A., 2008. Evaluation of iron chemical coagulation and electrocoagulation pretreatment for surface water microfiltration. Journal of Membrane Science 309 (1-2), 82-93.

Benavente, J., Hernandez, A., Jonsson, G., 1993. Proper and adsorbed charges on the surfaces of the polysulfonic support of a composite membrane from electrokinetic phenomena. Journal of Membrane Science 80 (1-3), 285-296.

Berube, P.R., Mavinic, D.S., Hall, E.R., Kenway, S.E., Roett, K., 2002. Evaluation of adsorption and coagulation as membrane pretreatment steps for the removal of organic material and disinfection-by-product precursors. Journal of Environmental Engineering and Science 1 (6), 465-476.

Bhattacharjee, C., Datta, S., 2003. Analysis of polarized layer resistance during ultrafiltration of PEG-6000: An approach based on filtration theory. Separation and Purification Technology 33 (2), 115-126.

Bhattacharjee, S., Sharma, A., Bhattacharya, P.K., 1996. A unified model for flux prediction during batch cell ultrafiltration. Journal of Membrane Science 111 (2), 243-258.

Bolton, G., LaCasse, D., Kuriyel, R., 2006. Combined models of membrane fouling: Development and application to microfiltration and ultrafiltration of biological fluids. Journal of Membrane Science 277 (1-2), 75-84.

Bottino, A., Capannelli, G., Petitbon, P., Cao, N., Pegoraro, M., Zoia, G., 1991. Pore-size and pore-size distribution in microfiltration membranes. Separation Science and Technology 26 (10-11), 1315-1327.

Bowen, W.R., Calvo, J.I., Hernandez, A., 1995. Steps of membrane blocking in flux decline during protein microfiltration. Journal of Membrane Science 101 (1-2), 153-165.

Bowen, W.R., Mukhtar, H., 1993. Properties of microfiltration membranes - the surface electrochemistry of mixed-oxide ceramic membranes. Colloids and Surfaces A-Physicochemical and Engineering Aspects 81, 93-101.

Brown, S.L., Leonard, K.M., Messimer, S.L., 2008. Evaluation of ozone pretreatment on flux parameters of reverse osmosis for surface water treatment. Ozone-Science & Engineering 30 (2), 152-164.

Cao, P.G., Tremblay, A.Y., Dube, M.A., Morse, K., 2007. Effect of membrane pore size on the performance of a membrane reactor for biodiesel production. Industrial & Engineering Chemistry Research 46 (1), 52-58.

Carroll, T., King, S., Gray, S.R., Bolto, B.A., Booker, N.A., 2000. The fouling of microfiltration membranes by NOM after coagulation treatment. Water Research 34 (11), 2861-2868.

Causserand, C., Nystrom, M., Aimar, P., 1994. Study of streaming potentials of clean and fouled ultrafiltration membranes. Journal of Membrane Science 88 (2-3), 211-222.

Childress, A.E., Elimelech, M., 1996. Effect of solution chemistry on the surface charge of polymeric reverse osmosis and nanofiltration membranes. Journal of Membrane Science 119 (2), 253-268.

Chiu, T.Y., James, A.E., 2007. Electrokinetic characterisation techniques on asymmetric microfiltration membranes. Colloids and Surfaces A-Physicochemical and Engineering Aspects 301 (1-3), 281-288.

Cho, J., Amy, G., Pellegrino, J., 2000. Membrane filtration of natural organic matter: Factors and mechanisms affecting rejection and flux decline with charged ultrafiltration (UF) membrane. Journal of Membrane Science 164 (1-2), 89-110.

Choi, K.Y.J., Dempsey, B.A., 2004. In-line coagulation with low-pressure membrane filtration. Water Research 38 (19), 4271-4281.

Ciston, S., Lueptow, R.M., Gray, K.A., 2008. Bacterial attachment on reactive ceramic ultrafiltration membranes. Journal of Membrane Science 320 (1-2), 101-107.

Cogan, N.G., Chellam, S., 2009. Incorporating pore blocking, cake filtration, and EPS production in a model for constant pressure bacterial fouling during dead-end microfiltration. Journal of Membrane Science 345 (1-2), 81-89.

Combe, C., Molis, E., Lucas, P., Riley, R., Clark, M.M., 1999. The effect of CA membrane properties on adsorptive fouling by humic acid. Journal of Membrane Science 154 (1), 73-87.

Costa, A.R., de Pinho, M.N., 2005. Effect of membrane pore size and solution chemistry on the ultrafiltration of humic substances solutions. Journal of Membrane Science 255 (1-2), 49-56.

de la Casa, E.J., Guadix, A., Ibanez, R., Guadix, E.M., 2007. Influence of pH and salt concentration on the cross-flow microfiltration of BSA through a ceramic membrane. Biochemical Engineering Journal 33 (2), 110-115.

de Lara, R., Benavente, J., 2009. Use of hydrodynamic and electrical measurements to determine protein fouling mechanisms for microfiltration membranes with different structures and materials. Separation and Purification Technology 66 (3), 517-524.

Duclos-Orsello, C., Li, W.Y., Ho, C.C., 2006. A three mechanism model to describe fouling of microfiltration membranes. Journal of Membrane Science 280 (1-2), 856-866.

Edzwald, J.K., 1993. Coagulation in drinking-water treatment - particles, organics and coagulants. Water Science and Technology 27 (11), 21-35.

Edzwald, J.K., Tobiason, J.E., 1999. Enhanced coagulation: US requirements and a broader view. Water Science and Technology 40 (9), 63-70.

Elimelech, M., Chen, W.H., Waypa, J.J., 1994. Measuring the zeta (electrokinetic) potential of reverse osmosis membranes by a streaming potential analyzer. Desalination 95 (3), 269-286.

Evans, P.J., Bird, M.R., Pihlajamäki, A., Nyström, M., 2008. The influence of hydrophobicity, roughness and charge upon ultrafiltration membranes for black tea liquor clarification. Journal of Membrane Science 313 (1-2), 250-262.

Fiksdal, L., Leiknes, T., 2006. The effect of coagulation with MF/UF membrane filtration for the removal of virus in drinking water. Journal of Membrane Science 279 (1-2), 364-371.

Freeman, S., Shorney-Darby, H., 2011. What's the buzz about ceramic membranes? Journal American Water Works Association 103 (12), 12-13.

Ganguly, S., Bhattacharya, P.K., 1994. Development of concentration profile and prediction of flux for ultrafiltration in a radial cross-flow cell. Journal of Membrane Science 97, 185-198.

Gao, Y., Chen, D., Weavers, L.K., Walker, H.W., 2012. Ultrasonic control of UF membrane fouling by natural waters: Effects of calcium, pH, and fractionated natural organic matter. Journal of Membrane Science 401–402 (0), 232-240.

Ghose, S., Bhattacharjee, C., Datta, S., 2000. Simulation of unstirred batch ultrafiltration process based on a reversible pore-plugging model. Journal of Membrane Science 169 (1), 29-38.

Ghosh, K., Schnitzer, M., 1980. Macromolecular structures of humic substances. Soil Science 129 (5), 266-276.

Gray, S.R., Ritchie, C.B., Tran, T., Bolto, B.A., 2007. Effect of NOM characteristics and membrane type on microfiltration performance. Water Research 41 (17), 3833-3841.

Gray, S.R., Ritchie, C.B., Tran, T., Bolto, B.A., Greenwood, P., Busetti, F., Allpike, B., 2008. Effect of membrane character and solution chemistry on microfiltration performance. Water Research 42 (3), 743-753.

Guo, H.L., Hu, J.Y., 2012. Effect of hybrid coagulation-membrane filtration on downstream UV disinfection. Desalination 290, 115-124.

Gupta, B.S., Hashim, M.A., Cui, Z.F., 1999. The effect of pore size distribution on the separation efficiency in surface force pore-flow model-system: Isopropanol-water. Bioprocess Engineering 21 (4), 349-353.

Hering, J.G., Morel, F.M.M., 1988. Humic-acid complexation of calcium and copper. Environmental Science & Technology 22 (10), 1234-1237.

Hermans, P.H., Bredee, H.L., 1936. Laws of filtration. Recueil des Travaux Chimigues des Pay-Bas 54, 680-700.

Hermia, J., 1982. Constant pressure blocking filtration laws - application to power-law non-newtonian fluids. Transactions of the Institution of Chemical Engineers 60 (3), 183-187.

Ho, C.C., Zydney, A.L., 2000. A combined pore blockage and cake filtration model for protein fouling during microfiltration. Journal of Colloid and Interface Science 232 (2), 389-399.

Hoek, E.M.V., Bhattacharjee, S., Elimelech, M., 2003. Effect of membrane surface roughness on colloid-membrane DLVO interactions. Langmuir 19 (11), 4836-4847.

Hofs, B., Ogier, J., Vries, D., Beerendonk, E.F., Cornelissen, E.R., 2011. Comparison of ceramic and polymeric membrane permeability and fouling using surface water. Separation and Purification Technology 79 (3), 365-374.

Hong, S.K., Elimelech, M., 1997. Chemical and physical aspects of natural organic matter (NOM) fouling of nanofiltration membranes. Journal of Membrane Science 132 (2), 159-181.

Howe, K.J., Clark, M.M., 2006. Effect of coagulation pretreatment on membrane filtration performance. Journal American Water Works Association 98 (4), 133-146.

Howe, K.J., Clark, M.M., 2002. Fouling of mcrofiltration and ultrafiltration membranes by natural waters. Environmental Science & Technology 36 (16), 3571-3576.

Howe, K.J., Marwah, A., Chiu, K.P., Adham, S.S., 2006. Effect of coagulation on the size of MF and UF membrane foulants. Environmental Science & Technology 40 (24), 7908-7913.

Hu, J., Song, H., Addison, J.W., Karanfil, T., 2010. Halonitromethane formation potentials in drinking waters. Water Research 44 (1), 105-114.

Huang, H., Schwab, K., Jacangelo, J.G., 2009. Pretreatment for low pressure membranes in water treatment: A review. Environmental Science & Technology 43 (9), 3011-3019.

Huang, H., Young, T.A., Jacangelo, J.G., 2008. Unified membrane fouling index for low pressure membrane filtration of natural waters: Principles and methodology. Environmental Science & Technology 42 (3), 714-720.

Huang, J.Y., Takizawa, S., Fujita, K. (2001) Membranes in drinking and industrial water production II. Balaban, M.Schippers, J.C. (eds), pp. 245-251.

Huisman, I.H., Tragardh, G., Tragardh, C., Pihlajamaki, A., 1998. Determining the zeta-potential of ceramic microfiltration membranes using the electroviscous effect. Journal of Membrane Science 147 (2), 187-194.

Hwang, K.J., Liao, C.Y., Tung, K.L., 2007. Analysis of particle fouling during microfiltration by use of blocking models. Journal of Membrane Science 287 (2), 287-293.

Jin, L., Ng, H.Y., Ong, S.L., 2009. Performance and fouling characteristics of different pore-sized submerged ceramic membrane bioreactors (SCMBR). Water Science and Technology 59 (11), 2213-2218.

Jones, K.L., O'Melia, C.R., 2000. Protein and humic acid adsorption onto hydrophilic membrane surfaces: Effects of pH and ionic strength. Journal of Membrane Science 165 (1), 31-46.

Judd, S.J., Hillis, P., 2001. Optimisation of combined coagulation and microfiltration for water treatment. Water Research 35 (12), 2895-2904.

Kanaya, S., Fujiura, S., Tomita, Y., Yonekawa, H., 2007. Performance of new generation ceramic membranes using coagulation and ozonation pretreatment. AWWA Membrane Technology Conference Proceedings, March 18-21, Tampa, FL.

Karanfil, T., Schlautman, M.A., Kilduff, J.E., Weber, W.J., 1996. Adsorption of organic macromolecules by granular activated carbon. 2. Influence of dissolved oxygen. Environmental Science & Technology 30 (7), 2195-2201.

Kennedy, M., Zhizhong, L., Febrina, E., Van Hoof, S., Shippers, J. (2003) Effects of coagulation on filtration mechanisms in dead-end ultrafiltration.

Kim, J., Shan, W., Davies, S.H.R., Baumann, M.J., Masten, S.J., Tarabara, V.V., 2009. Interactions of aqueous NOM with nanoscale TiO_2: Implications for ceramic membrane filtration-ozonation hybrid process. Environmental Science & Technology 43 (14), 5488-5494.

Kleijn, M., Norde, W., 1995. The adsorption of proteins from aqueous solution on solid surfaces. Heterogeneous Chemistry Reviews 2 (3), 157-172.

Kwon, B., Lee, S., Cho, J., Ahn, H., Lee, D., Shin, H.S., 2005. Biodegradability, DBP formation, and membrane fouling potential of natural organic matter: Characterization and controllability. Environmental Science & Technology 39 (3), 732-739.

Lee, E.K., Chen, V., Fane, A.G., 2008. Natural organic matter (NOM) fouling in low pressure membrane filtration - effect of membranes and operation modes. Desalination 218 (1-3), 257-270.

Lee, H., Amy, G., Cho, J.W., Yoon, Y.M., Moon, S.H., Kim, I.S., 2001. Cleaning strategies for flux recovery of an ultrafiltration membrane fouled by natural organic matter. Water Research 35 (14), 3301-3308.

Lee, J.D., Lee, S.H., Jo, M.H., Park, P.K., Lee, C.H., Kwak, J.W., 2000. Effect of coagulation conditions on membrane filtration characteristics in coagulation-microfiltration process for water treatment. Environmental Science & Technology 34 (17), 3780-3788.

Lee, N.H., Amy, G., Croue, J.P., Buisson, H., 2004. Identification and understanding of fouling in low-pressure membrane (MF/UF) filtration by natural organic matter (NOM). Water Research 38 (20), 4511-4523.

Lee, S.-J., Dilaver, M., Park, P.-K., Kim, J.-H., 2013. Comparative analysis of fouling characteristics of ceramic and polymeric microfiltration membranes using filtration models. Journal of Membrane Science 432, 97-105.

Lehman, S.G., Adham, S., Liu, L., 2008. Performance of new generation ceramic membranes using hybrid coagulation pretreatment. Journal of Environmental Engineering and Management 18 (4), 257-260.

Leiknes, T., Odegaard, H., Myklebust, H., 2004. Removal of natural organic matter (NOM) in drinking water treatment by coagulation-microfiltration using metal membranes. Journal of Membrane Science 242 (1-2), 47-55.

Li, Q.L., Elimelech, M., 2004. Organic fouling and chemical cleaning of nanofiltration membranes: Measurements and mechanisms. Environmental Science & Technology 38 (17), 4683-4693.

Li, X.F., Fu, X.Q., 2002. Effect of solution chemistry on membrane resistance and flux decline. Filtration & Separation 39 (10), 33-39.

Liang, S., Zhao, Y., Liu, C., Song, L., 2008. Effect of solution chemistry on the fouling potential of dissolved organic matter in membrane bioreactor systems. Journal of Membrane Science 310 (1-2), 503-511.

Lim, A.L., Bai, R., 2003. Membrane fouling and cleaning in microfiltration of activated sludge wastewater. Journal of Membrane Science 216 (1-2), 279-290.

Loi-Brugger, A., Panglisch, S., Buchta, P., Hattori, K., Yonekawa, H., Tomita, Y., Gimbel, R. (2006) 5th world water congress: Drinking water quality and treatment. Kroiss, H. (ed), pp. 89-98.

Loi-Brugger, A., Panglisch, S., Buchta, P., Hattori, K., Yonekawa, H., Tomita, Y., Gimbel, R., 2006. Ceramic membranes for direct river water treatment applying coagulation and microfiltration. Water Science and Technology: Water Supply 6 (4), 89-98.

Loi-Brugger, A., Panglisch, S., Hattori, K., Yonekawa, H., Tomita, Y., Gimbel, R., 2007. Open up new doors in water treatment with ceramic membranes. AWWA Membrane Technology Conference Proceedings, March 18-21, Tampa, FL.

Lopez-Duran, J.D.G., Khaldoun, A., Kerkeb, M.L., Ramos-Tejada, M.D., Gonzalez-Caballero, F., 2003. Wettability of montmorillonite clays in humic acid solutions. Clays and Clay Minerals 51 (1), 65-74.

Matsui, Y., Matsushita, T., Sakuma, S., Gojo, T., Mamiya, T., Suzuoki, H., Inoue, T., 2003. Virus inactivation in aluminum and polyaluminum coagulation. Environmental Science & Technology 37 (22), 5175-5180.

McAliley, I.E., D'Adamo, P., 2009. Advances in membrane treatment lead to more cost-effective options for drinking water providers. NC AWWA-WEA Annual conference, Novvember 15-18, Raleigh, NC.

Meng, F.G., Zhang, H.M., Yang, F.L., Liu, L.F., 2007. Characterization of cake layer in submerged membrane bioreactor. Environmental Science & Technology 41 (11), 4065-4070.

Meyn, T., Leiknes, T., 2010. Comparison of optional process configurations and operating conditions for ceramic membrane MF coupled with coagulation/flocculation pre-treatment for the removal of NOM in drinking water production. Journal of Water Supply Research and Technology-AQUA 59 (2-3), 81-91.

Mitch, W.A., Shah, A.S., A. D., Dotson, A.D., Linden, K.G., 2011. Impact of UF disinfection combined with chlorination/chloramination on the formation of halonitromethanes and haloacetonitriles in drinking water. Environmental Science & Technology 45 (8), 3657-3664.

Mo, L., Huang, X., 2003. Fouling characteristics and cleaning strategies in a coagulation-microfiltration combination process for water purification. Desalination 159 (1), 1-9.

Munson-McGee, S.H., 2002. Effect of particle-size and pore-size distributions in cross-flow filtration. Separation Science and Technology 37 (3), 493-513.

Nazzal, F.F., Wiesner, M.R., 1994. pH and ionic-strength effects on the performance of ceramic membranes in water filtration. Journal of Membrane Science 93 (1), 91-103.

Nguyen, S.T., Roddick, F.A., Harris, J.L., 2010. Membrane foulants and fouling mechanisms in microfiltration and ultrafiltration of an activated sludge effluent. Water Science and Technology 62 (9), 1975-1983.

Ohya, H., Kim, J.J., Chinen, A., Aihara, M., Semenova, S.I., Negishi, Y., Mori, O., Yasuda, M., 1998. Effects of pore size on separation mechanisms of microfiltration of oily water, using porous glass tubular membrane. Journal of Membrane Science 145 (1), 1-14.

Pendergast, M.M., Hoek, E.M.V., 2011. A review of water treatment membrane nanotechnologies. Energy & Environmental Science 4 (6), 1946-1971.

Rao, S.P., Tripathy, S.S., Raichur, A.M., 2007. Dispersion studies of sub-micron zirconia using Dolapix CE 64. Colloids and Surfaces A-Physicochemical and Engineering Aspects 302 (1-3), 553-558.

Renger, C., Kuschel, P., Kristoffersson, A., Clauss, B., Oppermann, W., Sigmund, W., 2006. Adsorption studies on nano-zirconia in water and a water-1,2-propanediol mixture. Journal of Ceramic Processing Research 7 (2), 106-112.

Ricq, L., Pierre, A., Bayle, S., Reggiani, J.C., 1997. Electrokinetic characterization of polyethersulfone UF membranes. Desalination 109 (3), 253-261.

Schippers, J.C., Verdouw, J., 1980. Modified fouling index, a method of determining the fouling characteristics of water. Desalination 32 (1-3), 137-148.

Shah, A.D., Dotson, A.D., Linden, K.G., Mitch, W.A., 2011. Impact of UV disinfection combined with chlorination/chloramination on the formation of halonitromethanes

and haloacetonitriles in drinking water. Environmental Science & Technology 45 (8), 3657-3664.

Shao, J., Hou, J., Song, H., 2011. Comparison of humic acid rejection and flux decline during filtration with negatively charged and uncharged ultrafiltration membranes. Water Research 45 (2), 473-482.

Sondhi, R., Bhave, R., 2001. Role of backpulsing in fouling minimization in crossflow filtration with ceramic membranes. Journal of Membrane Science 186 (1), 41-52.

Song, W., Ravindran, V., Koel, B.E., Pirbazari, M., 2004. Nanofiltration of natural organic matter with H_2O_2/UV pretreatment: Fouling mitigation and membrane surface characterization. Journal of Membrane Science 241 (1), 143-160.

Stawikowska, J., Livingston, A.G., 2013. Assessment of atomic force microscopy for characterisation of nanofiltration membranes. Journal of Membrane Science 425–426 (0), 58-70.

Sun, C., Fiksdal, L., Hanssen-Bauer, A., Rye, M.B., Leiknes, T., 2011. Characterization of membrane biofouling at different operating conditions (flux) in drinking water treatment using confocal laser scanning microscopy (CLSM) and image analysis. Journal of Membrane Science 382 (1–2), 194-201.

Taniguchi, M., Kilduff, J.E., Belfort, G., 2003. Modes of natural organic matter fouling during ultrafiltration. Environmental Science & Technology 37 (8), 1676-1683.

Tarabara, V.V., Hovinga, R.M., Wiesner, M.R., 2002. Constant transmembrane pressure vs. constant permeate flux: Effect of particle size on crossflow membrane filtration. Environmental Engineering Science 19 (6), 343-355.

Tracey, E.M., Davis, R.H., 1994. Protein fouling of track-etched polycarbonate microfiltration membranes. Journal of Colloid and Interface Science 167 (1), 104-116.

Urase, T., Yamamoto, K., Ohgaki, S., 1994. Effect of pore-size distribution of ultrafiltration membranes on virus rejection in cross-flow conditions. Water Science and Technology 30 (9), 199-208.

Vincent-Vela, M.C., Álvarez Blanco, S., Lora García, J., Bergantiños Rodríguez, E., 2009. Analysis of membrane pore blocking models adapted to crossflow ultrafiltration in the ultrafiltration of PEG. Chemical Engineering Journal 149 (1-3), 232-241.

Xu, L.C., Soman, P., Runt, J., Siedlecki, C.A., 2007. Characterization of surface microphase structures of poly(urethane urea) biomaterials by nanoscale indentation with AFM. Journal of Biomaterials Science-Polymer Edition 18 (4), 353-368.

Yang, X., Shang, C., 2004. Chlorination byproduct formation in the presence of humic acid, model nitrogenous organic compounds, ammonia, and bromide. Environmental Science & Technology 38 (19), 4995-5001.

Yonekawa, H., Tomita, Y., Watanabe, Y., 2004. Behavior of micro-particles in monolith ceramic membrane filtration with pre-coagulation. Water Science and Technology 50 (12), 317-325.

Yuan, W., Kocic, A., Zydney, A.L., 2002. Analysis of humic acid fouling during microfiltration using a pore blockage-cake filtration model. Journal of Membrane Science 198 (1), 51-62.

Yuan, W., Zydney, A.L., 1999. Effects of solution environment on humic acid fouling during microfiltration. Desalination 122 (1), 63-76.

Yuan, W., Zydney, A.L., 1999. Humic acid fouling during microfiltration. Journal of Membrane Science 157 (1), 1-12.

Yuan, W., Zydney, A.L., 2000. Humic acid fouling during ultrafiltration. Environmental Science & Technology 34 (23), 5043-5050.

Zarate-Rodriguez, E., Ortega-Rivas, E., Barbosa-Canovas, G.V., 2001. Effect of membrane pore size on quality of ultrafiltered apple juice. International Journal of Food Science and Technology 36 (6), 663-667.

Zhang, M.M., Li, C., Benjamin, M.M., Chang, Y.J., 2003. Fouling and natural organic matter removal in adsorben/membrane systems for drinking water treatment. Environmental Science & Technology 37 (8), 1663-1669.

Zhang, Q., Fan, Y.Q., Xu, N.P., 2009. Effect of the surface properties on filtration performance of A_2O_3-TiO_2 composite membrane. Separation and Purification Technology 66 (2), 306-312.

Zhang, W., Stack, A.G., Chen, Y.S., 2011. Interaction force measurement between E. Coli cells and nanoparticles immobilized surfaces by using AFM. Colloids and Surfaces B-Biointerfaces 82 (2), 316-324.